Progress In Electromagnetics Research, PIER 14, 89–180, 1996

SCATTERING, RADIATION AND PROPAGATION OVER TWO-DIMENSIONAL RANDOM SURFACE

–STOCHASTIC FUNCTIONAL APPROACH–

H. Ogura and N. Takahashi

1. Introduction

Scattering of waves from a random rough surface has long been a subject for a number of scholars, not only because of theoretical interest but also of practical importance in physics and engineering, and various techniques have been used and devised to tackle the problem, such as the Kirchhoff approximation [1–4], the small-perturbation method [3,5], the diagram and renormalization techniques [6,8–12], etc., where its theoretical difflculty arises from the multiple scattering.

In a series of preceding works since 1979 [13–23], the present authors with J.Nakayama have developed the scattering theory for various random surfaces by means of a stochastic functional approach combined with a group-theoretic consideration, which was originally introduced by one of the author in the theory of propagation in random media [24–27]. Some of those are; the scalar wave scattering from one-dimensional (1D) and 2D random plane [l3-15], electromagnetic scattering from a perfectly conducting random plane [l6,17], surface plasmon mode in a metal film [18], Green function and radiation over 1D random plane [19], scalar scattering from 1D and 2D random cylindrical surfaces [20,21], electromagnetic scattering from a random cylindrical surface [22], and scalar scattering from a random spherical surface [23].

First of all we note that our scattering problem is a stochastic boundary value problem, where the wave field satisfying the boundary condition is necessarily a stochastic field which should be treated as a stochastic functional of the random surface. For the sake of simplicity, we assume the random surface be described by a homogeneous Gaussian random field, and the scattered wave field can be regarded as a nonlinear functional of the Gaussian random surface or the Gaussian random measure [28–33], but if necessary, the random surface could be a non-Gaussian field generated by Gaussian random measure, or even the one generated by Poisson random measure [33]. Then, a nonlinear

functional of a Gaussian random field can be handled in the most convenient way by means of Wiener-Itô theory; the theory originally due to Wiener [28-33] has found diverse applications such as the turbulence [34,35], system theory [36,37], random propagation [24–27] and random scattering [13–23,38,39].

Secondly, another feature of our theory is that, in addition to the stochastic functional calculus, the formulation is firmly based on a group-theoretic consideration associated with the homogeneity of the random surface, where the random field is said to be homogeneous if its probability measure is invarinat under a group of motions on the surface; such as, translations on the plane, cylindrical motions on a cylinder, spherical rotations on a sphere, depending on the shape of random surfaces under discussion. The homogeneity associated with the translation group on a plane or a cylinder leads to a "stochastic Floquet theorem" [24]; this is an analogue to the Floquet theorem for a periodic surface, which obviously is a 1D representation of the periodic translation group. The stochastic Floquet theorem is no other than an irreducible "stochastic" representation of the motion group on the plane. Therefore, in the case of a random spherical surface [23], an irreducible "stochastic representation" of the rotation group plays a more crucial role than the "Floquet theorem", and yields the concept of "stochastic spherical harmonics" in terms of which the scattered wave can be represented.

It is further noted that the divergence difficulty arising in the multiple scattering theory, when dealing with a propagating mode on an infinite perturbing area, can be automatically circumvented by our method without recourse to the renormalization technique: this largely owes to the stochastic Floquet theorem and Wiener-Itô calculus.

As it is unable to give a complete review in this short article, we restrict ourselves to a 2D random plane described by a homogeneous and isotropic random field, which possesses two types of symmetry; homogeneity under translational motions and isotropy under rotational motions on the 2D plane. Then we discuss the scattering characteristics, reciprocity, backscattering enhancement, Green's function, radiation and propagation over the random surface, which are mostly new results. A brief account of the Wiener-Itô theory and several formulas adapted to the 2D Gaussian random field are summarized in the appendix.

2. Homogeneous Random Field and Shift Operator

2.1 Homogeneous Random Field on a Plane.

Let the two-dimensional (2D) plane be denoted by R_2 and a position vector on R_2 by $\mathbf{x} = (x, y)$, and the probability space under consideration be denoted by $(P, \mathcal{B}, \Omega)$ where Ω denotes the sample space, $\mathcal{B}$ the Borel field, and P the probability measure. Denote by $\langle \quad \rangle$ the average or expectation with respect to P. Let an infinitely extending 2D random surface be described by a homogeneous random field with parameter $\mathbf{x}$:

$$z = f(\mathbf{x}, \omega) = f(T^{\mathbf{x}}\omega), \qquad \omega \in \Omega, \qquad \mathbf{x} \in R_2 \tag{2.1}$$

where ω denotes a sample point in Ω, and $f(\omega) \equiv f(0, \omega)$. The implication of the right hand member is given later. For the time being, we assume that the random variables under consideration are generated from $f(\mathbf{x}, \omega)$ (i.e., linear or nonlinear functionals), that is, we regard $\mathcal{B}$ as the smallest Borel field where $f(\mathbf{x}, \omega)$ is measurable.

In our stochastic scattering theory, the homogeneity of the random surface, which is a certain symmetry of the ensemble of random surfaces, plays a crucial role in the formulation of the stochastic wave field. Homogeneity of $f(\mathbf{x}, \omega)$ implies its probability measure P is invariant under translational motions on R_2, that is, for a translation $\mathbf{a}(\in R_2)$ there is a measure-preserving set transformation $T^{\mathbf{a}}$ of $A(\in \mathcal{B}), A \to T^{\mathbf{a}}A$, such that

$$P(T^{\mathbf{a}}A) = P(A), \qquad \mathbf{a} \in R_2 \tag{2.2}$$

For our convenience, we regard $T^{\mathbf{a}}$ as a measure-preserving point transformation that brings a point ω to a new point ω' in Ω: $\omega \to \omega' = T^{\mathbf{a}}\omega$ [40]. That is, a translation of a sample function, $f(\mathbf{x}, \omega) \to f(\mathbf{x} + \mathbf{a}, \omega)$, can be expressed as an almost sure equality

$$f(\mathbf{x} + \mathbf{a}, \omega) = f(\mathbf{x}, T^{\mathbf{a}}\omega) \tag{2.3}$$

In this notation a sample point ω can be conveniently treated as if it is a coordinate parameter like $\mathbf{x}$. $T^{\mathbf{a}}$ is called the shift transformation, and has the additive group property with respect to $\mathbf{a}$:

$$T^{\mathbf{a}+\mathbf{b}} = T^{\mathbf{a}}T^{\mathbf{b}}, T^{\mathbf{0}} = I \text{ (identity)}, \qquad \mathbf{a}, \mathbf{b} \in R_2 \tag{2.4}$$

so that $T^{\mathbf{a}}$ gives a representation of the translation group on R_2 which we denote by R_2 also. Putting $\mathbf{x} \to 0$ and $\mathbf{a} \to \mathbf{x}$ in (2.3) we see that a homogeneous random field can be expressed as in the right-hand member of (2.1). We further assume that the shift transformation $T^{\mathbf{a}}$ be ergodic, that is, a $T^{\mathbf{a}}$ -invariant function $\psi(\omega)$, such that $\psi(T^{\mathbf{a}}\omega) = \psi(\omega)$ and $\mathbf{a} \in R_2$, always equal a constant for almost all ω.

2.2 Shift Operator

Let a random field $\psi(\mathbf{x}, \omega)$ be generated from $f(\mathbf{x}, \omega)$, and we introduce a measure-preserving transformation $D^{\mathbf{a}}$ on $R_2 \times \Omega$ operating on a random function $\psi(\mathbf{x}, \omega)$ by the definition:

$$D^{\mathbf{a}}\psi(\mathbf{x}, \omega) \equiv \psi(\mathbf{x} + \mathbf{a}, T^{-\mathbf{a}}\omega), \quad \mathbf{a} \in R_2 \tag{2.5}$$

We call $D^{\mathbf{a}}, \mathbf{a} \in R_2$, the shift operator, which has the additive group property also:

$$D^{\mathbf{a}+\mathbf{b}} = D^{\mathbf{a}}D^{\mathbf{b}}, \qquad D^{\mathbf{0}} = I, \qquad \mathbf{a}, \mathbf{b} \in R_2 \tag{2.6}$$

that is, $D^{\mathbf{a}}, \mathbf{a} \in R_2$, again gives a representation of the translation group R_2.

Consider a class of random functions $\psi(\mathbf{x}, \omega)$ such that

$$D^{\mathbf{a}}\psi(\mathbf{x}, \omega) = \Lambda^{\mathbf{a}}\psi(\mathbf{x}, \omega), \qquad \mathbf{a} \in R_2 \tag{2.7}$$

where $\Lambda^{\mathbf{a}}$ is an eigenvalue for the operator $D^{\mathbf{a}}$. Since $D^{\mathbf{a}}$ satisfies (2.6), $\Lambda^{\mathbf{a}}$ must satisfy $\Lambda^{\mathbf{a}+\mathbf{b}} = \Lambda^{\mathbf{a}}\Lambda^{\mathbf{b}}$, $\Lambda^{\mathbf{0}} = 1$, that is, $\Lambda^{\mathbf{a}}$ gives a 1D representation of the group R_2. Hence we can put $\Lambda^{\mathbf{a}} = e^{i\,\boldsymbol{\lambda}\cdot\mathbf{a}}$, where $\boldsymbol{\lambda}$ denotes generally a complex vector and $\boldsymbol{\lambda}\cdot\mathbf{a}$ the vector inner-product. We write an eigenfunction with eigenvalue $e^{i\,\boldsymbol{\lambda}\cdot\mathbf{a}}$ as $\phi(\mathbf{x}, \omega|\,\boldsymbol{\lambda})$, that is,

$$D^{\mathbf{a}}\phi(\mathbf{x}, \omega|\,\boldsymbol{\lambda}) = e^{i\,\boldsymbol{\lambda}\cdot\mathbf{a}}\phi(\mathbf{x}, \omega|\,\boldsymbol{\lambda}) \tag{2.8}$$

We denote by $\mathcal{D}_{\boldsymbol{\lambda}}$, the linear space of such eigenfunctions, which is an invariant space under $D^{\mathbf{a}}$, i.e., an irreducible space with respect to the operator group $D^{\mathbf{a}}$. As shown easily, a $D^{\mathbf{a}}$-invariant function can be written in the form $u(T^{\mathbf{x}}\omega)$:

$$D^{\mathbf{a}}u(T^{\mathbf{x}}\omega) = u(T^{\mathbf{x}}\omega) \tag{2.9}$$

so that it belongs to $\mathcal{D}_0$. Such a $D^{\mathbf{a}}$-invariant function is called a homogeneous random field generated by $f(T^{\mathbf{x}}\omega)$. Particularly, the original random field $f(T^{\mathbf{x}}\omega)$ is $D^{\mathbf{a}}$-invariant. A function belonging to $\mathcal{D}_{\boldsymbol{\lambda}}$ satisfying (2.8) can be generally expressed as

$$\phi(\mathbf{x},\omega|\,\boldsymbol{\lambda}\,) = e^{i\,\boldsymbol{\lambda}\cdot\mathbf{x}} u(T^{\mathbf{x}}\omega|\,\boldsymbol{\lambda}\,) \tag{2.10}$$

where $u(T^{\mathbf{x}}\omega|\ \boldsymbol{\lambda}\ )$ is a homogeneous random field in $\mathcal{D}_0$.

We consider a class of random field expressed as

$$\psi(\mathbf{x},\omega) = \int_{R_2} \phi(\mathbf{x},\omega|\,\boldsymbol{\lambda}\,)\,d\,\boldsymbol{\lambda} \tag{2.11}$$

or, using (2.10), we can write

$$\psi(\mathbf{x},\omega) = \int_{R_2} e^{i\,\boldsymbol{\lambda}\cdot\mathbf{x}} u(T^{\mathbf{x}}\omega|\,\boldsymbol{\lambda}\,)\,d\,\boldsymbol{\lambda} \tag{2.12}$$

where we assume $\boldsymbol{\lambda}$ is a real vector in R_2. This is a stochastic version of the "Fourier integral", and implies the decomposition of the function $\psi(\mathbf{x},\omega)$ into the sum of eigenfunctions in $\mathcal{D}_{\boldsymbol{\lambda}}$; this corresponds to the irreducible decomposition of the representation of the group $D^{\mathbf{a}}$. The representation (2.12), however, can be generalized to an integral over complex vector $\boldsymbol{\lambda}$ if the integration is properly defined. (2.11) or (2.12) can be considered as a general representation for an inhomogeneous random field, and will be used in a later chapter.

2.3 Homogeneous and Isotropic Random Field and Rotation Operator

Let g_α denote a rotation in R_2 by an angle α: that is, $g_\alpha\mathbf{x} = (\rho,\varphi+\alpha)_{cyl}$ where $\mathbf{x} = (\rho,\varphi)_{cyl}$ in cylindrical coordinates, and let G_2 denote the 2D rotation group consisting of g_α's. We note that the translation group R_2 and the rotation group G_2 are not commutative, and that $\mathcal{G} \equiv \{R_2, G_2\}$ forms the inhomogeneous rotation group called 2D Euclidean motion. If the homogeneous random field (2.1) is isotropic, that is, its probability measure is also invariant under rotations in addition to translations, then corresponding to a rotation g_α we can introduce a measure-preserving transformation T^α such that $P(T^\alpha A) = P(A), A \in \mathcal{B}$, and analogous to (2.3) we can express the isotropy,

$$f(g_\alpha\mathbf{x},\omega) = f(\mathbf{x},T^\alpha\omega) \tag{2.13}$$

For the sake of convenience, we use the same notation T^α as $T^{\mathbf{a}}$ to denote a shift transformation with respect to g_α, and discriminate them by the superscript. T^α possesses the additive group property similar to (2.4),

$$\begin{gathered} T^{\alpha+\beta} = T^\alpha T^\beta, \qquad T^{\mathbf{0}} = I \text{ (identity)}, \\ -\infty < \alpha, \beta < \infty \pmod{2\pi} \end{gathered} \tag{2.14}$$

$$\begin{gathered} T^{\mathbf{a}} T^\alpha = T^\alpha T^{g_\alpha \mathbf{a}}, \qquad T^\alpha T^{\mathbf{a}} = T^{g_{-\alpha}\mathbf{a}} T^\alpha, \\ \mathbf{a} \in R_2, \qquad g_\alpha \in G_2 \end{gathered} \tag{2.15}$$

where (2.15) shows that $T^{\mathbf{a}}$ and T^α are not commutative.

Similar to (2.5) we introduce the rotation operator D^α by the definition:

$$D^\alpha \psi(\mathbf{x}, \omega) \equiv \psi(g_\alpha \mathbf{x}, T^{-\alpha}\omega), \qquad g_\alpha \in G_2 \tag{2.16}$$

which satisfies the similar relations:

$$\begin{gathered} D^{\alpha+\beta} = D^\alpha D^\beta, \qquad D^{\mathbf{0}} = I \text{ (identity)}, \\ -\infty < \alpha, \beta < \infty \pmod{2\pi} \end{gathered} \tag{2.17}$$

$$\begin{gathered} D^{\mathbf{a}} D^\alpha = D^\alpha D^{g_\alpha \mathbf{a}}, \qquad D^\alpha D^{\mathbf{a}} = D^{g_{-\alpha}\mathbf{a}} D^\alpha, \\ \mathbf{a} \in R_2, \qquad g_\alpha \in G_2 \end{gathered} \tag{2.18}$$

By (2.17) D^α gives a representation of the rotation group G_2. By an argument analogous to (2.7)–(2.8), we write an eigenfunction with the eigenvalue $e^{im\alpha}$ as $\phi_m(\mathbf{x}, \omega)$;

$$D^\alpha \phi_m(\mathbf{x}, \omega) = e^{im\alpha} \phi_m(\mathbf{x}, \omega), \qquad m = 0, \pm 1, \pm 2, \ldots \tag{2.19}$$

We denote by $\mathcal{D}_m$ the linear space of such eigenfunctions, which is an invariant space under D^α. An isotropic random field belongs to $\mathcal{D}_O$, namely, it is D^α-invariant. Particularly,

$$D^\alpha f(\mathbf{x}, \omega) = f(\mathbf{x}, \omega) \tag{2.20}$$

It is not difflcult to show that a random field can be decomposed into the sum of such eigenfunctions:

$$\psi(\mathbf{x}, \omega) = \sum_{m=-\infty}^{\infty} \phi_m(\mathbf{x}, \omega). \tag{2.21}$$

which is the counterpart of (2.11).

2.4 Homogeneous Gaussian Random Field and Spectral Representation

In what follows we assume that the random surface is a homogeneous Gaussian random field generated by the 2D Gaussian random measure. Therefore, the shift transformation $T^{\mathbf{x}}$ is defined with respect to the random measure (see Appendix). Let the homogeneous random surface $z = f(T^{\mathbf{x}}\omega)$ be given in the form of a spectral representation:

$$z = f(T^{\mathbf{x}}\omega) = \int_{R_2} e^{i\,\boldsymbol{\lambda}\cdot\,\mathbf{x}} F(\boldsymbol{\lambda})\, dB(\boldsymbol{\lambda}, \omega), \quad \omega \in \Omega, \quad \mathbf{x} \in R_2 \tag{2.22}$$

$$\overline{F(\boldsymbol{\lambda})} = F(-\boldsymbol{\lambda}) \tag{2.23}$$

where $dB(\boldsymbol{\lambda}, \omega)$ is a 2D complex Gaussian random measure, and f is real-valued owing to (2.23) and (A.17). As easily demonstrated, the random surface has zero mean, $\langle f(T^{\mathbf{x}}\omega)\rangle = 0$, and the correlation function

$$R(\mathbf{x}) = \left\langle \overline{f(\omega)} f(T^{\mathbf{x}}\omega) \right\rangle = \int_{R_2} e^{i\,\boldsymbol{\lambda}\cdot\,\mathbf{x}} |F(\boldsymbol{\lambda})|^2 d\boldsymbol{\lambda}, \quad \boldsymbol{\lambda} \in R_2 \tag{2.24}$$

$$\sigma^2 \equiv R(0) = \int_{R_2} |F(\boldsymbol{\lambda})|^2 d\boldsymbol{\lambda} \tag{2.25}$$

where $|F(\boldsymbol{\lambda})|^2$ gives the spectral density (power spectrum) of the random surface, and σ^2 denote the variance, a parameter describing the surface roughness; $\sigma^2 = 0$ corresponds to a flat surface.

If the random field is homogeneous and isotropic, that is, if (2.22) is D^α -invariant according to (2.20), then using (A.20)

$$\begin{aligned} D^\alpha f(T^{\mathbf{x}}\omega) &= \int_{R_2} e^{i\boldsymbol{\lambda}\cdot_{g_\alpha}\mathbf{x}} F(\boldsymbol{\lambda}) dB(\boldsymbol{\lambda}, T^{-\alpha}\omega) \\ &= \int_{R_2} e^{i\boldsymbol{\lambda}\cdot\mathbf{x}} F(g_\alpha\boldsymbol{\lambda}) dB(\boldsymbol{\lambda}, \omega) \end{aligned} \tag{2.26}$$

so that we have

$$F(g_\alpha\,\boldsymbol{\lambda}) = F(\boldsymbol{\lambda}), \qquad g_\alpha \in G_2 \tag{2.27}$$

and can put $F(\boldsymbol{\lambda}) = F(\lambda)$, $\lambda \equiv |\boldsymbol{\lambda}| = \sqrt{\lambda_x^2 + \lambda_y^2}$. Then, the spectral representation (2.24) is transformed into

$$R(\rho) = 2\pi \int_0^\infty J_0(\lambda\rho)|F(\lambda)|^2 \lambda d\lambda, \quad 0 \le \rho < \infty \tag{2.28}$$

where $J_0(z)$ denotes the Bessel function, and $\rho \equiv |\mathbf{x}| = \sqrt{x^2 + y^2}$. Thus, the correlation function and the spectral density are both isotropic. One of such examples is a Gaussian correlation function, the spectrum of which is also in Gaussian form:

$$R(\rho) = \sigma^2 e^{-\rho^2/(4l^2)}, \quad |F(\lambda)|^2 = \sigma^2 \frac{l^2}{\pi} e^{-l^2\lambda^2} \tag{2.29}$$

where l gives the correlation length and $\sigma^2 = R(0)$ the variance.

3. Form of the Stochastic Wave Field for Plane Wave Incidence

3.1 Coordinates and Wave Vectors

We represent the 3D position vector $\mathbf{r} = (\mathbf{x}, z) = (x, y, z)$ in the polar and cylindrical coordinate system, respectively:

$$\mathbf{r} = (r, \theta, \varphi)_{pol} = (\mathbf{x}, z)_{cyl} \tag{3.1}$$

$$\mathbf{x} = (\rho, \varphi)_{cyl}, \quad \rho = r\sin\theta, \quad z = r\cos\theta \tag{3.2}$$

Similarly, let the 3D wave vector $\mathbf{k}$ be represented as

$$\mathbf{k} = (k, \alpha, \beta)_{pol} = (\boldsymbol{\lambda}, S(\boldsymbol{\lambda}))_{cyl} \tag{3.3}$$

$$\boldsymbol{\lambda} = (\lambda_x, \lambda_y) = (\lambda, \beta)_{cyl} \tag{3.4}$$

where k is the wave number and

$$\lambda = k\sin\alpha \tag{3.5}$$

$$S(\boldsymbol{\lambda}) \equiv \sqrt{k^2 - \boldsymbol{\lambda}^2} = k\cos\alpha \tag{3.6}$$

The branch of $S(\boldsymbol{\lambda})$ is taken as $argS = 0\,,\ k^2 > \boldsymbol{\lambda}^2\,;\ argS = \pi/2\,,$ $k^2 < \boldsymbol{\lambda}^2\,.$

Now let $\mathbf{k}_0$ and $\mathbf{k}_0'$ be the wave vectors of the incident and the specularly reflected plane wave, respectively, and we write the wave vectors,

$$\begin{aligned} \mathbf{k}_0 &= (k, \pi - \theta_0, \varphi_0)_{pol} = (\boldsymbol{\lambda}_0, -S(\boldsymbol{\lambda}_0))_{cyl}, \quad \text{(incidence)} \\ \mathbf{k}_0' &= (k, \theta_0, \varphi_0)_{pol} = (\boldsymbol{\lambda}_0, S(\boldsymbol{\lambda}_0))_{cyl}, \quad \text{(reflection)} \\ \boldsymbol{\lambda}_0 &= (k \sin\theta_0, \varphi_0)_{cyl} \end{aligned} \tag{3.7}$$

where θ_0 denotes the incident angle and φ_0 the azimuth angle, as shown in Fig. 3.1.

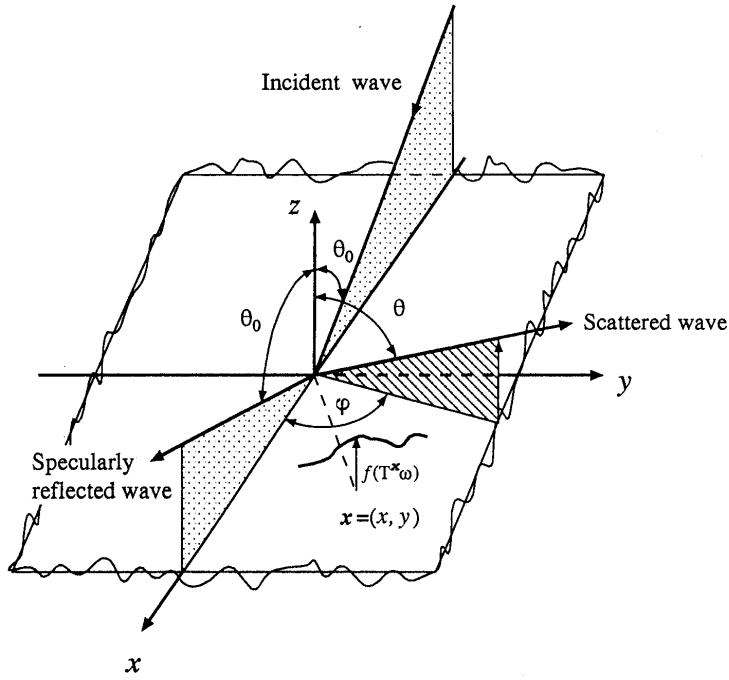

Figure 3.1. Plane wave incident on a random plane. $(\theta_0, 0)$ **: the angle of incidence,** (θ, ϕ) **: the scattering angle.**

3.2 Stochastic Floquet Theorem for Plane Wave Incidence

When a plane wave with the wave vector $\mathbf{k}_0$ is incident on the 2D random surface, we write the wave field as $\psi(\mathbf{x}, z; \omega | \boldsymbol{\lambda}_0)$, which

satisfies the wave equation:

$$(\boldsymbol{\nabla}^2 + k^2)\psi(\mathbf{x}, z, \omega|\,\boldsymbol{\lambda}_0) = 0, \qquad z > f(T^{\mathbf{x}}\omega), \mathbf{x} \in R_2 \tag{3.8}$$

in the upper half space above the random surface, where $\boldsymbol{\nabla}^2$ denote the 3D Laplacian. We assume that ψ satisfies either of the two boundary conditions on the random surface:

$$\psi(\mathbf{x}, z; \omega|\,\boldsymbol{\lambda}_0) = 0, z = f(T^{\mathbf{x}}\omega) \quad \text{(Dirichlet)} \tag{3.9}$$

$$\frac{\partial\psi(\mathbf{x}, z; \omega|\,\boldsymbol{\lambda}_0)}{\partial n} = 0, z = f(T^{\mathbf{x}}\omega) \quad \text{(Neumann)} \tag{3.10}$$

as well as the radiation condition in the far region ($z \to \infty$). In (3.10) $\partial\psi/\partial n \equiv \mathbf{n}\cdot\boldsymbol{\nabla}\psi$ implies the normal derivative relative to the normal vector of the random surface:

$$\mathbf{n} = \frac{\boldsymbol{\nabla} f - \mathbf{e}_z}{(|\,\boldsymbol{\nabla} f|^2 + 1)^{1/2}} \tag{3.11}$$

where $\mathbf{e}_z$ denotes the unit vector along the z-axis.

Now we consider the form of the stochastic wave field in the case of plane wave incidence. Let the primary (unperturbed) field be written

$$\psi_\iota(\mathbf{x}, z|\,\boldsymbol{\lambda}_0) = e^{i\,\boldsymbol{\lambda}_0\cdot\mathbf{x}}\left[e^{-iS(\boldsymbol{\lambda}_0)z} \mp e^{iS(\boldsymbol{\lambda}_0)z}\right], \qquad \iota = D, N \tag{3.12}$$

where $\mp$ corresponds to the Dirichlet or Neumann condition on the flat surface $z = 0$. First of all we note that the boundary condition on the random surface is $D^{\mathbf{a}}$-invariant and that the Laplacian commutes with the operator $D^{\mathbf{a}}, \mathbf{a} \in R_2$. Therefore, if a random function $\psi(\mathbf{x}, z; \omega)$ is a solution of the wave equation, $D^{\mathbf{a}}\psi(\mathbf{x}, z; \omega)$ is also a solution. The primary wave (3.12) composed of the incident and reflected plane is an eigenfunction of the operator $D^{\mathbf{a}}$ with the eigenvalue $e^{i\,\boldsymbol{\lambda}_0\cdot\mathbf{a}}$; that is,

$$D^{\mathbf{a}}\psi_\iota(\mathbf{x}, z|\,\boldsymbol{\lambda}_0) = e^{i\,\boldsymbol{\lambda}_0\cdot\mathbf{a}}\psi_\iota(\mathbf{x}, z|\,\boldsymbol{\lambda}_0), \qquad \iota = D, N \tag{3.13}$$

Thus, the scattered wave field as well as the total wave field also has to be an eigenfunction with the same eigenvalue, that is,

$$D^{\mathbf{a}}\psi(\mathbf{x}, z; \omega|\,\boldsymbol{\lambda}_0) = \psi(\mathbf{x} + \mathbf{a}, z; T^{\mathbf{a}}\omega|\,\boldsymbol{\lambda}_0) = e^{i\,\boldsymbol{\lambda}_0\cdot\mathbf{a}}\psi(\mathbf{x}, z; \omega|\,\boldsymbol{\lambda}_0) \tag{3.14}$$

Therefore, in view of (2.8) and (2.10), the wave field for the incident plane wave with the wave vector (3.7) can be written in the form:

$$\psi(\mathbf{x}, z; \omega | \boldsymbol{\lambda}_0) = e^{i \boldsymbol{\lambda}_0 \cdot \mathbf{x}} \left[e^{-iS(\boldsymbol{\lambda}_0) z} \mp e^{iS(\boldsymbol{\lambda}_0) z} \mp U(T^{\mathbf{x}} \omega, z | \boldsymbol{\lambda}_0) \right] \tag{3.15}$$

$$\psi_s(\mathbf{x}, z; \omega | \boldsymbol{\lambda}_0) \equiv \mp e^{i \boldsymbol{\lambda}_0 \cdot \mathbf{x}} U(T^{\mathbf{x}} \omega, z | \boldsymbol{\lambda}_0) \tag{3.16}$$

where ψ_s, denotes the scattered wave due to the surface roughness. This form of solution is the stochastic analogue of the "Floquet theorem" for a homogeneous random surface: that is, it is the product of an exponential function and a $D^{\mathbf{a}}$-invariant homogeneous random field in [ ]. The "stochastic Floquet theorem" (3.15) is generally valid for complex $\boldsymbol{\lambda}_0$, when the primary wave is evanescent. The first and the second terms in [ ] give the primary wave field for the flat surface ($\sigma^2 = 0$), and the third term U gives the scattered wave field due to the roughness ($\sigma^2 > 0$); we take $-$ sign for Dirichlet and $+$ sign for Neumann condition, for convenience.

3.3 Wiener-Itô Expansion of Wave Field

Since the random surface is given by (2.22), the scattered wave field can be regarded as a nonlinear stochastic functional of the Gaussian random measure, and the homogeneous random field $U(T^{\mathbf{x}} \omega, z | \boldsymbol{\lambda}_0)$ can be expressed by a Wiener-Itô expansion as in (A.46), which we write in the form,

$$U(T^{\mathbf{x}} \omega, z | \boldsymbol{\lambda}_0) = \sum_{n=0}^{\infty} U_n(T^{\mathbf{x}} \omega, z | \boldsymbol{\lambda}_0) \tag{3.17}$$

$$\begin{aligned} U_n(T^{\mathbf{x}} \omega, z | \boldsymbol{\lambda}_0) \equiv & \int \cdots \int_{R_2} e^{i(\boldsymbol{\lambda}_1 + \cdots + \boldsymbol{\lambda}_n) \cdot \mathbf{x} + iS(\boldsymbol{\lambda}_0 + \cdots + \boldsymbol{\lambda}_n) z} \\ & \times A_n(\boldsymbol{\lambda}_1, \cdots, \boldsymbol{\lambda}_n | \boldsymbol{\lambda}_0) \hat{h}_n[dB(\boldsymbol{\lambda}_1), \cdots, dB(\boldsymbol{\lambda}_n)], \\ & n = 0, 1, 2, \cdots \end{aligned} \tag{3.18}$$

where $A_n(\boldsymbol{\lambda}_1, \cdots, \boldsymbol{\lambda}_n | \boldsymbol{\lambda}_0)$ denotes the n-th order Wiener kernel which is symmetric with respect to n variables $(\boldsymbol{\lambda}_1, \cdots, \boldsymbol{\lambda}_n)$. We note here that $e^{i \boldsymbol{\lambda}_0 \cdot \mathbf{x}} U_n$, $n = 1, 2, \cdots$, satisfies the wave equation (3.8) termwise, and that U_n's in (3.17) are orthogonal to each other

in the sense of (A.27): that is,

$$\begin{aligned}\left\langle \overline{U_n} U_m \right\rangle =& \delta_{nm} n! \int \cdots \int_{R_2} e^{-2ImS(\boldsymbol{\lambda}_0+\boldsymbol{\lambda}_1+\cdots+\boldsymbol{\lambda}_n)z} \\ & |A_n(\boldsymbol{\lambda}_1, \cdots, \boldsymbol{\lambda}_n|\boldsymbol{\lambda}_0)|^2 d\boldsymbol{\lambda}_1 \cdots d\boldsymbol{\lambda}_n \\ & n, m = 0, 1, 2, \cdots\end{aligned} \tag{3.19}$$

3.4 Isotropy

Next we consider the case when the homogeneous random surface is isotropic, that is, it is invariant under the rotation operator D^α. Since the Laplacian operator is D^α-invariant as well as the boundary condition, $D^\alpha \psi(\mathbf{x}, z; \omega|\, \boldsymbol{\lambda}_0)$ is a solution to the wave equation (3.8). Using (3.14) and (2.18) it is easily shown that

$$D^{\mathbf{a}} D^\alpha \psi(\mathbf{x}, z; \omega|\, \boldsymbol{\lambda}_0) = e^{i\, \boldsymbol{\lambda}_0 \cdot g_\alpha \mathbf{a}} D^\alpha \psi(\mathbf{x}, z; \omega|\, \boldsymbol{\lambda}_0) \tag{3.20}$$

Therefore, comparing this with (3.15), we see that

$$D^{-\alpha} \psi(\mathbf{x}, z; \omega|\, \boldsymbol{\lambda}_0) = \psi(\mathbf{x}, z; \omega| g_\alpha\, \boldsymbol{\lambda}_0) \tag{3.21}$$

which means that, when the random surface is homogeneous and isotropic, a solution for any azumuth direction of incidence with $\boldsymbol{\lambda}' = g_{-\alpha}\, \boldsymbol{\lambda}_0$ can be obtained by operating D^α on the solution for a fixed $\boldsymbol{\lambda}_0$. Furthermore, using (3.21), (A.42) and (3.18), we can show the symmetric property of Wiener kernels:

$$A_n(g_\alpha\, \boldsymbol{\lambda}_1, \cdots, g_\alpha\, \boldsymbol{\lambda}_n | g_\alpha\, \boldsymbol{\lambda}_0) = A_n(\boldsymbol{\lambda}_1, \cdots, \boldsymbol{\lambda}_n|\, \boldsymbol{\lambda}_0) \tag{3.22}$$

$$g_\alpha \in G_2$$

3.5 Reciprocity

Let the two solutions for different incident angles be $\psi_1 = \psi(\mathbf{x}, z; \omega|\, \boldsymbol{\lambda}_0)$ and $\psi_2 = \psi(\mathbf{x}, z; \omega|\, \boldsymbol{\lambda}_0')$. Integrating the equality $\boldsymbol{\nabla} \cdot [\psi_1 \boldsymbol{\nabla} \psi_2 - \psi_2 \boldsymbol{\nabla} \psi_1]/k = 0$ over the cylindrical volume placed on the random surface (Fig. 4.1), we obtain the equality

$$\frac{1}{k} \int_{S_t + S_c} \left[\psi_1 \frac{\partial \psi_2}{\partial n} - \psi_2 \frac{\partial \psi_1}{\partial n} \right] dS = 0 \tag{3.23}$$

for almost all ω, where S_t stands for the top surface of the cylinder at the height z with radius ρ, and S_c the cylindrical surface. The contribution to the integral from the bottom surface vanishes due to the boundary condition (3.9) or (3.10). Since the top area and the side area are proportional to ρ^2 and ρ, respectively, we obtain the following equality for almost all ω,

$$\lim_{\rho\to\infty} \frac{1}{\pi\rho^2 k} \int_{S_t} \left[\psi_1 \frac{\partial \psi_2}{\partial z} - \psi_2 \frac{\partial \psi_1}{\partial z} \right] d\mathbf{x} = 0 \tag{3.24}$$

where $\pi\rho^2$ is the area of S_t. Using this equality we can obtain the following reciprocal relation for the Wiener kernels:

$$A_0(\boldsymbol{\lambda}_0) = A_0(-\boldsymbol{\lambda}_0) \tag{3.25}$$

$$a_1(\boldsymbol{\lambda}_1|\boldsymbol{\lambda}_0) = a_1(\boldsymbol{\lambda}_1| - \boldsymbol{\lambda}_0 - \boldsymbol{\lambda}_1) \tag{3.26}$$

$$a_n(\boldsymbol{\lambda}_1, \cdots, \boldsymbol{\lambda}_n|\boldsymbol{\lambda}_0) = a_n(\boldsymbol{\lambda}_1, \cdots, \boldsymbol{\lambda}_n|-\boldsymbol{\lambda}) \tag{3.27}$$

$$\boldsymbol{\lambda} \equiv \boldsymbol{\lambda}_0 + \boldsymbol{\lambda}_1 + \cdots + \boldsymbol{\lambda}_n, \tag{3.28}$$

$$n = 1, 2, \cdots$$

where $A_n, n \geq 1$ can be put in the form

$$A_n(\boldsymbol{\lambda}_1, \cdots, \boldsymbol{\lambda}_n|\boldsymbol{\lambda}_0 \equiv S(\boldsymbol{\lambda}_0) a_n(\boldsymbol{\lambda}_1, \cdots, \boldsymbol{\lambda}_n|\boldsymbol{\lambda}_0), \tag{3.29}$$

$$n = 1, 2, \cdots$$

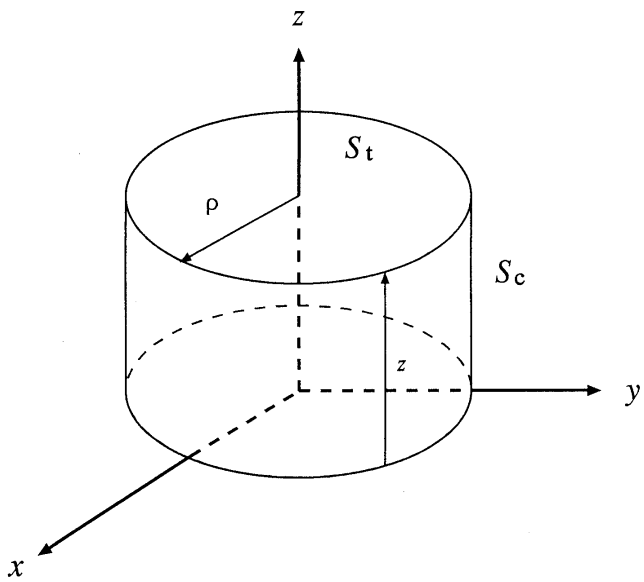

Figure 4.1. Cylindrical surface for divergence theorem.

The outline for the derivation of above reciprocal relations is as follows: We substitute into (3.24) the Weiner-Itô expansions (3.15)-(3.18) for $\psi_1 = \psi(\mathbf{x}, z; \omega | \boldsymbol{\lambda}_0)$ and $\psi_2 = \psi(\mathbf{x}, z; \omega | \boldsymbol{\lambda}'_0)$. Then we obtain the sum of terms $[\ \ ]_{mn} = [\psi_1]_m[\psi_{2z}]_n - [\psi_{1z}]_m[\psi_2]_n, m, n = 0, 1, 2, \cdots$, which consist of the product of m- and n-tuple Wiener integrals, $[\ \ ]_n$, indicating the component in $L^2_n[\Omega]$. The termwise integration with respect to $\mathbf{x}$ gives nonvanishing terms when $\boldsymbol{\lambda}_0 + \boldsymbol{\lambda}_1 + \cdots + \boldsymbol{\lambda}_m + \boldsymbol{\lambda}'_0 + \boldsymbol{\lambda}'_1 + \cdots + \boldsymbol{\lambda}'_n = 0$ is satisfied. We find that all terms of the form $[\ \ ]_{mn} + [\ \ ]_{nm}$ with $m \geq 1$ and $n \geq 1$, vanish identically, that the term $[\ \ ]_{00}$ yields the recirocity (3.25) for A_0, and that the term $[\ \ ]_{0n} + [\ \ ]_{n0}$, by virtue of the orthogonality of Wiener-Hermite differentials, gives the equality:

$$S(\boldsymbol{\lambda}_0)A_n(\boldsymbol{\lambda}_1, \cdots, \boldsymbol{\lambda}_n | \boldsymbol{\lambda}'_0) - S(\boldsymbol{\lambda}'_0)A_n(\boldsymbol{\lambda}_1, \cdots, \boldsymbol{\lambda}_n | \boldsymbol{\lambda}_0) = 0 \quad (3.30)$$

$$\boldsymbol{\lambda}'_0 + \boldsymbol{\lambda}_0 + \boldsymbol{\lambda}_1 + \cdots \boldsymbol{\lambda}_n = 0 \quad (3.31)$$

which implies the reciprocity (3.27) for A_n.

We note here that the reciprocity does hold for $\boldsymbol{\lambda}'_0 = -\boldsymbol{\lambda} \equiv -(\boldsymbol{\lambda}_0 + \cdots + \boldsymbol{\lambda}_n)$, where, in view of (3.18), $\boldsymbol{\lambda}$ gives the scattering direction of partial waves for the incident direction $\boldsymbol{\lambda}_0$. The reciprocal relation (3.27) implies that the partial wave amplitude for the scattering process $\{\boldsymbol{\lambda}_0 \to \boldsymbol{\lambda}\}$ equals that of $\{-\boldsymbol{\lambda} \to -\boldsymbol{\lambda}_0\}$, where $-\boldsymbol{\lambda}$ gives the reciprocal incident direction, and $-\boldsymbol{\lambda}_0$ the scattering direction.

4. Statistical Quantities of the Scattered Wave Field

The stochastic wave field $\psi(\mathbf{x}, z; \omega | \boldsymbol{\lambda}_0)$ is expressed by (3.15)–(3.18) in terms of the Wiener kernels A_n's and the random measure. Therefore, once the kernels are obtained, we can even draw a spatial realization of the stochastic wave field corresponding to a given realization of the random surface. However, various statistical quantities of the random wave field can be easily calculated by means of averaging procedure as follows.

4.1 Coherent Scattering Amplitude

By taking the average of (3.15) using (3.17) and (A.10), we obtain the coherent field

$$\langle \psi(\mathbf{x}, z; \omega | \boldsymbol{\lambda}_0) \rangle = e^{i \boldsymbol{\lambda}_0 \cdot \mathbf{x}} \left[e^{-iS(\boldsymbol{\lambda}_0)z} \mp (1 + A_0(\boldsymbol{\lambda}_0)) e^{iS(\boldsymbol{\lambda}_0)z} \right] \quad (4.1)$$

where the constant $A_0(\boldsymbol{\lambda}_0)$ is the 0-th order Wiener kernel. Apparently the coherent scattering takes place into the direction of specular reflection, and $(1 + A_0)$ is the reflection coefficient of the random surface.

4.2 Power Flow Conservation and Optical Theorem

Putting $\psi_1 = \overline{\psi}$ and $\psi_2 = \psi$ in (3.24), we obtain the following equality for all realizations of the random surface;

$$\lim_{\rho \to \infty} \frac{1}{\pi \rho^2 k} \int_{S_t} \mathrm{Im} \left[\overline{\psi} \frac{\partial \psi}{\partial z} \right] d\mathbf{x} = 0 \quad (4.2)$$

where $\pi \rho^2$ is the area of S_t. At this point we note that the power flow $\mathrm{Im}[\overline{\psi} \partial \psi / \partial z]$ is a $D^{\mathbf{a}}$-invariant homogeneous random field, and that the lefthand member of (4.2) which is a spatial average over R_2 is invariant under the shift $T^{\mathbf{a}}$. Therefore, by the ergodicity of $T^{\mathbf{a}}$, it equals a constant for almost all ω, and hence equals its average. Thus we obtain the equality,

$$\frac{1}{k} \left\langle \mathrm{Im} \left[\overline{\psi} \frac{\partial \psi}{\partial z} \right] \right\rangle = 0 \quad (4.3)$$

which is the power-flow conservation law for random surface scattering.

Substituting (3.15)–(3.18) into (4.3) we obtain the power conservation formula in terms of A_n's;

$$\begin{aligned} \frac{S(\boldsymbol{\lambda}_0)}{k} =& \frac{S(\boldsymbol{\lambda}_0)}{k} |1 + A_0(\boldsymbol{\lambda}_0)|^2 \\ &+ \frac{1}{k} \sum_{n=1}^{\infty} n! \int \cdots \int_{(\boldsymbol{\lambda}_0 + \boldsymbol{\lambda}_1 + \cdots + \boldsymbol{\lambda}_n)^2 < k^2} S(\boldsymbol{\lambda}_0 + \boldsymbol{\lambda}_1 + \cdots + \boldsymbol{\lambda}_n) \\ &\qquad \times |A_n(\boldsymbol{\lambda}_1, \cdots, \boldsymbol{\lambda}_n | \boldsymbol{\lambda}_0)|^2 d\boldsymbol{\lambda}_1 \cdots d\boldsymbol{\lambda}_n \end{aligned} \quad (4.4)$$

The left member is the incident power falling on a unit area, whereas the first term on the righthand side is the coherently reflected power P_c and the second terms consisting of the sum of integrals gives the incoherently scattered power from a unit area.

The power conservation formula (4.4) can be cast into the form of the optical theorem:

$$-\frac{2S(\boldsymbol{\lambda}_0)}{k} Re A_0(\boldsymbol{\lambda}_0) = p_c + P_{ic} \tag{4.5}$$

$$p_c \equiv \frac{S(\boldsymbol{\lambda}_0)}{k} |A_0(\boldsymbol{\lambda}_0)|^2 \tag{4.6}$$

$$\begin{aligned} P_{ic} \equiv & \frac{1}{k} \sum_{n=1}^{\infty} n! \int \cdots \int_{(\boldsymbol{\lambda}_0+\boldsymbol{\lambda}_1+\cdots+\boldsymbol{\lambda}_n)^2<k^2} S(\boldsymbol{\lambda}_0 + \boldsymbol{\lambda}_1 + \cdots + \boldsymbol{\lambda}_n) \\ & \times |A_n(\boldsymbol{\lambda}_1, \cdots, \boldsymbol{\lambda}_n | \boldsymbol{\lambda}_0)|^2 d\boldsymbol{\lambda}_1 \cdots d\boldsymbol{\lambda}_n \end{aligned} \tag{4.7}$$

where p_c and P_{ic} respectively, give the coherently and incoherently scattered power due to the surface roughness. The optical theorem (4.5) implies that -Re A_0 , a decrease in the reflection coefficient, gives the scattered power $p_c + P_{ic}$. The power conservation formula or the optical theorem can be used as a measure to estimate the accuracy of the approximate solution.

4.3 Angular Distribution of Incoherent Scattering

The incident plane wave is scattered into various directions. By $P(\boldsymbol{\theta} \,|\, \boldsymbol{\theta}_0)$ we denote the angular distribution of the incoherent scattering, that is, the average power scattered incoherently from unit surface area into unit solid angle of the direction $\boldsymbol{\theta} = (\theta, \varphi)_{pol}$ when the angle of incidence is $\boldsymbol{\theta}_0 = (\theta_0, \varphi_0)_{pol}$. Since P_{ic} which is the second term in (4.4) describes the incoherent power flow in the z direction per unit area, it equals the integral of $P(\boldsymbol{\theta} \,|\, \boldsymbol{\theta}_0)$ over 2π steradians:

$$\begin{aligned} P_{ic} = & \int_{2\pi} P(\boldsymbol{\theta}|\boldsymbol{\theta}_0) d\boldsymbol{\theta} \\ = & \frac{1}{k} \sum_{n=1}^{\infty} n! \int \cdots \int_{(\boldsymbol{\lambda}_0+\boldsymbol{\lambda}_1+\cdots+\boldsymbol{\lambda}_n)^2<k^2} S(\boldsymbol{\lambda}_0 + \boldsymbol{\lambda}_1 + \cdots + \boldsymbol{\lambda}_n) \\ & \times |A_n(\boldsymbol{\lambda}_1, \cdots \boldsymbol{\lambda}_n | \boldsymbol{\lambda}_0)|^2 d\boldsymbol{\lambda}_1 \cdots d\boldsymbol{\lambda}_n \end{aligned} \tag{4.8}$$

where $d\boldsymbol{\theta} \equiv \sin\theta d\theta d\phi$ and $A_n \equiv S(\boldsymbol{\lambda}_0)a_n$ by (3.29). The vector $\boldsymbol{\lambda} = \boldsymbol{\lambda}_0 + \boldsymbol{\lambda}_1 + \cdots + \boldsymbol{\lambda}_n = (k\sin\theta, \varphi)_{cyl}$ can be interpreted as a scattering vector. Therefore, putting $d\boldsymbol{\lambda} = \lambda d\lambda d\phi = k^2 \cos\theta d\boldsymbol{\theta}$, $S(\boldsymbol{\lambda}) \equiv k\cos\theta$ and $\boldsymbol{\lambda}_0 = (k\sin\theta_0, \varphi_0)_{cyl}$ we obtain

$$\begin{aligned} P(\boldsymbol{\theta}|\boldsymbol{\theta}_0) =& \sum_{n=1}^{\infty} P_n(\boldsymbol{\theta}|\boldsymbol{\theta}_0) \\ =& k^4 \cos^2\theta \cos^2\theta_0 \\ & \left[|a_1(\boldsymbol{\lambda} - \boldsymbol{\lambda}_0|\boldsymbol{\lambda}_0)|^2 + 2! \int_{R^2} |a_2(\boldsymbol{\lambda} - \boldsymbol{\lambda}_0 - \boldsymbol{\lambda}_2, \boldsymbol{\lambda}_2|\boldsymbol{\lambda}_0)|^2 d\boldsymbol{\lambda}_2 + \cdots \right] \end{aligned} \tag{4.9}$$

where $P_n(\boldsymbol{\theta}\,|\,\boldsymbol{\theta}_0)$ represents the contribution from A_n. $\boldsymbol{\lambda} - \boldsymbol{\lambda}_0$ is a Bragg vector of the random surface scattering. As mentioned earlier, the reciprocal relation (3.28) for a_n holds when the boundary condition (3.9) or (3.10) is satisfied, and the partial wave amplitude of the scattering process $\{\boldsymbol{\lambda}_0 \to \boldsymbol{\lambda}\}$ equals to that of the reciprocal scattering process $\{-\boldsymbol{\lambda} \to -\boldsymbol{\lambda}_0\}$ (c.f. Fig. 6.8(a)). Therefore, it follows from (4.9) and (3.27) that $P(\boldsymbol{\theta}\,|\,\boldsymbol{\theta}_0)$ has the reciprocity also:

$$P(\boldsymbol{\theta}\,|\,\boldsymbol{\theta}_0) = P(\boldsymbol{\theta}_0|\,\boldsymbol{\theta}) \tag{4.10}$$

$4\pi P(\boldsymbol{\theta}\,|\,\boldsymbol{\theta}_0)$ is called the scattering cross section per unit area. If the angular distribution of incoherent scattering is observed with a lens or a parabola with a fixed aperture which is directed toward the scattering surface at an angle θ, the observed scattering area is then increased by a factor $1/\cos\theta$. Therefore, the angular distribution $S(\boldsymbol{\theta}\,|\,\boldsymbol{\theta}_0)$, such as adopted in [14,13], is related to $P(\boldsymbol{\theta}\,|\,\boldsymbol{\theta}_0)$ by the equation,

$$S(\boldsymbol{\theta}\,|\,\boldsymbol{\theta}_0) = P(\boldsymbol{\theta}\,|\,\boldsymbol{\theta}_0)/\cos\theta \tag{4.11}$$

4.4 Power Flow of the Surface Wave

The surface wave part $\psi_{sf}(\mathbf{x}, z; \omega)$ of the scattered field obviously comes from the integrals of (3.18) over the regions such that $(\boldsymbol{\lambda}_0 + \boldsymbol{\lambda}_1 + \cdots + \boldsymbol{\lambda}_n)^2 > k^2$. Its average power $\mathbf{P}_{sf}(z)$ along the surface at

the height z, though neglected in (4.8), can be written

$$\begin{aligned}\mathbf{P}_{sf}(z) =& \frac{1}{k}\sum_{n=1}^{\infty} n! \int\cdots\int_{(\boldsymbol{\lambda}_0+\boldsymbol{\lambda}_1+\cdots+\boldsymbol{\lambda}_n)^2>k^2} (\boldsymbol{\lambda}_0+\boldsymbol{\lambda}_1+\cdots+\boldsymbol{\lambda}_n) \\ & \times |A_n(\boldsymbol{\lambda}_1,\cdots,\boldsymbol{\lambda}_n|\boldsymbol{\lambda}_0)|^2 \\ & \times \exp\left[-2z[(\boldsymbol{\lambda}_0+\boldsymbol{\lambda}_1+\cdots+\boldsymbol{\lambda}_n)^2-k^2)^{1/2}]\right] d\boldsymbol{\lambda}_1\cdots d\boldsymbol{\lambda}_n \end{aligned} \tag{4.12}$$

In the special case of interest when the random surface is homogeneous and isotropic such that the relation (3.22) does hold, we can show that the average power flow has the same direction with $\boldsymbol{\lambda}_0$. The power flow P_{sf} of surface wave along this direction per unit width is obtained by integrating $\mathbf{P}_{sf}(z)\cdot\boldsymbol{\lambda}_0/\lambda_0$ over $0\le z<\infty$:

$$P_{sf} = \int_{(\boldsymbol{\lambda}_0+\boldsymbol{\lambda})^2>k^2} \frac{(\boldsymbol{\lambda}_0+\boldsymbol{\lambda})\cdot\boldsymbol{\lambda}_0}{2k\lambda_0} \frac{|A_1(\boldsymbol{\lambda}\,|\,\boldsymbol{\lambda}_0)|^2}{[(\boldsymbol{\lambda}_0+\boldsymbol{\lambda})^2-k^2]^{1/2}} d\boldsymbol{\lambda} + \cdots \tag{4.13}$$

where higher terms can be written likewise.

5. Approximate Method of Solution

The foregoing argument is applicable to any homogeneous random surface. To obtain concrete solutions for the scattering problem here, we limit ourselves to the case of small roughness, where the Wiener-Itô functional calculus can be very effectively used as shown below. In the case of very rough surface, however, the boundary condition and the stochastic functional calculus has to be dealt with somewhat differently, which the authors intend to discuss elsewhere.

5.1 Effective Boundary Condition

We assume that the 2D random surface has small roughness relative to the wavelength and is smooth enough, namely, $k^2\langle f^2\rangle \ll 1$ and $\langle|\nabla f|^2\rangle \ll 1$. Then the boundary condition (3.9) and (3.10) can be expanded in terms of f and $\boldsymbol{\nabla} f$:

$$[\psi]_{z=f} = \left[\psi + f\frac{\partial\psi}{\partial z}\right]_{z=0} = 0 \qquad \text{(Dirichlet)} \tag{5.1}$$

$$-\frac{1}{kn_z}[\mathbf{n}\cdot\boldsymbol{\nabla}\psi]_{z=f} = \frac{1}{k}\left[\frac{\partial\psi}{\partial z} - (\boldsymbol{\nabla}f\cdot\boldsymbol{\nabla}\psi) + f\cdot\frac{\partial^2\psi}{\partial z^2}\right]_{z=0} = 0 \qquad \text{(Neumann)} \tag{5.2}$$

where we have kept the terms up to the first-order in f for simplicity. Although we are concernred with small roughness here, higher-order terms could be added if necessary. These simplified equations given in terms of the boundary values on $z = 0$ represent the effective boundary conditions for a slightly random surface, and we use them as the models of random boundary conditions in what follows.

5.2 Stochastic Functional Equation

To solve the boundary condition we can avail ourselves of the homogeneity of the random surface, or in other words, $D^{\mathbf{a}}$ transformation property (3.14). Inserting (3.15) into (5.1) and (5.2), the boundary conditions are rewritten

$$\left[U + f\left[2iS(\boldsymbol{\lambda}_0) + \frac{\partial U}{\partial z}\right]\right]_{z=0} = 0 \qquad \text{(Dirichlet)} \tag{5.3}$$

$$\left[\frac{\partial U}{\partial z} - \boldsymbol{\nabla}f\cdot[i\boldsymbol{\lambda}_0(2+U) + \boldsymbol{\nabla}U] + f\left[-2S^2(\boldsymbol{\lambda}_0) + \frac{\partial^2 U}{\partial z^2}\right]\right]_{z=0} = 0 \qquad \text{(Neumann)} \tag{5.4}$$

Since f, U, and their partial derivatives are all $D^{\mathbf{a}}$-invariant, the boundary condition over $\mathbf{x} \in R_2$ is reduced to the equation of $D^{\mathbf{a}}$-invariant random field, and consequently, can be regarded as a functional equation with $\mathbf{x}$ fixed at any point in R_2, say, $\mathbf{x} = 0$. Thus, the boundary condition turns into an equation for a stochastic functional where the coordinate parameter $\mathbf{x}$ is suppressed. This is one of advantages of the stochastic Floquet theorem (3.15). Then, invoking the Wiener-Itô expansion (3.17) and (3.18), we can manipulate the stochastic functional equation in a systematic manner. Though the procedure bears some similarity to the Rayleigh-Rice method [5], the decomposition of the functional equation into a hierachy of function equations is made by means of the Wiener functional calculus instead of the perturbation method.

5.3 Dirichlet Condition

Let us insert (2.22) and (3.15)–(3.18) into the boundary condition (5.1) or (5.3), and set $z = 0$ and $\mathbf{x} = 0$. Denoting by U_n the n-th orthogonal component of U, we should note that the product of f and $U_n (n \geq 1)$ can be split into $(n+1)-$ and $(n-1)-$tuple Wiener integrals by means of the recurrence formula (A.33): that is, it is written in the following form,

$$\left[f \frac{\partial U_n}{\partial z} \right]_{z=0,\mathbf{x}=0} = \int \tilde{K}_{n+1}(\boldsymbol{\lambda}_1, \cdots \boldsymbol{\lambda}_{n+1}) \hat{h}_{n+1}[dB(\boldsymbol{\lambda}_1), \cdots, dB(\boldsymbol{\lambda}_{n+1})] + n \int \tilde{L}_{n-1}(\boldsymbol{\lambda}_1, \cdots, \boldsymbol{\lambda}_{n-1}) \hat{h}_{n-1}[dB(\boldsymbol{\lambda}_1), \cdots, dB(\boldsymbol{\lambda}_{n-1})] \tag{5.5}$$

where the symmetrized kernels $\tilde{K}_{n+1}$ and $\tilde{L}_{n-1}$ are, according to (A.35), (A.36) and (2.23), given by

$$\tilde{K}_{n+1}(\boldsymbol{\lambda}_1, \cdots \boldsymbol{\lambda}_{n+1}) \equiv \frac{i}{n+1} \sum_{k=1}^{n+1} F(\boldsymbol{\lambda}_k) S(\boldsymbol{\lambda}_0 + \cdots + \boldsymbol{\lambda}_{k-1} + \boldsymbol{\lambda}_{k+1} + \cdots + \boldsymbol{\lambda}_{n+1}) \times A_n(\boldsymbol{\lambda}_1, \cdots, \boldsymbol{\lambda}_{k-1}, \boldsymbol{\lambda}_{k+1}, \cdots \boldsymbol{\lambda}_{n+1} | \boldsymbol{\lambda}_0) d\boldsymbol{\lambda}_k \tag{5.6}$$

$$\tilde{L}_{n-1}(\boldsymbol{\lambda}_1, \cdots, \boldsymbol{\lambda}_{n-1}) \equiv i \int_{E_2} \overline{F(\boldsymbol{\lambda}_n)} S(\boldsymbol{\lambda}_0 + \cdots + \boldsymbol{\lambda}_n) A_n(\boldsymbol{\lambda}_1, \cdots, \boldsymbol{\lambda}_n | \boldsymbol{\lambda}_0) d\boldsymbol{\lambda}_n \tag{5.7}$$

Then, making use of these relations the boundary condition (3.9), as a functional equation in $L^2[\Omega]$, can be decomposed into a set of equations in the orthogonal subspaces $L_n^2[\Omega], n = 0, 1, 2, \cdots$, which in turn yield a hierarchy of function equations for the Wiener kernels A_n's:

$(n = 0)$

$$A_0(\boldsymbol{\lambda}_0) + i \int_{R_2} S(\boldsymbol{\lambda}_0 + \boldsymbol{\lambda}) A_1(\boldsymbol{\lambda} | \boldsymbol{\lambda}_0) \overline{F(\boldsymbol{\lambda})} d\boldsymbol{\lambda} = 0 \tag{5.8}$$

$(n = 1)$

$$A_1(\boldsymbol{\lambda}|\boldsymbol{\lambda}_0) + iS(\boldsymbol{\lambda}_0)[2 + A_0(\boldsymbol{\lambda}_0)]F(\boldsymbol{\lambda}) + 2i \int_{R_2} S(\boldsymbol{\lambda}_0 + \boldsymbol{\lambda} + \boldsymbol{\lambda}_1) A_2(\boldsymbol{\lambda}, \boldsymbol{\lambda}_1 | \boldsymbol{\lambda}_0) \overline{F(\boldsymbol{\lambda}_1)} d\boldsymbol{\lambda}_1 = 0 \tag{5.9}$$

$(n = 2)$

$$
\begin{aligned}
&A_2(\boldsymbol{\lambda}_1, \boldsymbol{\lambda}_2|\boldsymbol{\lambda}_0) + \frac{i}{2} S(\boldsymbol{\lambda}_0 + \boldsymbol{\lambda}_1) A_1(\boldsymbol{\lambda}_1|\boldsymbol{\lambda}_0) F(\boldsymbol{\lambda}_2) \\
&\quad + \frac{i}{2} S(\boldsymbol{\lambda}_0 + \boldsymbol{\lambda}_2) A_1(\boldsymbol{\lambda}_2|\boldsymbol{\lambda}_0) F(\boldsymbol{\lambda}_1) \\
&\quad + 3i \int_{R_2} S(\boldsymbol{\lambda}_0 + \boldsymbol{\lambda}_1 + \boldsymbol{\lambda}_2 + \boldsymbol{\lambda}_3) A_3(\boldsymbol{\lambda}_1, \boldsymbol{\lambda}_2, \boldsymbol{\lambda}_3|\boldsymbol{\lambda}_0) \overline{F(\boldsymbol{\lambda}_3)} d\boldsymbol{\lambda}_3 = 0
\end{aligned}
\tag{5.10}
$$

$(n = 3)$

$$
\begin{aligned}
&A_3(\boldsymbol{\lambda}_1, \boldsymbol{\lambda}_2, \boldsymbol{\lambda}_3|\boldsymbol{\lambda}_0) + \frac{i}{3} S(\boldsymbol{\lambda}_0 + \boldsymbol{\lambda}_1 + \boldsymbol{\lambda}_2) A_2(\boldsymbol{\lambda}_1, \boldsymbol{\lambda}_2|\boldsymbol{\lambda}_0) F(\boldsymbol{\lambda}_3) \\
&\quad + \frac{i}{3} S(\boldsymbol{\lambda}_0 + \boldsymbol{\lambda}_1 + \boldsymbol{\lambda}_3) A_2(\boldsymbol{\lambda}_1, \boldsymbol{\lambda}_3|\boldsymbol{\lambda}_0) F(\boldsymbol{\lambda}_2) \\
&\quad + \frac{i}{3} S(\boldsymbol{\lambda}_0 + \boldsymbol{\lambda}_2 + \boldsymbol{\lambda}_3) A_2(\boldsymbol{\lambda}_2, \boldsymbol{\lambda}_3|\boldsymbol{\lambda}_0) F(\boldsymbol{\lambda}_1) \\
&\quad + 4i \int_{R_2} S(\boldsymbol{\lambda}_0 + \boldsymbol{\lambda}_1 + \boldsymbol{\lambda}_2 + \boldsymbol{\lambda}_3 + \boldsymbol{\lambda}_4) \\
&\qquad\qquad \times A_4(\boldsymbol{\lambda}_1, \boldsymbol{\lambda}_2, \boldsymbol{\lambda}_3, \boldsymbol{\lambda}_4|\boldsymbol{\lambda}_0) \overline{F(\boldsymbol{\lambda}_4)} d\boldsymbol{\lambda}_4 = 0
\end{aligned}
\tag{5.11}
$$

and so on. The equation (5.8) for $n = 0$ is just the average of (5.3). Higher-order equations $(n \geq 2)$ have self-similar structures as easily observed in (5.10) and (5.11). However, the equations (5.8)-(5.11) are almost sufficient for our purpose. Since $F(\boldsymbol{\lambda})$ is a function of the order of σ^1, these equation shows that A_0 and $A_n (n \geq 1)$ are at least of the order of σ^2 and σ^n, respectively. Therefore, we can solve these equations approximately by neglecting higher order functions for sufficiently small σ. Leaving the details of the method of solution until later, we first show the approximate solutions for A_0, A_1 and A_2 here, although A_3 and higher kernels are taken into consideration in the solution.

$$
A_0(\boldsymbol{\lambda}) \equiv S(\boldsymbol{\lambda}) a_o(\boldsymbol{\lambda}) = -\frac{2 Z_D(\boldsymbol{\lambda})}{1 + Z_D(\boldsymbol{\lambda})} \tag{5.12}
$$

$$
A_1(\boldsymbol{\lambda}_1|\boldsymbol{\lambda}) \equiv S(\boldsymbol{\lambda}) a_1(\boldsymbol{\lambda}_1|\boldsymbol{\lambda}) \tag{5.13}
$$

$$
A_2(\boldsymbol{\lambda}_1, \boldsymbol{\lambda}_2|\boldsymbol{\lambda}) \equiv S(\boldsymbol{\lambda}) a_2(\boldsymbol{\lambda}_1, \boldsymbol{\lambda}_2|\boldsymbol{\lambda}) \tag{5.14}
$$

$$
Z_D(\boldsymbol{\lambda}) \equiv S(\boldsymbol{\lambda}) \xi(\boldsymbol{\lambda}) \tag{5.15}
$$

where we have put

$$a_0(\boldsymbol{\lambda}) = -\frac{2\xi(\boldsymbol{\lambda})}{1+S(\boldsymbol{\lambda})\xi(\boldsymbol{\lambda})} \tag{5.16}$$

$$a_1(\boldsymbol{\lambda}_1|\boldsymbol{\lambda}) = \frac{-2iF(\boldsymbol{\lambda}_1)[1-\xi^*(\boldsymbol{\lambda}+\boldsymbol{\lambda}_1,\boldsymbol{\lambda})]}{[1+S(\boldsymbol{\lambda})\xi(\boldsymbol{\lambda})][1+S(\boldsymbol{\lambda}+\boldsymbol{\lambda}_1)\xi(\boldsymbol{\lambda}+\boldsymbol{\lambda}_1)]} \tag{5.17}$$

$$a_2(\boldsymbol{\lambda}_1,\boldsymbol{\lambda}_2|\boldsymbol{\lambda}) \simeq -\frac{i}{2}\frac{S(\boldsymbol{\lambda}+\boldsymbol{\lambda}_1)a_1(\boldsymbol{\lambda}_1|\boldsymbol{\lambda})F(\boldsymbol{\lambda}_2)+S(\boldsymbol{\lambda}+\boldsymbol{\lambda}_2)a_1(\boldsymbol{\lambda}_2|\boldsymbol{\lambda})F(\boldsymbol{\lambda}_1)}{1+S(\boldsymbol{\lambda}+\boldsymbol{\lambda}_1+\boldsymbol{\lambda}_2)\xi(\boldsymbol{\lambda}+\boldsymbol{\lambda}_1+\boldsymbol{\lambda}_2)} \tag{5.18}$$

and

$$\xi(\boldsymbol{\lambda}) \equiv \int_{R_2} \frac{S(\boldsymbol{\lambda}_1|F(\boldsymbol{\lambda}_1-\boldsymbol{\lambda})|^2}{1+S(\boldsymbol{\lambda}_1)\xi(\boldsymbol{\lambda}_1)}d\boldsymbol{\lambda}_1 \tag{5.19}$$

$$\simeq \int_{R_2} S(\boldsymbol{\lambda}_1)|F(\boldsymbol{\lambda}_1-\boldsymbol{\lambda})|^2 d\boldsymbol{\lambda}_1 \tag{5.20}$$

$$\xi^*(\boldsymbol{\lambda},\boldsymbol{\lambda}_0) \simeq \int_{R_2} S(\boldsymbol{\lambda}+\boldsymbol{\lambda}_1)S(\boldsymbol{\lambda}_0+\boldsymbol{\lambda}_1)|F(\boldsymbol{\lambda}_1)|^2 d\boldsymbol{\lambda}_1 \tag{5.21}$$

(5.19) is actually the dispersion equation for determining $\xi(\boldsymbol{\lambda})$, and (5.20) can be used for approximate evaluation since ξ is of the order of σ^2. Particularly, at $\boldsymbol{\lambda}=\mathbf{k}$, we note that

$$Z_D(\mathbf{k})=0, \qquad A_0(\mathbf{k})=0, \qquad A_n(\boldsymbol{\lambda}_1,\cdots,\boldsymbol{\lambda}_n|\mathbf{k})=0 \tag{5.22}$$

$$(n \geq 1)$$

First, we note that for $(k\sigma)^2 \ll 1$, (5.12) and (5.13) can be written, neglecting ξ^* and ξ in (5.16) and (5.17),

$$A_0^{(2)}(\boldsymbol{\lambda}) = -2S(\boldsymbol{\lambda})\xi(\boldsymbol{\lambda}) = -2Z_D(\boldsymbol{\lambda}) \tag{5.23}$$

$$A_1^{(1)}(\boldsymbol{\lambda}_1|\boldsymbol{\lambda}) = -2iS(\boldsymbol{\lambda})F(\boldsymbol{\lambda}_1) \tag{5.24}$$

which correspond to the second- and the first-order perturbation solution for A_0 and A_1, respectively, a superscript in the parentheses indicating the order of perturbation. These solutions can be immediately obtained as follows: neglecting A_0 and A_2 in (5.9) yields $A_1^{(1)}$,

and inserting $A_1^{(1)}$ in (5.8) gives $A_0^{(2)}$. Now we improve the approximate solutions. A better approximation for A_0 can be obtained if we keep A_0 in (5.9); substituting

$$A_1(\boldsymbol{\lambda}\,|\,\boldsymbol{\lambda}_0) \simeq -iS(\boldsymbol{\lambda}_0)[2 + A_0(\boldsymbol{\lambda}_0)]F(\boldsymbol{\lambda}) \tag{5.25}$$

into (5.8) we obtain the equation

$$A_0(\boldsymbol{\lambda}_0) + S(\boldsymbol{\lambda}_0)[2 + A_0(\boldsymbol{\lambda}_0)] \int_{R_2} S(\boldsymbol{\lambda}_0 + \boldsymbol{\lambda})|F(\boldsymbol{\lambda})|^2 d\boldsymbol{\lambda} = 0 \tag{5.26}$$

Solving this for A_0 yields the solution (5.12) where ξ is given by (5.20). The equation for ξ, (5.19), is obtained if we use a better solution for A_1 instead of (5.25). A better solution for A_1 can be obtained as follows. First, we get an approximate solution for A_2 from (5.10), neglecting A_3;

$$\begin{aligned} &A_2(\boldsymbol{\lambda}_1, \boldsymbol{\lambda}_2|\boldsymbol{\lambda}_0) \simeq \\ &-\frac{i}{2}[S(\boldsymbol{\lambda}_0 + \boldsymbol{\lambda}_1)A_1(\boldsymbol{\lambda}_1|\boldsymbol{\lambda}_0)F(\boldsymbol{\lambda}_2) + S(\boldsymbol{\lambda}_0 + \boldsymbol{\lambda}_2)A_1(\boldsymbol{\lambda}_2|\boldsymbol{\lambda}_0)F(\boldsymbol{\lambda}_1)] \end{aligned} \tag{5.27}$$

Substituting this into (5.9) we obtain a more rigorous equation for A_1 than (5.25),

$$\begin{aligned} &A_1(\boldsymbol{\lambda}|\boldsymbol{\lambda}_0)\left[1 + S(\boldsymbol{\lambda}_0 + \boldsymbol{\lambda})\int_{R_2} S(\boldsymbol{\lambda}_0 + \boldsymbol{\lambda} + \boldsymbol{\lambda}_1)|F(\boldsymbol{\lambda}_1)|^2 d\boldsymbol{\lambda}_1\right] \\ &\quad \simeq -iS(\boldsymbol{\lambda}_0)F(\boldsymbol{\lambda})[2 + A_0(\boldsymbol{\lambda}_0)] \\ &\qquad - F(\boldsymbol{\lambda})\int_{R_2} S(\boldsymbol{\lambda}_0 + \boldsymbol{\lambda}_1)S(\boldsymbol{\lambda}_0 + \boldsymbol{\lambda} + \boldsymbol{\lambda}_1)A_1(\boldsymbol{\lambda}_1|\boldsymbol{\lambda}_0)\overline{F(\boldsymbol{\lambda}_1)}d\boldsymbol{\lambda}_1 \end{aligned} \tag{5.28}$$

If we substitute (5.12) for A_0 and (5.24) for A_1 in the righthand side, we obtain (5.13) and (5.17) where ξ is given by (5.20) and σ^5-order term is neglected in the numerator. The equation (5.19) for ξ can be obtained again by making a higher-order correction to A_2 using A_3 from (5.11). The solution (5.27) for A_2 can be improved in the same way, and we get the solution (5.18) for a_2. In this stepwise manner we can improve the approximate solutions. However, the above solutions are already good enough for small roughness. We note that the approximate solutions (5.16) and (5.17) satisfy the reciprocal relation (3.28).

5.4 Neumann Condition

We can proceed with the Neumann condition (5.2) or (5.4) in the same manner as the Dirichlet. To rewrite $[f\partial^2 U_n/\partial z^2]$ in the form of (5.5) we only replace iS by $[iS]^2$ in (5.6) and (5.7), and similarly, to obtain $[\boldsymbol{\nabla} f \cdot \boldsymbol{\nabla} U_n]$, we can put $F(\boldsymbol{\lambda}) \to i\boldsymbol{\lambda} F(\boldsymbol{\lambda})$ and $iS(\boldsymbol{\lambda}_0 + \cdots + \boldsymbol{\lambda}_n) \to i(\boldsymbol{\lambda}_0 + \cdots + \boldsymbol{\lambda}_n)$.

In this manner we can derive a hierarchy of equations for A_n's from (5.4):

$(n = 0)$

$$iS(\boldsymbol{\lambda}_0)A_0(\boldsymbol{\lambda}_0) - \int_{R_2} \left[S^2(\boldsymbol{\lambda}_0 + \boldsymbol{\lambda}) + \boldsymbol{\lambda} \cdot (\boldsymbol{\lambda}_0 + \boldsymbol{\lambda})\right] A_1(\boldsymbol{\lambda}|\boldsymbol{\lambda}_0)\overline{F(\boldsymbol{\lambda})}d\boldsymbol{\lambda} = 0 \tag{5.29}$$

$(n = 1)$

$$\begin{aligned} iS(\boldsymbol{\lambda}_0+\boldsymbol{\lambda})A_1(\boldsymbol{\lambda}|\boldsymbol{\lambda}_0) &- (2 + A_0(\boldsymbol{\lambda}_0))(S^2(\boldsymbol{\lambda}_0) - \boldsymbol{\lambda}_0 \cdot \boldsymbol{\lambda})F(\boldsymbol{\lambda}) \\ &- 2\int_{R_2} \left[S^2(\boldsymbol{\lambda}_0 + \boldsymbol{\lambda} + \boldsymbol{\lambda}_1) + \boldsymbol{\lambda}_1 \cdot (\boldsymbol{\lambda}_0 + \boldsymbol{\lambda} + \boldsymbol{\lambda}_1)\right] \\ &\qquad \times \overline{F(\boldsymbol{\lambda}_1)}A_2(\boldsymbol{\lambda}, \boldsymbol{\lambda}_1|\boldsymbol{\lambda}_0)d\boldsymbol{\lambda}_1 = 0 \end{aligned} \tag{5.30}$$

$(n = 2)$

$$\begin{aligned} iS(\boldsymbol{\lambda}_0+\boldsymbol{\lambda}_1 + \boldsymbol{\lambda}_2)A_2(\boldsymbol{\lambda}_1, \boldsymbol{\lambda}_2|\boldsymbol{\lambda}_0) &+ \frac{1}{2}\left[\boldsymbol{\lambda}_1 \cdot (\boldsymbol{\lambda}_0 + \boldsymbol{\lambda}_2) - S^2(\boldsymbol{\lambda}_0 + \boldsymbol{\lambda}_2)\right] A_1(\boldsymbol{\lambda}_2|\boldsymbol{\lambda}_0)F(\boldsymbol{\lambda}_1) \\ &+ \frac{1}{2}\left[\boldsymbol{\lambda}_2 \cdot (\boldsymbol{\lambda}_0 + \boldsymbol{\lambda}_1) - S^2(\boldsymbol{\lambda}_0 + \boldsymbol{\lambda}_1)\right] A_1(\boldsymbol{\lambda}_1|\boldsymbol{\lambda}_0)F(\boldsymbol{\lambda}_2) \\ &- 3\int_{R_2} \left[S^2(\boldsymbol{\lambda}_0 + \boldsymbol{\lambda}_1 + \boldsymbol{\lambda}_2 + \boldsymbol{\lambda}_3)\right. \\ &\qquad \left. + \boldsymbol{\lambda}_3 \cdot (\boldsymbol{\lambda}_0 + \boldsymbol{\lambda}_1 + \boldsymbol{\lambda}_2 + \boldsymbol{\lambda}_3)\right] \\ &\qquad \times A_3(\boldsymbol{\lambda}_1, \boldsymbol{\lambda}_2, \boldsymbol{\lambda}_3|\boldsymbol{\lambda}_0)\overline{F(\boldsymbol{\lambda}_3)}d\boldsymbol{\lambda}_3 = 0 \end{aligned} \tag{5.31}$$

$(n = 3)$

$$
\begin{aligned}
&iS(\boldsymbol{\lambda}_0 + \boldsymbol{\lambda}_1 + \boldsymbol{\lambda}_2 + \boldsymbol{\lambda}_3) A_3(\boldsymbol{\lambda}_1, \boldsymbol{\lambda}_2, \boldsymbol{\lambda}_3 | \boldsymbol{\lambda}_0) \\
&\quad + \frac{1}{3}\left[\boldsymbol{\lambda}_1 \cdot (\boldsymbol{\lambda}_0 + \boldsymbol{\lambda}_2 + \boldsymbol{\lambda}_3) - S^2(\boldsymbol{\lambda}_0 + \boldsymbol{\lambda}_2 + \boldsymbol{\lambda}_3)\right] A_2(\boldsymbol{\lambda}_2, \boldsymbol{\lambda}_3 | \boldsymbol{\lambda}_0) F(\boldsymbol{\lambda}_1) \\
&\quad + \frac{1}{3}\left[\boldsymbol{\lambda}_2 \cdot (\boldsymbol{\lambda}_0 + \boldsymbol{\lambda}_3 + \boldsymbol{\lambda}_1) - S^2(\boldsymbol{\lambda}_0 + \boldsymbol{\lambda}_3 + \boldsymbol{\lambda}_1)\right] A_2(\boldsymbol{\lambda}_3, \boldsymbol{\lambda}_1 | \boldsymbol{\lambda}_0) F(\boldsymbol{\lambda}_2) \\
&\quad + \frac{1}{3}\left[\boldsymbol{\lambda}_3 \cdot (\boldsymbol{\lambda}_0 + \boldsymbol{\lambda}_1 + \boldsymbol{\lambda}_2) - S^2(\boldsymbol{\lambda}_0 + \boldsymbol{\lambda}_1 + \boldsymbol{\lambda}_2)\right] A_2(\boldsymbol{\lambda}_1, \boldsymbol{\lambda}_2 | \boldsymbol{\lambda}_0) F(\boldsymbol{\lambda}_3) \\
&\quad - 4 \int_{R_2} \left[S^2(\boldsymbol{\lambda}_0 + \boldsymbol{\lambda}_1 + \boldsymbol{\lambda}_2 + \boldsymbol{\lambda}_3 + \boldsymbol{\lambda}_4)\right. \\
&\qquad\qquad \left. + \boldsymbol{\lambda}_4 \cdot (\boldsymbol{\lambda}_0 + \boldsymbol{\lambda}_1 + \boldsymbol{\lambda}_2 + \boldsymbol{\lambda}_3 + \boldsymbol{\lambda}_4)\right] \\
&\qquad\qquad \times A_4(\boldsymbol{\lambda}_1, \boldsymbol{\lambda}_2, \boldsymbol{\lambda}_3, \boldsymbol{\lambda}_4 | \boldsymbol{\lambda}_0) \overline{F(\boldsymbol{\lambda}_4)} d\boldsymbol{\lambda}_4 = 0
\end{aligned}
\tag{5.32}
$$

and so on. Higher order equations can be written similarly. As before, (5.30) for $n = 0$ is just the average of (5.4).

We first write out the approximate solutions for A_0, A_1 and A_2:

$$A_0(\boldsymbol{\lambda}) \equiv -2 + S(\boldsymbol{\lambda}) a_0(\boldsymbol{\lambda}) = -\frac{2Z_N(\boldsymbol{\lambda})}{1 + Z_N(\boldsymbol{\lambda})} \tag{5.33}$$

$$A_1(\boldsymbol{\lambda}_1 | \boldsymbol{\lambda}) \equiv S(\boldsymbol{\lambda}) a_1(\boldsymbol{\lambda}_1 | \boldsymbol{\lambda}) \tag{5.34}$$

$$A_2(\boldsymbol{\lambda}_1, \boldsymbol{\lambda}_2 | \boldsymbol{\lambda}) \equiv S(\boldsymbol{\lambda}) a_2(\boldsymbol{\lambda}_1, \boldsymbol{\lambda}_2 | \boldsymbol{\lambda}) \tag{5.35}$$

$$Z_N(\boldsymbol{\lambda}) \equiv \frac{\eta(\boldsymbol{\lambda})}{S(\boldsymbol{\lambda})} \tag{5.36}$$

where

$$a_0(\boldsymbol{\lambda}) = \frac{2}{S(\boldsymbol{\lambda}) + \eta(\boldsymbol{\lambda})} \tag{5.37}$$

$$a_1(\boldsymbol{\lambda}_1 | \boldsymbol{\lambda}) = \frac{-2iF(\boldsymbol{\lambda}_1)\left[k^2 - (\boldsymbol{\lambda} + \boldsymbol{\lambda}_1) \cdot \boldsymbol{\lambda} - \eta^*(\boldsymbol{\lambda} + \boldsymbol{\lambda}_1, \boldsymbol{\lambda})\right]}{\left[S(\boldsymbol{\lambda}) + \eta(\boldsymbol{\lambda})\right]\left[S(\boldsymbol{\lambda} + \boldsymbol{\lambda}_1) + \eta(\boldsymbol{\lambda} + \boldsymbol{\lambda}_1)\right]} \tag{5.38}$$

$$
\begin{aligned}
&a_2(\boldsymbol{\lambda}_1,\boldsymbol{\lambda}_2|\boldsymbol{\lambda}) \\
&\quad \simeq \frac{i}{2}\left\{\left[\boldsymbol{\lambda}_1\cdot(\boldsymbol{\lambda}+\boldsymbol{\lambda}_2)-S^2(\boldsymbol{\lambda}+\boldsymbol{\lambda}_2)\right]a_1(\boldsymbol{\lambda}_2|\boldsymbol{\lambda})F(\boldsymbol{\lambda}_1)\right. \\
&\qquad\qquad \left.+\left[\boldsymbol{\lambda}_2\cdot(\boldsymbol{\lambda}+\boldsymbol{\lambda}_1)-S^2(\boldsymbol{\lambda}+\boldsymbol{\lambda}_1)\right]a_1(\boldsymbol{\lambda}_1|\boldsymbol{\lambda})F(\boldsymbol{\lambda}_2)\right\} \\
&\qquad\qquad \Big/\left[S(\boldsymbol{\lambda}+\boldsymbol{\lambda}_1+\boldsymbol{\lambda}_2)+\eta(\boldsymbol{\lambda}+\boldsymbol{\lambda}_1+\boldsymbol{\lambda}_2)\right] \qquad (5.39) \\
&\quad = \frac{i}{2}\left\{\left[(\boldsymbol{\lambda}+\boldsymbol{\lambda}_2)\cdot(\boldsymbol{\lambda}+\boldsymbol{\lambda}_1+\boldsymbol{\lambda}_2)-k^2\right]a_1(\boldsymbol{\lambda}_2|\boldsymbol{\lambda})F(\boldsymbol{\lambda}_1)\right. \\
&\qquad\qquad \left.+\left[(\boldsymbol{\lambda}+\boldsymbol{\lambda}_1)\cdot(\boldsymbol{\lambda}+\boldsymbol{\lambda}_1+\boldsymbol{\lambda}_2)-k^2\right]a_1(\boldsymbol{\lambda}_1|\boldsymbol{\lambda})F(\boldsymbol{\lambda}_2)\right\} \\
&\qquad\qquad \Big/\left[S(\boldsymbol{\lambda}+\boldsymbol{\lambda}_1+\boldsymbol{\lambda}_2)+\eta(\boldsymbol{\lambda}+\boldsymbol{\lambda}_1+\boldsymbol{\lambda}_2)\right] \qquad (5.40)
\end{aligned}
$$

and

$$
\eta(\boldsymbol{\lambda}) \equiv \int_{R_2}\frac{\left[k^2-\boldsymbol{\lambda}_1\cdot\boldsymbol{\lambda}\right]^2|F(\boldsymbol{\lambda}_1-\boldsymbol{\lambda})|^2}{S(\boldsymbol{\lambda}_1)+\eta(\boldsymbol{\lambda}_1)}d\boldsymbol{\lambda}_1 \qquad (5.41)
$$

$$
\simeq \int_{R_2}\frac{\left[k^2-\boldsymbol{\lambda}_1\cdot\boldsymbol{\lambda}\right]^2|F(\boldsymbol{\lambda}_1-\boldsymbol{\lambda})|^2}{S(\boldsymbol{\lambda}_1)}d\boldsymbol{\lambda}_1 \qquad (5.42)
$$

$$
\begin{aligned}
&\eta^*(\boldsymbol{\lambda},\boldsymbol{\lambda}_0) \\
&\quad = \int_{R_2}\frac{\left[k^2-(\boldsymbol{\lambda}+\boldsymbol{\lambda}_1)\cdot\boldsymbol{\lambda}\right]\left[k^2-(\boldsymbol{\lambda}_0+\boldsymbol{\lambda}_1)\cdot\boldsymbol{\lambda}_0\right]}{\left[S(\boldsymbol{\lambda}+\boldsymbol{\lambda}_1)+\eta(\boldsymbol{\lambda}+\boldsymbol{\lambda}_1)\right]\left[S(\boldsymbol{\lambda}_0+\boldsymbol{\lambda}_1)+\eta(\boldsymbol{\lambda}_0+\boldsymbol{\lambda}_1)\right]} \\
&\qquad\qquad \times\left[k^2-(\boldsymbol{\lambda}+\boldsymbol{\lambda}_1)\cdot(\boldsymbol{\lambda}_0+\boldsymbol{\lambda}_1)\right]|F(\boldsymbol{\lambda}_1)|^2d\boldsymbol{\lambda}_1 \qquad (5.43) \\
&\quad \simeq \int_{R_2}\frac{\left[k^2-(\boldsymbol{\lambda}+\boldsymbol{\lambda}_1)\cdot\boldsymbol{\lambda}\right]\left[k^2-(\boldsymbol{\lambda}_0+\boldsymbol{\lambda}_1)\cdot\boldsymbol{\lambda}_0\right]}{S(\boldsymbol{\lambda}+\boldsymbol{\lambda}_1)S(\boldsymbol{\lambda}_0+\boldsymbol{\lambda}_1)} \\
&\qquad\qquad \times\left[k^2-(\boldsymbol{\lambda}+\boldsymbol{\lambda}_1)\cdot(\boldsymbol{\lambda}_0+\boldsymbol{\lambda}_1)\right]|F(\boldsymbol{\lambda}_1)|^2d\boldsymbol{\lambda}_1 \qquad (5.44)
\end{aligned}
$$

Particularly at $\boldsymbol{\lambda}=\mathbf{k}$, we have

$$
Z_N(\mathbf{k})=\infty, \qquad 2+A_0(\mathbf{k})=0, \qquad A_n(\boldsymbol{\lambda}_1,\cdots,\boldsymbol{\lambda}_n|\mathbf{k})=0 \quad (n\geq 1) \qquad (5.45)
$$

which should be compared with (5.22). The equation (5.41) is actually the dispersion equation for determining η. However, the integral (5.42) is finite and can be regarded as an approximate value of η. If necessary,

it could be used for the initial value to iterate the integral (3.10) for better values.

We first note that neglecting η and η^* in (5.34) and (5.35) we obtain the expressions,

$$A_0^{(2)}(\boldsymbol{\lambda}) = -2\frac{\eta(\boldsymbol{\lambda})}{S(\boldsymbol{\lambda})} = -2Z_N(\boldsymbol{\lambda}) \tag{5.46}$$

$$A_1^{(1)}(\boldsymbol{\lambda}_1|\boldsymbol{\lambda}) = -\frac{2\left[k^2 - (\boldsymbol{\lambda}+\boldsymbol{\lambda}_1)\cdot\boldsymbol{\lambda}\right]}{iS(\boldsymbol{\lambda}+\boldsymbol{\lambda}_1)}F(\boldsymbol{\lambda}_1) \tag{5.47}$$

which correspond to the second- and the first-order perturbation solution for A_0 and A_1, respectively. $A_1^{(1)}$ immediately follows from (5.30), neglecting A_0 and A_2, and $A_0^{(2)}$ is given by (5.29), using $A_1^{(1)}$ and (3.6). We note that these perturbation solutions for the Neumann surface diverge at $\boldsymbol{\lambda}$ such that $S=0$ whereas for the Dirichlet surface (5.23) and (5.24) are finite.

For a better approximation of A_0, we keep A_0 in (5.30) to get

$$A_1(\boldsymbol{\lambda}\,|\,\boldsymbol{\lambda}_0) \simeq -i\frac{[2+A_0(\boldsymbol{\lambda}_0)]}{S(\boldsymbol{\lambda}_0+\boldsymbol{\lambda})}\left[k^2 - \boldsymbol{\lambda}_0\cdot(\boldsymbol{\lambda}_0+\boldsymbol{\lambda})\right]F(\boldsymbol{\lambda}) \tag{5.48}$$

Substituting this into (5.29) we have

$$\begin{aligned} &S(\boldsymbol{\lambda}_0)A_0(\boldsymbol{\lambda}_0) \\ &\quad + [2+A_0(\boldsymbol{\lambda})]\int_{R_2}\frac{[k_2 - \boldsymbol{\lambda}_0\cdot(\boldsymbol{\lambda}_0+\boldsymbol{\lambda})]^2}{S(\boldsymbol{\lambda}_0+\boldsymbol{\lambda})}|F(\boldsymbol{\lambda})|^2 d\boldsymbol{\lambda} = 0 \end{aligned} \tag{5.49}$$

Solving this for A_0 yields the solution (5.33) where η is given by (5.42). The equation (5.41) for η is obtained if we use a better approximation for A_1 than (5.48), taking into account the correction due to A_2.

To obtain a better solution for A_1, we first get an approximate solution for A_2 from (5.31) and (5.32),

$$\begin{aligned} &A_2(\boldsymbol{\lambda}_1,\boldsymbol{\lambda}_2|\boldsymbol{\lambda}_0) \\ &\quad\simeq\frac{i}{2}\left\{\left[\boldsymbol{\lambda}_1\cdot(\boldsymbol{\lambda}_0+\boldsymbol{\lambda}_2) - S^2(\boldsymbol{\lambda}_0+\boldsymbol{\lambda}_2)\right]A_1(\boldsymbol{\lambda}_2|\boldsymbol{\lambda}_0)F(\boldsymbol{\lambda}_1)\right. \\ &\qquad\left. + \left[\boldsymbol{\lambda}_2\cdot(\boldsymbol{\lambda}_0+\boldsymbol{\lambda}_1) - S^2(\boldsymbol{\lambda}_0+\boldsymbol{\lambda}_1)\right]A_1(\boldsymbol{\lambda}_1|\boldsymbol{\lambda}_0)F(\boldsymbol{\lambda}_2)\right\} \\ &\qquad / \left[S(\boldsymbol{\lambda}_0+\boldsymbol{\lambda}_1+\boldsymbol{\lambda}_2) + \eta(\boldsymbol{\lambda}_0+\boldsymbol{\lambda}_1+\boldsymbol{\lambda}_2)\right] \end{aligned} \tag{5.50}$$

where an approximate solution A_3 from (5.32) is inserted to (5.31) to give a corrective term η in the denominator. From this follows (5.39). Substituting (5.50) into (5.30) gives

$$iS(\boldsymbol{\lambda}_0+\boldsymbol{\lambda})A_1(\boldsymbol{\lambda}|\boldsymbol{\lambda}_0)-(2+A_0(\boldsymbol{\lambda}_0))F(\boldsymbol{\lambda})[k^2-(\boldsymbol{\lambda}_0+\boldsymbol{\lambda})\cdot\boldsymbol{\lambda}_0] + iA_1(\boldsymbol{\lambda}|\boldsymbol{\lambda}_0)\eta(\boldsymbol{\lambda}_0+\boldsymbol{\lambda})+iF(\boldsymbol{\lambda})I(\boldsymbol{\lambda}+\boldsymbol{\lambda}_0,\boldsymbol{\lambda}_0)=0 \tag{5.51}$$

$$I(\boldsymbol{\lambda},\boldsymbol{\lambda}_0)\equiv\int_{R_2}\frac{\left[k^2-(\boldsymbol{\lambda}+\boldsymbol{\lambda}_1)\cdot\boldsymbol{\lambda}\right]\left[k^2-(\boldsymbol{\lambda}+\boldsymbol{\lambda}_1)\cdot(\boldsymbol{\lambda}_0+\boldsymbol{\lambda}_1)\right]}{S(\boldsymbol{\lambda}+\boldsymbol{\lambda}_1)+\eta(\boldsymbol{\lambda}+\boldsymbol{\lambda}_1)} \times A_1(\boldsymbol{\lambda}_1|\boldsymbol{\lambda}_0)\overline{F(\boldsymbol{\lambda}_1)}d\boldsymbol{\lambda}_1 \tag{5.52}$$

where η is defined by (5.41) and the integral I involves unknown A_1. We first neglect I to solve (5.51) for A_1, and then insert this A_1 into (5.52) to obtain I:

$$I(\boldsymbol{\lambda},\boldsymbol{\lambda}_0)=-i[2+A_0]\eta^*(\boldsymbol{\lambda},\boldsymbol{\lambda}_0) \tag{5.53}$$

where η^* is defined by (5.43). Next insert (5.53) into (5.51), and using $(2+A_0)=2S(\boldsymbol{\lambda}_0)/[S(\boldsymbol{\lambda}_0)+\eta(\boldsymbol{\lambda}_0)]$, we finally obtain the solution (5.34) with (5.38). Although η appearing in the denominator of (5.37) and (5.38) plays a crucial role of making A_0 and A_1 finite, η^* in the numerator of (5.38) is only a corrective term that could be neglected for practical application. The quantities $\xi(\boldsymbol{\lambda})$ and $\eta(\boldsymbol{\lambda})$ represent the effect of multiple scattering and can be also obtained by a renormalization technique in the multiple scattering theory.

If the random surface is homogeneous and isotropic such that $F(\boldsymbol{\lambda})=F(\lambda)$, $\lambda\equiv|\boldsymbol{\lambda}|$, by (2.27), then we immediately see that above solutions for A_n's satisfy (3.22), and accordingly that Z_D, Z_N, ξ and η depend only on λ.

5.5 Average Surface Impedence

It should be noticed that the righthand members of (5.12) and (5.33) have the same form in Z's and satisfy the relation,

$$1+A_0(\boldsymbol{\lambda})=\frac{1-Z_\iota(\boldsymbol{\lambda})}{1+Z_\iota(\boldsymbol{\lambda})},\qquad \iota=D,N \tag{5.54}$$

By (4.1) $1 + \mathrm{A}_o$ gives the amplitude of the coherent reflection occuring in the direction of specular reflection. Therefore, the equation (5.54) enables us to interpret Z_ι, $\iota = D, N$, as the average surface impedance of the random surface for each boundary condition. $Re(Z_\iota)$ represents equivalent energy dissipation due to incoherent scattering, and $Im(Z_\iota)$ suggests the reaction due to the surface wave.

The equation (5.19) or (5.41) can be considered as a dispersion equation determining $\xi(\boldsymbol{\lambda})$ (or $\eta(\boldsymbol{\lambda})$), which can be obtained using an approximate solution for A_3 and neglecting kernels higher than A_4. These equations can be rewritten in the form of integral equations for the surface impedance:

$$Z_D(\boldsymbol{\lambda}) = S(\boldsymbol{\lambda}) \int_{R_2} \frac{S(\boldsymbol{\lambda}')|F(\boldsymbol{\lambda}' - \boldsymbol{\lambda})|^2}{1 + Z_D(\boldsymbol{\lambda}')} d\boldsymbol{\lambda}' \qquad \text{(Dirichlet)} \quad (5.55)$$

$$Z_N(\boldsymbol{\lambda}) = \frac{1}{S(\boldsymbol{\lambda})} \int_{R_2} \frac{[k^2 - \boldsymbol{\lambda}' \cdot \boldsymbol{\lambda}]^2 |F(\boldsymbol{\lambda}' - \boldsymbol{\lambda})|^2}{S(\boldsymbol{\lambda}')[1 + Z_N(\boldsymbol{\lambda}')]} d\boldsymbol{\lambda}' \qquad \text{(Neumann)} \quad (5.56)$$

The above integral equation for Z_ι can be solved by the iteration method, starting from the first solution given in terms of (5.20) or (5.42), that is, n-th solution is obtained by substituting $(n-1)$-th solution into the righthand side; however, the first or the second solution is good enough for small roughness.

6. Scattering Characteristics

Here we show some examples of the numerical scattering characteristics using the approximate solutions obtained above.

6.1 Isotropic Gaussian Spectrum

For numerical calculation we conveniently assume an isotropic Gaussian form (2.29) for the spectral density of the random surface, where the parameter l denotes the isotropic correlation length. Using the isotropy (2.27), we easily see that ξ^* and η^* as well as a_n satisfy the rotational invariance of the form (3.22), and that ξ and η depend only on $\lambda \equiv |\boldsymbol{\lambda}|$.

The Gaussian spectrum implies a smooth random surface in the sense that it can be differentiated arbitrarily many times [41]: however, for our purpose, it is sufficient that the random surface is differentiable only once, or equivalently, $|F(\lambda)|^2\lambda^3$ is integrable over $[0,\infty)$.

6.2 Coherent Scattering Amplitude

As mentioned above the coherent scattering amplitude is described by the 0-th Wiener kernel A_0 which is

$$A_0(\boldsymbol{\lambda}) = -\frac{2Z_\iota(\boldsymbol{\lambda})}{1+Z_\iota(\boldsymbol{\lambda})}, \qquad \iota = D, N \tag{6.1}$$

where Z's are surface impedances given by (5.55) and (5.56); that is

$$Z_D(\boldsymbol{\lambda}) = S(\boldsymbol{\lambda})\int_{R_2} \frac{S(\boldsymbol{\lambda}')|F(\boldsymbol{\lambda}'-\boldsymbol{\lambda})|^2}{1+S(\boldsymbol{\lambda}')\xi(\boldsymbol{\lambda}')} d\boldsymbol{\lambda}' \qquad \text{(Dirichlet)} \tag{6.2}$$

$$Z_N(\boldsymbol{\lambda}) = \frac{1}{S(\boldsymbol{\lambda})}\int_{R_2} \frac{[k^2-\boldsymbol{\lambda}'\cdot\boldsymbol{\lambda}]^2|F(\boldsymbol{\lambda}'-\boldsymbol{\lambda})|^2}{S(\boldsymbol{\lambda}')+\eta(\boldsymbol{\lambda}')} d\boldsymbol{\lambda}' \qquad \text{(Neumann)} \tag{6.3}$$

For ξ and η on the righthand sides, we can use the approximate expressions (5.20) and (5.42). The amplitude and phase of the coherent scattering amplitude $1+A_0$ are plotted againt the incident angle θ in Fig. 6.1 (Dirichlet) and Fig. 6.2 (Neumann) for the surface roughness $k\sigma = \pi/10$. In the enlarged portion of Fig. 6.2 we notice the anomalous behavior of $1+A_0$ near the grazing angle $\theta = 90^\circ$, which is due to the multiple scattering along the Neumann surface.

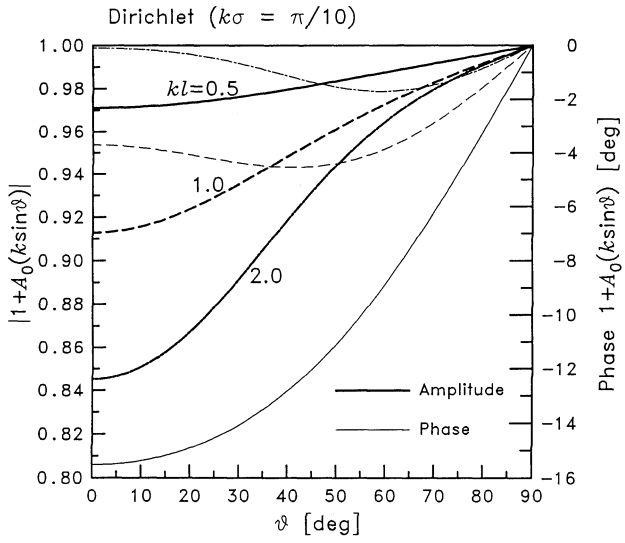

Figure 6.1. Coherent scattering amplitude $1 + A_0$ versus incident angle (Dirichlet). $k\sigma = \pi/10, kl = 0.5$ (solid line), 1.0 (broken line), 2.0 (chain line); amplitude (thick line), phase (thin line).

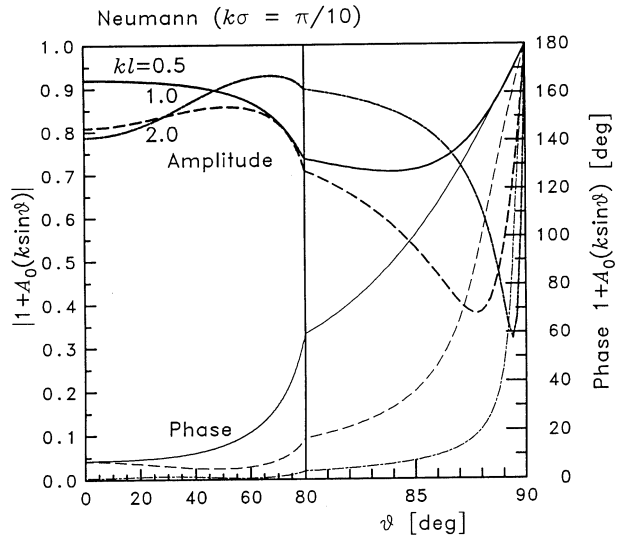

Figure 6.2. Coherent scattering amplitude $1 + A_0$ versus incident angle (Neumann). $k\sigma = \pi/10, kl = 0.5$ (solid line), 1.0 (broken line), 2.0 (chain line); amplitude (thick line), phase (thin line).

6.3 Average Surface Impedance

The surface impedances can be calculated by means of (6.2) and (6.3). We note that, if the spectrum $|F(\boldsymbol{\lambda})|^2$ is anisotropic, the surface impedance $Z_\iota(\boldsymbol{\lambda})$ is anisotropic either, i.e., dependent on the direction, and so is $A_0(\boldsymbol{\lambda})$. For an isotropic spectrum like (2.29), however, Z_ι is isotropic and depends only on λ.

The surface impedances Z_D and Z_N are shown in Figs. 6.3 and 6.4, respectively. The anomalous behavior of Z_N is shown in the Neumann case.

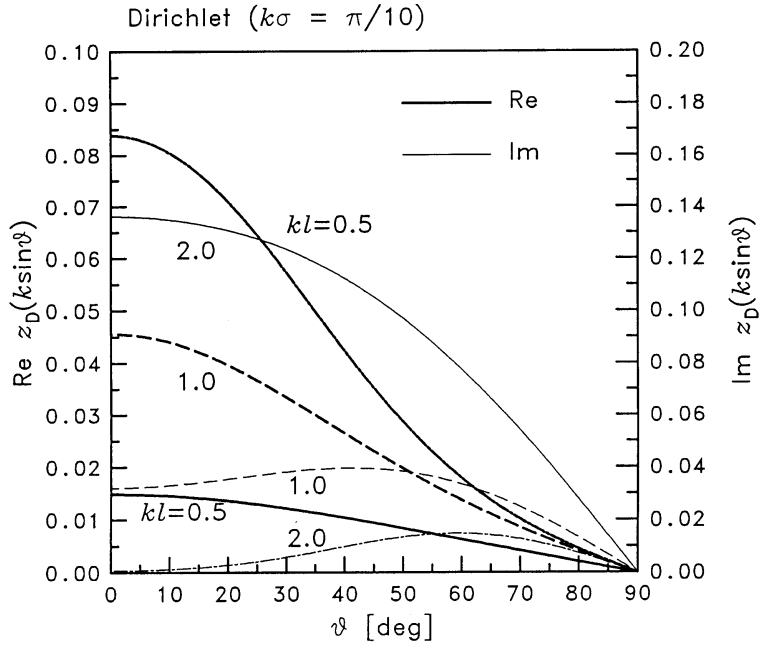

Figure 6.3. Average surface impedance versus incident angle (Dirichlet). $k\sigma = \pi/10, kl = 0.5$ **(solid line), 1.0 (broken line), 2.0 (chain line),** $\mathrm{Re}\, Z_D$ **(thick line),** $\mathrm{Im}\, Z_D$ **(thin line).**

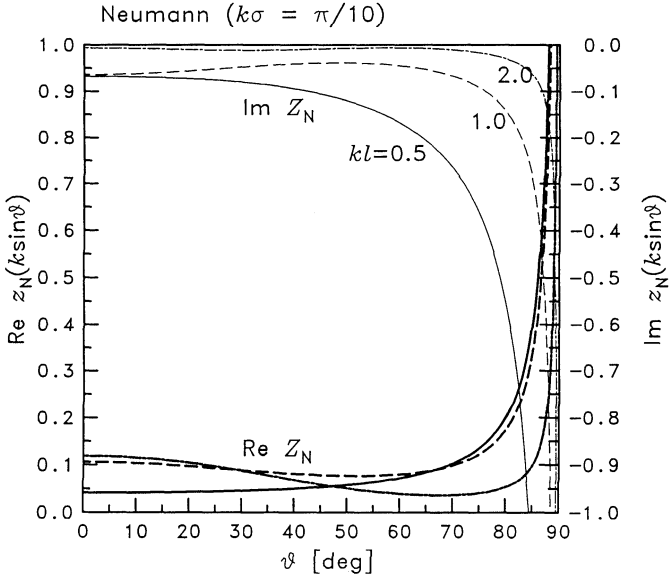

Figure 6.4. Average surface impedance versus incident angle (Neumann). $k\sigma = \pi/10, kl = 0.5$ **(solid line), 1.0 (broken line), 2.0 (chain line),** $\mathrm{Re}\, Z_D$ **(thick line),** $\mathrm{Im}\, Z_D$ **(thin line).**

6.4 Angular Distribution of Incoherent Scattering

The angular distribution $P(\theta, \phi|\theta_0, \phi_0)$ given by (4.9) can be calculated using the approximate solutions for the Wiener kernels. Using A_1 and A_2 given by (5.13), (5.14), (5.34), and (5.35), we obtain the following:

$$\begin{aligned} P(\theta, \phi|\theta_0, \phi_0) &= P_1(\theta, \phi|\theta_0, \phi_0) + P_2(\theta, \phi|\theta_0, \phi_0) \\ &\equiv k^4 \cos^2\theta \cos^2\theta_0 \\ &\quad \times \left[|a_1(\boldsymbol{\lambda} - \boldsymbol{\lambda}_0|\boldsymbol{\lambda}_0)|^2 + 2\int_{R_2} |a_2(\boldsymbol{\lambda} - \boldsymbol{\lambda}_1, \boldsymbol{\lambda}_1 - \boldsymbol{\lambda}_0|\boldsymbol{\lambda}_0)|^2 d\boldsymbol{\lambda}_1 \right] \end{aligned} \tag{6.4}$$

where P_1, the contribution from A_1, is given by

$$P_1(\theta,\phi|\theta_0,\phi_0) = \frac{4k^2\cos^2\theta\cos^2\theta_0|1-\xi^*(\boldsymbol{\lambda},\boldsymbol{\lambda}_0)|^2|F(\boldsymbol{\lambda}-\boldsymbol{\lambda}_0)|^2}{|\,[1+S(\boldsymbol{\lambda}_0)\xi(\boldsymbol{\lambda}_0)]\,[1+S(\boldsymbol{\lambda})\xi(\boldsymbol{\lambda})]\,|^2} \quad (6.5)$$

(Dirichlet)

$$= \frac{4k^4\cos^2\theta\cos^2\theta_0|k^2-\boldsymbol{\lambda}\cdot\boldsymbol{\lambda}_0-\eta^*(\boldsymbol{\lambda},\boldsymbol{\lambda}_0)|^2|F(\boldsymbol{\lambda}-\boldsymbol{\lambda}_0)|^2}{|\,[S(\boldsymbol{\lambda}_0)+\eta(\boldsymbol{\lambda}_0)]\,[S(\boldsymbol{\lambda})+\eta(\boldsymbol{\lambda})]\,|^2} \quad (6.6)$$

(Neumann)

with

$$\boldsymbol{\lambda} = (\lambda,\phi)_{cyl}, \qquad \boldsymbol{\lambda}_0 = (\lambda_0,\phi_0)_{cyl} \quad (6.7)$$

$$\lambda = k\sin\theta, S(\boldsymbol{\lambda}) = k\cos\theta, \quad \lambda_0 = k\sin\theta_0, \quad S(\boldsymbol{\lambda}_0) = k\cos\theta_0 \quad (6.8)$$

$$|\boldsymbol{\lambda}-\boldsymbol{\lambda}_0| = k\sqrt{\sin^2\theta+\sin^2\theta_0-2\sin\theta\sin\theta_0\cos(\phi-\phi_0)} \quad (6.9)$$

$$\boldsymbol{\lambda}\cdot\boldsymbol{\lambda}_0 = k^2\sin\theta\sin\theta_0\cos(\phi-\phi_0) \quad (6.10)$$

and P_2, the contribution from A_2, is written approximately

$$\begin{aligned} &P_2(\theta,\phi|\theta_0,\phi_0) \\ &= \frac{k^4\cos^2\theta\cos^2\theta_0}{2|1+S(\boldsymbol{\lambda})\xi(\boldsymbol{\lambda})|^2}\int_{R_2}\Big|S(\boldsymbol{\lambda}_1)a_1(\boldsymbol{\lambda}_1-\boldsymbol{\lambda}_0|\boldsymbol{\lambda}_0)F(\boldsymbol{\lambda}-\boldsymbol{\lambda}_1) \\ &\quad + S(\boldsymbol{\lambda}_0+\boldsymbol{\lambda}-\boldsymbol{\lambda}_1)a_1(\boldsymbol{\lambda}-\boldsymbol{\lambda}_1|\boldsymbol{\lambda}_0)F(\boldsymbol{\lambda}_1-\boldsymbol{\lambda}_0)\Big|^2 d\boldsymbol{\lambda}_1 \quad (6.11) \\ &\simeq \frac{4k^4\cos^2\theta\cos^2\theta_0}{|\,[1+S(\boldsymbol{\lambda}_0)\xi(\boldsymbol{\lambda}_0)]\,[1+S(\boldsymbol{\lambda})\xi(\boldsymbol{\lambda})]\,|^2}\int_{R_2}\left\{\Big|\frac{S(\boldsymbol{\lambda}_1)}{1+S(\boldsymbol{\lambda}_1)\xi(\boldsymbol{\lambda}_1)}\Big|^2\right. \\ &\quad \left. + Re\left(\frac{\overline{S(\boldsymbol{\lambda}_1)}}{1+\overline{S(\boldsymbol{\lambda}_1)\xi(\boldsymbol{\lambda}_1)}}\frac{S(\boldsymbol{\lambda}_0+\boldsymbol{\lambda}-\boldsymbol{\lambda}_1)}{1+S(\boldsymbol{\lambda}_0+\boldsymbol{\lambda}-\boldsymbol{\lambda}_1)\xi(\boldsymbol{\lambda}_0+\boldsymbol{\lambda}-\boldsymbol{\lambda}_1)}\right)\right\} \\ &\quad \times\Big|F(\boldsymbol{\lambda}_1-\boldsymbol{\lambda}_0)F(\boldsymbol{\lambda}-\boldsymbol{\lambda}_1)\Big|^2 d\boldsymbol{\lambda}_1 \qquad \text{(Dirichlet)} \quad (6.12) \end{aligned}$$

$$\begin{aligned} &P_2(\theta,\phi|\theta_0,\phi_0) \\ &= \frac{k^4\cos^2\theta\cos^2\theta_0}{2|S(\boldsymbol{\lambda})+\eta(\boldsymbol{\lambda})|^2}\int_{R_2}\Big|\left[k^2-\boldsymbol{\lambda}_1\cdot\boldsymbol{\lambda}\right]a_1(\boldsymbol{\lambda}_1-\boldsymbol{\lambda}_0|\boldsymbol{\lambda}_0)F(\boldsymbol{\lambda}-\boldsymbol{\lambda}_1) \\ &\quad + \left[k^2-(\boldsymbol{\lambda}_0+\boldsymbol{\lambda}-\boldsymbol{\lambda}_1)\cdot\boldsymbol{\lambda}\right]a_1(\boldsymbol{\lambda}-\boldsymbol{\lambda}_1|\boldsymbol{\lambda}_0)F(\boldsymbol{\lambda}_1-\boldsymbol{\lambda}_0)\Big|^2 d\boldsymbol{\lambda}_1 \quad (6.13) \end{aligned}$$

$$\simeq \frac{4k^4 \cos^2\theta \cos^2\theta_0}{|\,[S(\boldsymbol{\lambda}_0)+\eta(\boldsymbol{\lambda}_0)]\,[S(\boldsymbol{\lambda})+\eta(\boldsymbol{\lambda})]\,|^2}$$
$$\int_{R_2} \left\{ \left| \frac{\left[k^2-\boldsymbol{\lambda}_1\cdot\boldsymbol{\lambda}\right]\left[k^2-\boldsymbol{\lambda}_1\cdot\boldsymbol{\lambda}_0\right]}{S(\boldsymbol{\lambda}_1)+\eta(\boldsymbol{\lambda}_1)} \right|^2 \right.$$
$$+ Re\left(\frac{\left[k^2-\boldsymbol{\lambda}_1\cdot\boldsymbol{\lambda}\right]\left[k^2-\boldsymbol{\lambda}_1\cdot\boldsymbol{\lambda}_0\right]}{\overline{S(\boldsymbol{\lambda}_1)}+\overline{\eta(\boldsymbol{\lambda}_1)}} \right.$$
$$\left. \left. \times \frac{\left[k^2-(\boldsymbol{\lambda}_0+\boldsymbol{\lambda}-\boldsymbol{\lambda}_1)\cdot\boldsymbol{\lambda}\right]\left[k^2-(\boldsymbol{\lambda}_0+\boldsymbol{\lambda}-\boldsymbol{\lambda}_1)\cdot\boldsymbol{\lambda}_0\right]}{S(\boldsymbol{\lambda}_0+\boldsymbol{\lambda}-\boldsymbol{\lambda}_1)+\eta(\boldsymbol{\lambda}_0+\boldsymbol{\lambda}-\boldsymbol{\lambda}_1)} \right) \right\}$$
$$\times |F(\boldsymbol{\lambda}_1-\boldsymbol{\lambda}_0)F(\boldsymbol{\lambda}-\boldsymbol{\lambda}_1)|^2 d\boldsymbol{\lambda}_1 \qquad \text{(Neumann)} \tag{6.14}$$

In the above equations, ξ, ξ^*, η and η^* are calculated by (5.19), (5.21), (5.41) and (5.43), respectively, and ξ^* and η^* are neglected to simplify the approximate equations for P_2.

It should be noticed that our approximate solutions for $P(\boldsymbol{\theta}\,|\,\boldsymbol{\theta}_0)$ satisfy the reciprocity relation (4.10).

Figures 6.5–6.6 show the zenithal distributions of $P(\boldsymbol{\theta}\,|\,\boldsymbol{\theta}_0)$ on the plane of incidence with $\phi = 0^\circ, 180^\circ$, and on the plane across with $\phi = 90^\circ, 270^\circ$ for three incident angles $\theta_0 = 0^\circ$, 30°, 60°, with $\phi_0 = 0^\circ$. The presence of the factor $1/|[S(\boldsymbol{\lambda}_0)+\eta(\boldsymbol{\lambda}_0)][S(\boldsymbol{\lambda})+\eta(\boldsymbol{\lambda})]|^2$ in (6.6) and (6.14) of the Neumann case, implies that the anomalous scattering occurs at the incident or scattering angle close to the grazing angle θ_0 or $\theta \simeq 90^\circ$, where $S(\boldsymbol{\lambda}_0)$ or $S(\boldsymbol{\lambda}) \simeq 0$ [15-17]; this phenomenon is analogous to the well known Wood's anomaly in the grating scattering. In the profile of $P(\boldsymbol{\theta}\,|\,\boldsymbol{\theta}_0)$ shown in Fig. 6.6, such an anomaly appears nearly cancelled by the factor $\cos^2\theta_0 \cos^2\theta$. However, the anomaly is clearly observed in the practical scattering distribution $S(\boldsymbol{\theta}\,|\,\boldsymbol{\theta}_0)$ defined by (4.11), as shown in Fig. 6.7, where a sharp scattering occurs in the direction close to the surface. Such anomalous scattering becomes much sharper as kl increases. As discussed in a later section, the anomalous scattering is closely related to the propagating mode along the Neumann random surface.

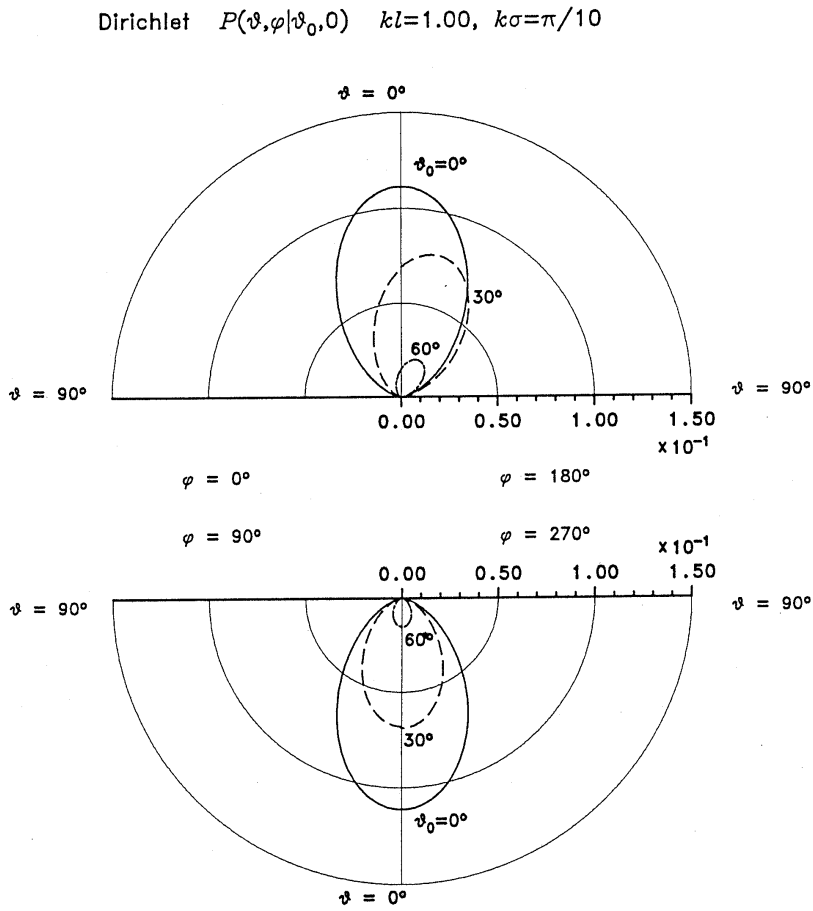

Figure 6.5. Angular distribution of incoherent scattering $P(\theta, \phi|\theta_0, 0)$ (Dirichlet). $kl = 1.0$. The upper half shows the distribution on the incident plane, $\phi = 0°, 180°$ and the lower half the crossing plane, $\phi = 90°, 270°$. $\theta_0 = 0°$ (solid line), $30°$ (broken line), $60°$ (chain line).

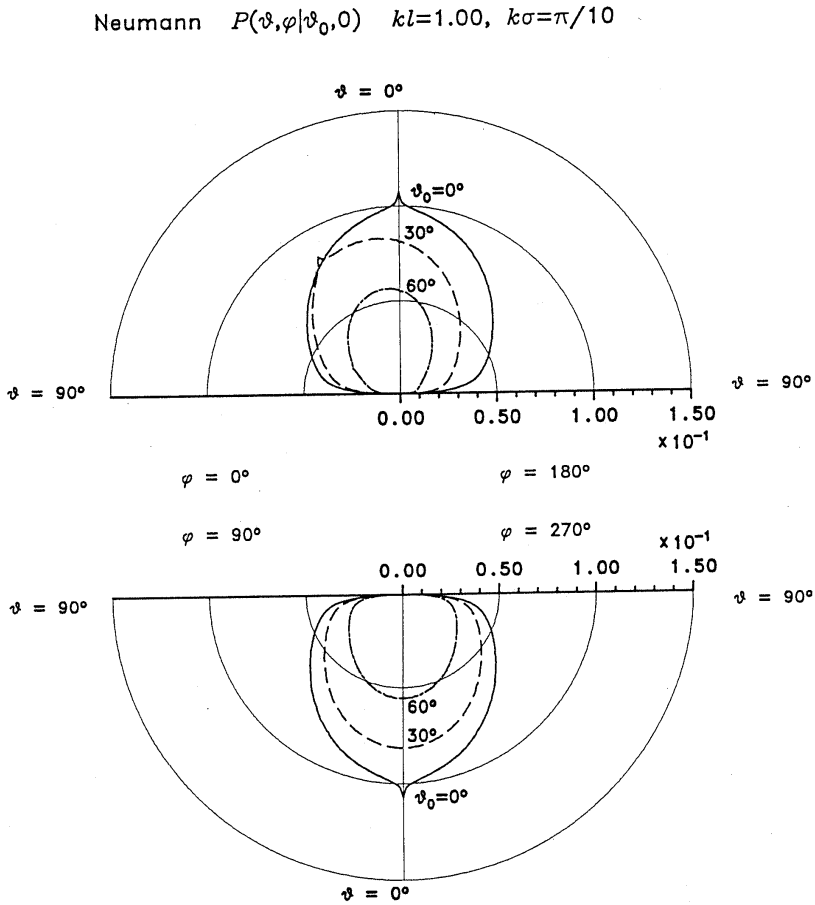

Figure 6.6. Angular distribution of incoherent scattering $P(\theta, \phi|\theta_0, 0)$ (Neumann). $kl = 1.0$.

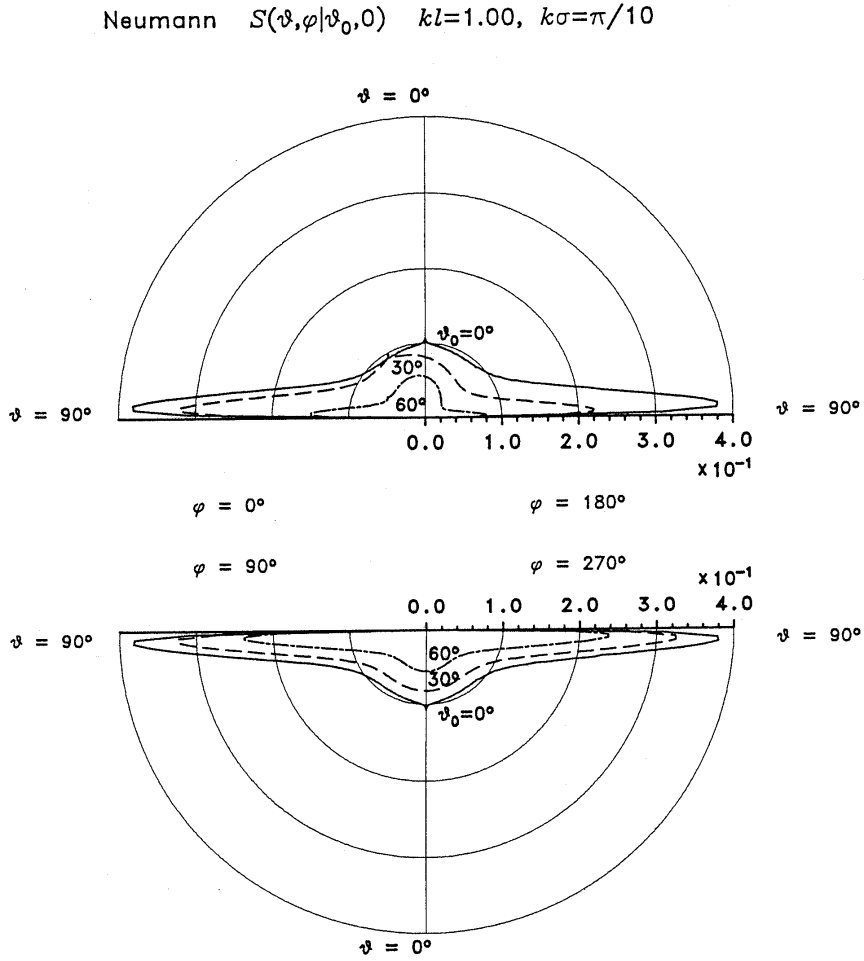

Figure 6.7. Angular distribution of incoherent scattering $S(\theta, \phi|\theta_0, 0)$ (Neumann). $kl = 1.0$.

6.5 Enhanced Backscattering

As shown in Fig. 6.6, on a broad angular distribution a small peak juts out in the backward scattering direction satisfying

$$\boldsymbol{\lambda} + \boldsymbol{\lambda}_0 = 0 \tag{6.15}$$

This is the phenomenon of the enhanced backscattering from a slightly random Neumann surface, whereas the enhancement is hardly observ-

able in the case of a slightly random Dirichlet surface. Although the backscattering enhancement has been studied for a very rough surface [42] or a random metal surface [43], the enhancement of the backscattering from a slightly random surface can be explained in the following manner.

First, from P_1 in (6.4), we may interprete the first Wiener kernel $a_1(\boldsymbol{\lambda} - \boldsymbol{\lambda}_0|\boldsymbol{\lambda}_0)$ as describing a "renormalized" or "dressed" single scattering process which we express sympolically as $\{\boldsymbol{\lambda}_0 \to \boldsymbol{\lambda}\}$ (See Fig. 6.8 (a).).

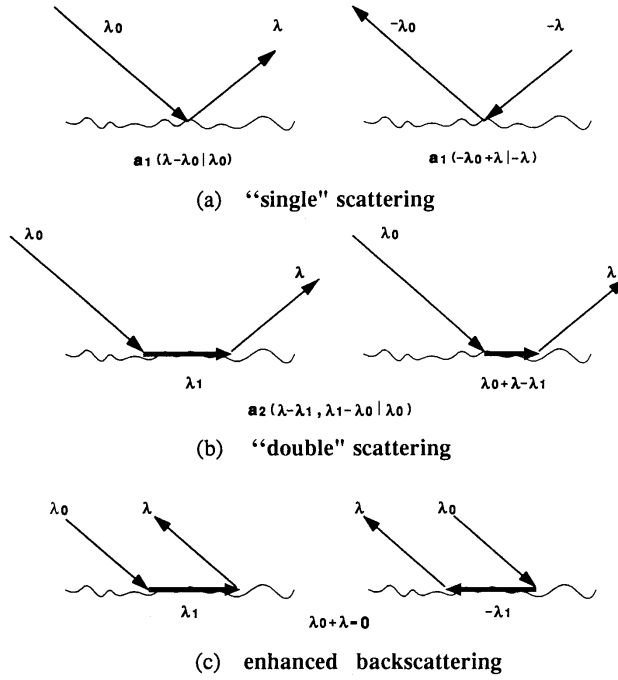

Figure 6.8. Scattering diagrams for "single" and "double" scattering processes. (a) "single" scattering process $\{\lambda_0 \to \lambda\}$ described by a_1 and its reciprocal process $\{-\lambda \to -\lambda_0\}$ (b) two "double" scattering processes described by a_2. A thick arrow shows an intermediate state. (c) enhanced "double" scattering processes for the backward direction with $\lambda_0 + \lambda = 0$.

Second, we note that the enhancement comes from P_2 given by the integral of the second kernel a_2, which is composed of two terms involving a_1 as in (6.11) or (6.13). Using (5.17) and (5.38), we can

rewrite a_2 in (6.4) in terms of a_1 in the following way:

$$
\begin{aligned}
&a_2(\boldsymbol{\lambda}-\boldsymbol{\lambda}_1,\boldsymbol{\lambda}_1-\boldsymbol{\lambda}_0|\boldsymbol{\lambda}_0)\\
&\quad=\frac{1}{4}\{S(\boldsymbol{\lambda}_1)\,[1+S(\boldsymbol{\lambda}_1)\xi(\boldsymbol{\lambda}_1)]\,a_1(\boldsymbol{\lambda}-\boldsymbol{\lambda}_1|\boldsymbol{\lambda}_1)a_1(\boldsymbol{\lambda}_1-\boldsymbol{\lambda}_0|\boldsymbol{\lambda}_0)\\
&\qquad+S(\boldsymbol{\lambda}_0+\boldsymbol{\lambda}-\boldsymbol{\lambda}_1)\,[1+S(\boldsymbol{\lambda}_0+\boldsymbol{\lambda}-\boldsymbol{\lambda}_1)\xi(\boldsymbol{\lambda}_0+\boldsymbol{\lambda}-\boldsymbol{\lambda}_1)]\\
&\quad\cdot a_1(\boldsymbol{\lambda}-(\boldsymbol{\lambda}_0+\boldsymbol{\lambda}-\boldsymbol{\lambda}_1)|\boldsymbol{\lambda}_0+\boldsymbol{\lambda}-\boldsymbol{\lambda}_1)\\
&\qquad\times a_1((\boldsymbol{\lambda}_0+\boldsymbol{\lambda}-\boldsymbol{\lambda}_1)-\boldsymbol{\lambda}_0|\boldsymbol{\lambda}_0)\}\quad\text{(Dirichlet)} \qquad (6.16)\\
&\quad=\frac{1}{4}\{[S(\boldsymbol{\lambda}_1)+\eta(\boldsymbol{\lambda}_1)]\,a_1(\boldsymbol{\lambda}-\boldsymbol{\lambda}_1|\boldsymbol{\lambda}_1)a_1(\boldsymbol{\lambda}_1-\boldsymbol{\lambda}_0|\boldsymbol{\lambda}_0)\\
&\qquad+[S(\boldsymbol{\lambda}_0+\boldsymbol{\lambda}-\boldsymbol{\lambda}_1)+\eta(\boldsymbol{\lambda}_0+\boldsymbol{\lambda}-\boldsymbol{\lambda}_1)]\,a_1(\boldsymbol{\lambda}-(\boldsymbol{\lambda}_0+\boldsymbol{\lambda}-\boldsymbol{\lambda}_1)|\boldsymbol{\lambda}_0+\boldsymbol{\lambda}-\boldsymbol{\lambda}_1)\\
&\qquad\times a_1((\boldsymbol{\lambda}_0+\boldsymbol{\lambda}-\boldsymbol{\lambda}_1)-\boldsymbol{\lambda}_0|\boldsymbol{\lambda}_0)\}\quad\text{(Neumann)} \qquad (6.17)
\end{aligned}
$$

where the correcting terms ξ^* and η^* are neglected for simplicity. They can be more concisely cast into an approximate equation,

$$
\begin{aligned}
&a_2(\boldsymbol{\lambda}-\boldsymbol{\lambda}_1,\boldsymbol{\lambda}_1-\boldsymbol{\lambda}_0|\boldsymbol{\lambda}_0)\\
&\quad\simeq\frac{1}{4}\,[S(\boldsymbol{\lambda}_1)a_1(\boldsymbol{\lambda}-\boldsymbol{\lambda}_1|\boldsymbol{\lambda}_1)a_1(\boldsymbol{\lambda}_1-\boldsymbol{\lambda}_0|\boldsymbol{\lambda}_0)\\
&\qquad+S(\boldsymbol{\lambda}_0+\boldsymbol{\lambda}-\boldsymbol{\lambda}_1)a_1(\boldsymbol{\lambda}-(\boldsymbol{\lambda}_0+\boldsymbol{\lambda}-\boldsymbol{\lambda}_1)\\
&\qquad\cdot|\boldsymbol{\lambda}_0+\boldsymbol{\lambda}-\boldsymbol{\lambda}_1)a_1((\boldsymbol{\lambda}_0+\boldsymbol{\lambda}-\boldsymbol{\lambda}_1)-\boldsymbol{\lambda}_0|\boldsymbol{\lambda}_0)] \qquad (6.18)
\end{aligned}
$$

Now, with the interpretation for a_1 in mind, we may reinterpret the decomposition of a_2 into the products of a_1's as follows: The process described by a_2 is composed of two "double scattering" processes: the first one gives the "double scattering" process, $\{\boldsymbol{\lambda}_0\to\boldsymbol{\lambda}_1\to\boldsymbol{\lambda}\}$, and the second is $\{\boldsymbol{\lambda}_0\to\boldsymbol{\lambda}+\boldsymbol{\lambda}_0-\boldsymbol{\lambda}_1\to\boldsymbol{\lambda}\}$ (See Fig. 6.8(b).). Thus, P_2 in (6.4) consists of the integration over intermediate states.

In the case of backscattering, that is, $\boldsymbol{\lambda}+\boldsymbol{\lambda}_0=0$, however, the two "double scattering" processes, $\{\boldsymbol{\lambda}_0\to\boldsymbol{\lambda}_1\to\boldsymbol{\lambda}\}$ and $\{\boldsymbol{\lambda}_0\to-\boldsymbol{\lambda}_1\to\boldsymbol{\lambda}\}$, can interfere with each other to enhance the backscattering amplitude (Fig. 6.8(c)). The reason that the enhancement is more conspicuous in the Neumann case than in Dirichlet is attributable to the anomalous scattering that occurs in the Neumann case for both incident and scattering angles close to the surface (cf. Fig. 6.7). And the anomalous scattering, closely related to the propagating mode along

the random surface, can produce a fairly large amplitude for the "double scattering" process. Therefore, on integrating over intermediate states, the contribution to the integral largely comes from such anomalous, propagating modes with $\lambda_1 \simeq k$, and as a result, the enhanced interference takes place in the backward direction, $\boldsymbol{\lambda} + \boldsymbol{\lambda}_0 = 0$. We note that there is some similarity between the enhanced backscattering from a slightly random Neumann surface and that of a metal random surface where the surface plasmon mode takes part in the scattering process [43,18].

6.6 Surface Wave Power-Flow

The surface-wave power flow P_{sf} along the surface toward the direction of incidence, as given by (4.13), is shown in Figs. 6.9 and 6.10. We note that on the Neumann random surface the surface-wave power can flow into the negative direction depending on kl and θ_0.

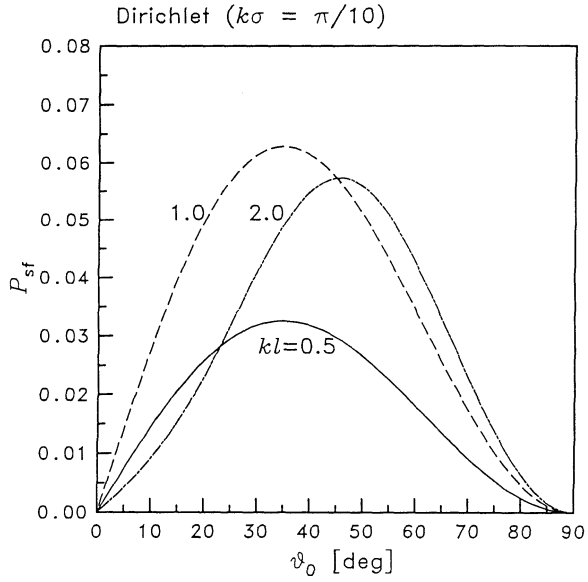

Figure 6.9. Surface wave flow P_{sf} versus incident angle θ_0 (Dirichlet). $kl = 0.5$ (solid line), 1.0 (broken line), 2.0 (chain line).

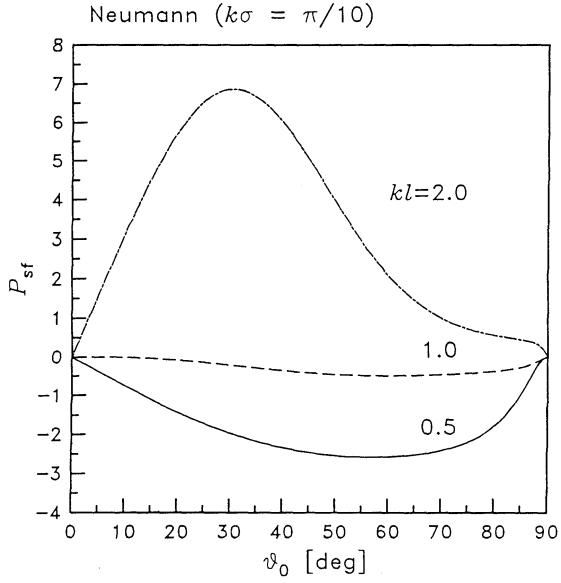

Figure 6.10. Surface wave flow P_{sf} versus incident angle θ_0 (Neumann). $kl = 0.5$ (solid line), 1.0 (broken line), 2.0 (chain line).

7. Relations to Other Theories

7.1 Perturbation Theory

The familiar Rayleigh-Rice perturbation solution can be readily obtained from our results by expanding them in powers of σ. In this section we let a parenthesized superscript indicate the order of perturbation.

7.1.1 Dirichlet Condition.

The coherent scattering amplitude is obviously the result of the second order perturbation, which is given by (5.23) and (5.20):

$$A_0^{(2)}(\boldsymbol{\lambda}) = -2S(\boldsymbol{\lambda})\xi(\boldsymbol{\lambda}) \simeq -2S(\boldsymbol{\lambda}) \int_{R_2} S(\boldsymbol{\lambda}_1)|F(\boldsymbol{\lambda}_1 - \boldsymbol{\lambda})|^2 d\boldsymbol{\lambda}_1 \tag{7.19}$$

Then the coherently scattered power is given by (4.6), i.e.,

$$p_c^{(2)} = \cos\theta_0 |A_0^{(2)}(\boldsymbol{\lambda}_0)|^2 \tag{7.20}$$

The perturbation solution for the incoherent scattering distribution can be readily obtained by expanding (6.4) in powers of σ^2. We show the expression correct up to the second-order perturbation, i.e., the term $P_1^{(1)}$ of the order of σ^2, and $P_1^{(2)}$ and $P_2^{(2)}$ of the order of σ^4.

$$\begin{aligned} P_{ptb}(\boldsymbol{\theta}|\boldsymbol{\theta}_0) =& P_1^{(1)}(\boldsymbol{\theta}|\boldsymbol{\theta}_0) + P_1^{(2)}(\boldsymbol{\theta}|\boldsymbol{\theta}_0) + P_2^{(2)}(\boldsymbol{\theta}|\boldsymbol{\theta}_0) \\ =& k^4 \cos^2\theta \cos^2\theta_0 \left\{ 4|F(\boldsymbol{\lambda}-\boldsymbol{\lambda}_0)|^2[1 - 2Re\Xi(\boldsymbol{\lambda},\boldsymbol{\lambda}_0)] \right. \\ &+ 4\int_{R_2} \left[|k^2 - \lambda_1^2| + ReS(\boldsymbol{\lambda}_1)\overline{S(\boldsymbol{\lambda}_0+\boldsymbol{\lambda}-\boldsymbol{\lambda}_1)} \right] \\ &\left. \times |F(\boldsymbol{\lambda}-\boldsymbol{\lambda}_1)F(\boldsymbol{\lambda}_1-\boldsymbol{\lambda}_0)|^2 d\boldsymbol{\lambda}_1 \right\} \qquad \text{(Dirichlet)} \end{aligned} \tag{7.21}$$

$$\Xi(\boldsymbol{\lambda},\boldsymbol{\lambda}_0) \equiv S(\boldsymbol{\lambda}_0)\xi(\boldsymbol{\lambda}_0) + S(\boldsymbol{\lambda})\xi(\boldsymbol{\lambda}) + \xi^*(\boldsymbol{\lambda},\boldsymbol{\lambda}_0) \tag{7.22}$$

$$\begin{aligned} \simeq \int_{R_2} & [S(\boldsymbol{\lambda}_0)S(\boldsymbol{\lambda}_0+\boldsymbol{\lambda}_1) + S(\boldsymbol{\lambda})S(\boldsymbol{\lambda}+\boldsymbol{\lambda}_1) \\ & + S(\boldsymbol{\lambda}+\boldsymbol{\lambda}_1)S(\boldsymbol{\lambda}_0+\boldsymbol{\lambda}_1)]\,|F(\boldsymbol{\lambda}_1)|^2 d\boldsymbol{\lambda}_1 \end{aligned} \tag{7.23}$$

where $P_1^{(1)}$ represents the well known first-order perturbation solution:

$$P_1^{(1)}(\,\boldsymbol{\theta}\,|\,\boldsymbol{\theta}_0) = 4k^4 \cos^2\theta \cos^2\theta_0 |F(\,\boldsymbol{\lambda} - \boldsymbol{\lambda}_0)|^2 \tag{7.24}$$

which follows directly from (5.24).

The perturbation solution (11.8) agrees with the result of conventional perturbation method (c.f. [44] for Dirichlet case). An extra minor term appears if we add to the effective boundary condition (5.1) the second-order correction proportional to σ^2.

7.1.2 Neumann Condition.

The perturbation expansion in the Neumann case can be obtained similarly. It is well known that the second-order perturbation gives a diverging result in the Neumann case [15] as well as in the electromagnetic case [5], unless the multiple scattering is taken into account. We can see this as follows. For instance, the coherent scattering amplitude, as a result of the second-order perturbation, is given by (5.46) and (5.42):

$$\begin{aligned} A_0^{(2)}(\boldsymbol{\lambda}) =& -\frac{2}{S(\boldsymbol{\lambda})}\eta(\boldsymbol{\lambda}) \\ \simeq& -\frac{2}{S(\boldsymbol{\lambda})}\int_{R_2} \frac{[k^2 - \boldsymbol{\lambda}_1\cdot\boldsymbol{\lambda}]^2}{S(\boldsymbol{\lambda}_1)} |F(\boldsymbol{\lambda}_1-\boldsymbol{\lambda})|^2 d\boldsymbol{\lambda}_1 \end{aligned} \tag{7.25}$$

which obviously diverges at the grazing angle $\theta_0 = 90^\circ$. Similarly we can obtain the perturbation solution for the incoherent scattering distribution, the details of which are omitted here. Although $P_1^{(1)} = 4|(k^2 - \boldsymbol{\lambda} \cdot \boldsymbol{\lambda}_0)F(\boldsymbol{\lambda} - \boldsymbol{\lambda}_0)|^2$ is finite, it does not vanish at the grazing angle $\theta = 90^\circ$ or $\theta_0 = 90^\circ$, where it ought to. Thus the first-order solution for the angular distribution $S^{(1)} = P^{(1)}/\cos\theta$ defined by (4.11) is divergent at the grazing angle. The second-order terms $P_1^{(2)}$ and $P_2^{(2)}$ are also divergent. We note that such divergence arises from the factor $1/S(\boldsymbol{\lambda})$ due to the presence of a propagating mode along the unperturbed Neumann surface, and that it causes a multiple scattering effect however small the roughness is. We have seen that such a divergence difficulty is easily overcome by the stochastic functional method, which automatically involves the multiple scattering process within the theory and calculi.

7.2 Multiple Scattering Theory

The theoretical analyses concerning the multiple scattering process on the random surface have been developed by several scholars along the line of scattering formalism, such as the diagrammatic approach by Freilikher and Fuks [6, 7], Zipfel and DeSanto [8], and the Green function approach by Ito [12] and others. S.Ito derived the Dyson and Bethe-Salpeter type integral equations for the first- and second-order moments of the Green function, from which he obtained several statistics of the random surface scattering.

We compare our results with S. Ito's [12], and see that the two different formulations give rise to almost the same results, if we properly translate the notations and definitions between the two theories. That is, the coherent reflection coefficients ([12] (33a),(33b)) are equivalent to (5.54), and the integral equations for the surface impedance ([12] (37a),(37b)) perfectly agree with (5.55) and (5.56). By a careful comparison of Ito's 2nd-order solution ([12] (54a),(54b)) with $P_1 + P_2$ given by (6.4), although it nearly agrees with the latter, we observe that his derivation of the 2nd-order solutions might yet be incomplete because the solution is devoid of the reciprocity, and not reducible to the correct 2nd-order perturbation solution when expanded in powers of σ^2 because of a missing term. We anticipate, however, that the two approaches, if correctly solved, are most probably equivalent to each other in terms of the scattering statistics. However, we stress further

that the stochastic functional approach is not only more versatile in deriving various statistical quantities but even capable of numerically calculating a random wave field for a given realization of the random surface.

8. Green Function over a 2D Random Surface

Making use of the stochastic solution for plane wave incidence, we will treat the radiation problem over a random surface, namely, the stochastic Green function. Once such a Green function is explicitly obtained, various forms of radiation and propagation can be handled in terms of the Green function. The argument goes in parallel with the case of a 1D random surface [19].

8.1 Stochastic Green Function

We denote by P_0 the location of a point source at $\mathbf{r}_0 = (r_0, \theta_0, \varphi_0)_{pol} = (\mathbf{x}_0, z_0)_{cyl}$, and by P the observation position at $\mathbf{r} = (r, \theta, \varphi)_{pol} = (\mathbf{x}, z)_{cyl}$, with $z_0, z > 0$. Let the stochastic Green function G (in cylindrical coordinates) satisfy the equation

$$(\boldsymbol{\nabla}^2 + k^2) G(\mathbf{x}, z|\mathbf{x}_0, z_0; \omega) = -\delta(\mathbf{x} - \mathbf{x}_0)\delta(z - z_0), \qquad z, z_0 > 0 \quad (8.1)$$

in the half space above the random surface. Moreover we assume that G satisfies the random boundary condition (3.9) or (3.10) as well as the radiation condition at infinity ($z \to \infty$).

For the time being we assume that the source point P_0 be located at $(0, z)$ on the z axis without loss of generality. For an arbitrary location of the source $(\mathbf{x}_0, z)$, however, the corresponding Green function can be immediately obtained from $G(\mathbf{x}, z|0, z_0; \omega)$ by means of the shift operator as follows:

$$G(\mathbf{x}, z|\mathbf{x}_0, z_0; \omega) = D^{-\mathbf{x}_0} G(\mathbf{x}, z|0, z_0; \omega) = G(\mathbf{x} - \mathbf{x}_0, z|0, z_0; T^{\mathbf{x}_0}\omega) \quad (8.2)$$

This is the translation rule for the stochastic Green function over a homogeneous random surface, though such a rule is trivial for a nonrandom flat surface.

According to (2.11) or (2.12), the stochastic Green function that is a functional of the random surface can be generally represented by a linear combination of eigenfunctions of $D^{\mathbf{a}}$ operator:

$$G(\mathbf{x}, z|0, z_0; \omega) = \int_{R_2} \phi(\mathbf{x}, z|z_0; \omega|\boldsymbol{\lambda}) d\boldsymbol{\lambda} \tag{8.3}$$

$$= \int_{R_2} e^{i\boldsymbol{\lambda}_{\mathbf{x}}} u(T^{\mathbf{x}}\omega; z, z_0|\boldsymbol{\lambda}) d\boldsymbol{\lambda}, \quad \mathbf{x} \in R_2, \qquad z, z_0 > 0 \tag{8.4}$$

that is, the stochastic Green function can be given as a superposition of the stochastic solutions for plane wave incidence. By the translation rule (8.2) we have

$$G(\mathbf{x}, z|\mathbf{x}_0, z_0; \omega) = \int_{R_2} e^{i\,\boldsymbol{\lambda}\cdot(\mathbf{x}-\mathbf{x}_0)} u(T^{\mathbf{x}}\omega; z, z_0|\,\boldsymbol{\lambda}\,) d\,\boldsymbol{\lambda}\,, \qquad z, z_0 > 0 \tag{8.5}$$

8.2 Primary Field

To start with we give the expression for the primary wave $G_0(\mathbf{x}, z|0, z_0)$, namely, the Green function over the flat surface with $\sigma^2 = 0$;

$$(\boldsymbol{\nabla}^2 + k^2) G_0(\mathbf{x}, z|0, z_0) = -\delta(\mathbf{x})\delta(z - z_0) \tag{8.6}$$

We make use of an integral representation for the free space Green function g_0,

$$g_0(\mathbf{x}, z|0, 0) = \frac{k}{4\pi} h_0^{(1)}(kr) \equiv \frac{1}{4\pi}\frac{e^{ikr}}{r} \tag{8.7}$$

$$= \frac{i}{8\pi^2} \int_{R_2} e^{i\boldsymbol{\lambda}\cdot\mathbf{x} + iS(\boldsymbol{\lambda})z} \frac{d\boldsymbol{\lambda}}{S(\boldsymbol{\lambda})} = \frac{i}{4\pi} \int_0^\infty J_0(\lambda x) \frac{e^{iS(\lambda)z}}{S(\lambda)} \lambda d\lambda, \qquad z > 0 \tag{8.8}$$

where $h_0^{(1)}(z)$ denotes the 0-th order spherical Hankel function of the first kind, $S(\boldsymbol{\lambda}) = S(\lambda) \equiv \sqrt{k^2 - \lambda^2} = k \sin\alpha$ and the branch of $S(\lambda)$ is defined as in (3.6) (cf. Fig. 11.1 below). Using (8.8), the integral representation for the Green function G_0 can be written

$$G_0(\mathbf{x}, z|0, z_0) = \frac{k}{4\pi}\left[h_0^{(1)}(kR) \mp h_0^{(1)}(kR')\right]$$
$$= \frac{i}{8\pi^2}\int_{R_2} \frac{e^{i\boldsymbol{\lambda}\cdot\mathbf{x}}}{S(\boldsymbol{\lambda})}\left[e^{iS(\boldsymbol{\lambda})|z-z_0|} \mp e^{iS(\boldsymbol{\lambda})(z+z_0)}\right] d\boldsymbol{\lambda} \quad (8.9)$$

$$R \equiv \sqrt{x^2 + (z - z_0)^2}, R' \equiv \sqrt{x^2 + (z + z_0)^2} \quad (8.10)$$

where R and R' denote the distance from P to the source P_0 and from P to the image P_0', respectively (Fig. 8.1), and the composite sign $\mp$ corresponds to the Dirichlet and Neumann condition as denoted in (3.15), and will be used throughout this section.

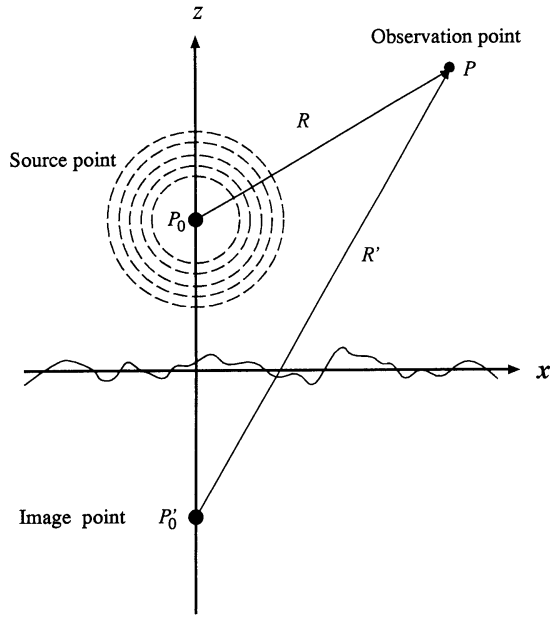

Figure 8.1. Source point P_0, image point P_0' and observation point P.

8.3 Representation of the Stochastic Green Function

When the surface is rough ($\sigma^2 > 0$) the Green function G is composed of the primary wave G_0 and the secondary wave G_s. i.e., the scattered wave due to surface roughness:

$$G(\mathbf{x}, z|0, z_0; \omega) = G_0(\mathbf{x}, z|0, z_0) \mp G_s(\mathbf{x}, z|0, z_0; \omega), \qquad z, z_0 > 0 \tag{8.11}$$

where the composite sign $\mp$ corresponds to the Dirichlet and Neumann conditions again. Comparing (3.15) and (8.3) with (8.9) and (8.11) in the region $z < z_0$ we find the relationship;

$$\phi(\mathbf{x}, z|z_0; \omega|\boldsymbol{\lambda}) = \psi(\mathbf{x}, z; \omega|\boldsymbol{\lambda}) \frac{e^{iS(\boldsymbol{\lambda})z_0}}{2iS(\boldsymbol{\lambda})}, \qquad z < z_0 \tag{8.12}$$

Hence in the region $z < z_0$ the stochastic Green function is expressed in the form:

$$G(\mathbf{x}, z|0, z_0; \omega) = \frac{i}{8\pi^2} \int_{R_2} e^{i\boldsymbol{\lambda}\cdot\mathbf{x}} \left[e^{-iS(\boldsymbol{\lambda})z} \mp e^{iS(\boldsymbol{\lambda})z} \mp U(T^x\omega, z|\boldsymbol{\lambda}) \right] \frac{e^{iS(\boldsymbol{\lambda})z_0}}{S(\boldsymbol{\lambda})} d\boldsymbol{\lambda}, \qquad z < z_0 \tag{8.13}$$

where U is given by (3.17). To obtain the Green function in the region $z > z_0$, one has to replace the first term $e^{iS(\boldsymbol{\lambda})(z_0 - z)}$ in (8.13) by $e^{iS(\boldsymbol{\lambda})(z - z_0)}$ in accordance with (8.9). Thus the scattered part G_s of the stochastic Green function can be given by the third term in (8.13), namely,

$$G_s(\mathbf{x}, z|0, z_0; \omega) = \frac{i}{8\pi^2} \int_{R_2} e^{i\boldsymbol{\lambda}\cdot\mathbf{x}} U(T^x\omega, z|\boldsymbol{\lambda}) \frac{e^{iS(\boldsymbol{\lambda})z_0}}{S(\boldsymbol{\lambda})} d\boldsymbol{\lambda} \qquad \mathbf{x} \in R_2, \qquad z, z_0 > 0 \tag{8.14}$$

$$U(T^{\mathbf{x}}\omega, z|\boldsymbol{\lambda}) = e^{iS(\boldsymbol{\lambda})z} A_0(\boldsymbol{\lambda}) + \sum_{n=1}^{\infty} \int \cdots \int_{R_2} e^{i(\boldsymbol{\lambda}_1 + \cdots + \boldsymbol{\lambda}_n)\cdot\mathbf{x} + iS(\boldsymbol{\lambda} + \boldsymbol{\lambda}_1 + \cdots + \boldsymbol{\lambda}_n)z} \times A_n(\boldsymbol{\lambda}_1, \cdots, \boldsymbol{\lambda}_n|\boldsymbol{\lambda}) \hat{h}_n[dB(\boldsymbol{\lambda}_1), \cdots, dB(\boldsymbol{\lambda}_n)], \qquad z > 0 \tag{8.15}$$

We note that the expression (8.14) holds in either region $z > z_0$ or $z < z_0$. In view of (8.15) we further divide G_s into the coherent part g_c and the incoherent part g_{ic};

$$G_s(\mathbf{x}, z|0, z_0; \omega) \equiv g_c(\mathbf{x}, z|0, z_0) + g_{ic}(\mathbf{x}, z|0, z_0; \omega) \tag{8.16}$$

where

$$g_c(\mathbf{x}, z|0, z_0) = \frac{i}{8\pi^2} \int_{R_2} e^{i\boldsymbol{\lambda}\cdot\mathbf{x} + iS(\boldsymbol{\lambda})(z+z_0)} \frac{A_0(\boldsymbol{\lambda})}{S(\boldsymbol{\lambda})} d\boldsymbol{\lambda} \tag{8.17}$$

$$g_{ic}(\mathbf{x}, z|0, z_0; \omega) = \int_{R_2} K(\mathbf{x}, z, z_0|\boldsymbol{\lambda}_1) dB(\boldsymbol{\lambda}_1) + \cdots \tag{8.18}$$

$$K(\mathbf{x}, z, z_0|\boldsymbol{\lambda}_1) \equiv \frac{i}{8\pi^2} \int_{R_2} e^{i(\boldsymbol{\lambda}+\boldsymbol{\lambda}_1)\cdot\mathbf{x} + iS(\boldsymbol{\lambda}+\boldsymbol{\lambda}_1)z + iS(\boldsymbol{\lambda})z_0} a_1(\boldsymbol{\lambda}_1|\boldsymbol{\lambda}) d\boldsymbol{\lambda} \tag{8.19}$$

$$= \frac{i}{8\pi^2} \int_{R_2} e^{i\boldsymbol{\lambda}\cdot\mathbf{x} + iS(\boldsymbol{\lambda})z + iS(\boldsymbol{\lambda}-\boldsymbol{\lambda}_1)z_0} a_1(\boldsymbol{\lambda}_1|\boldsymbol{\lambda}-\boldsymbol{\lambda}_1) d\boldsymbol{\lambda} \tag{8.20}$$

$$\mathbf{x} \in R_2, z, z_0 > 0$$

We have shown in (8.18) the contribution from the first Wiener kernel a_1, and for simplicity we will discard the terms due to a_2 and higher order kernels in the following argument.

Therefore, the total coherent part G_c can be written

$$G_c(\mathbf{x}, z|0, z_0) \equiv G_0(\mathbf{x}, z|0, z_0) \mp g_c(\mathbf{x}, z|0, z_0)$$
$$= \frac{i}{8\pi^2} \int_{R_2} \frac{e^{\boldsymbol{\lambda}\cdot\mathbf{x}}}{S(\boldsymbol{\lambda})} \left[e^{iS(\boldsymbol{\lambda})|z-z_0|} \mp (1 + A_0(\boldsymbol{\lambda})) e^{iS(\boldsymbol{\lambda})(z+z_0)} \right] d\boldsymbol{\lambda} \tag{8.21}$$
$$z, z_0 > 0$$

If we substitute into the above equations the solutions (5.12), (5.16), (5.17), (5.33), (5.37) and (5.38) for $A_0(\boldsymbol{\lambda})$ and $a_1(\boldsymbol{\lambda}_1|\boldsymbol{\lambda})$, we then obtain the Green function satisfying the Dirichlet and Neumann conditions on the random surface.

8.4 Reciprocity of Green Functions

Using the reciprocity of the Wiener kernels (3.27) in (8.15) we can easily derive the following reciprocal relation for the Green function G_s and G:

$$G_s(\mathbf{x}, z|\mathbf{x}_0, z_0) = G_s(\mathbf{x}_0, z_0|\mathbf{x}, z), \quad G(\mathbf{x}, z|\mathbf{x}_0, z_0) = G(\mathbf{x}_0, z_0|\mathbf{x}, z) \tag{8.22}$$

8.5 Distributed Image Source under the Rough Surface

For the coherent radiation we can define an equivalent image source distribution under the rough surface. We note that g_c in (8.17) reduces to (8.8) if the factor $e^{is(\boldsymbol{\lambda})z_0}A_0(\boldsymbol{\lambda})$ is removed. Therefore, the coherent part g_c can be rewritten in the form,

$$g_c(\mathbf{x}, z|0, z_0) = \int_{R_3} g_0(\mathbf{x} - \mathbf{x}', z - z')Q_c(\mathbf{r}')d\mathbf{r}' \tag{8.23}$$

where g_0 is the free space Green function and $Q_c(\mathbf{r}), \mathbf{r} = (\mathbf{x}, z)$, is the source distribution given by

$$Q_c(\mathbf{r}) \equiv \delta(z + z_0)q_c(\mathbf{x}) \tag{8.24}$$

$$q_c(\mathbf{x}) = \frac{1}{(2\pi)^2}\int_{R_2} e^{i\boldsymbol{\lambda}\cdot\mathbf{x}}A_0(\boldsymbol{\lambda})d\boldsymbol{\lambda} \tag{8.25}$$

That is, $q_c(\mathbf{x})$ represents a distributed source at the same depth with the image $z = -z_0$ which is radiating the coherent wave g_c.

Particularly when the random surface is homogeneous and isotropic so that $A_0(\boldsymbol{\lambda})$ is a function of $\lambda = |\boldsymbol{\lambda}|$ in view of (3.22), we have a revolutionary distribution,

$$g_c(\rho) = \frac{1}{2\pi}\int_0^\infty J_0(\lambda\rho)A_0(\lambda)\lambda d\lambda, \qquad \rho \equiv |\mathbf{x}| \tag{8.26}$$

9 Radiation over a Random Surface - Far Field from the Source and the Surface -

We evaluate an asymptotic form of the stochastic Green function in the region far from the radiating source. Using the asymptotic representation we can discuss various types of radiation, such as the dipole radiation or beam transmission. Assuming that the source P_0 is fixed at a position not very high above the surface, we evaluate the integrals (8.17) and (8.18) asymptotically.

9.1 Asymptotic Form of the Coherent Green Function

We first gives an integral representation for the free space Green function g_0 convenient for our purpose:

$$\begin{aligned} g_0(\mathbf{x}, z|0,0) =& \frac{1}{4\pi}\frac{e^{ikr}}{r} \\ =& \frac{ik}{16\pi^2}\int_0^{2\pi} d\beta \int_C e^{i\mathbf{k}\cdot\mathbf{r}} \sin\alpha d\alpha = \frac{ik}{8\pi}\int_{C'} e^{ikr\cos\alpha'} \sin\alpha' d\alpha' \end{aligned} \tag{9.1}$$

where $r = \sqrt{p^2+z^2}$, $\mathbf{r} = (r,\theta,\varphi)_{pol}$, $\mathbf{k} = (k,\alpha,\beta)_{pol}$, and

$$\mathbf{k}\cdot\mathbf{r} = kr\cos(\boldsymbol{\theta}-\boldsymbol{\alpha}) \equiv kr[\cos\theta\cos\alpha + \sin\theta\sin\alpha\cos(\varphi-\beta)] \tag{9.2}$$

C and C' stand for the integration contours on the complex α- and α'-plane, respectively, going from $-\epsilon+i\infty$ to $\epsilon - i\infty, \pi/2 > \epsilon > 0$.

Now we obtain an asymptotic expression of g_c given by (8.17) in the far region, $kr \equiv k\sqrt{p^2+z^2} \to \infty$. Though there are several ways for asymptotic evaluation, we apply the stationary phase method to the integral (8.17), which can be rewritten in the polar coordinates,

$$g_c(\mathbf{x}, z|0,z_0) = \frac{ik}{16\pi^2}\int_0^{2\pi} d\beta \int_C e^{ikr\cos(\alpha-\boldsymbol{\theta})} e^{ikz_0\cos\alpha} A_0(\boldsymbol{\lambda}) \sin\alpha d\alpha \tag{9.3}$$

where $\cos(\boldsymbol{\alpha}-\boldsymbol{\theta})$ is given by (9.2), and $\boldsymbol{\lambda} \equiv (\lambda,\beta)_{cyl} = (k\sin\alpha,\beta)_{cyl}$. For $kr \gg 1$ with fixed kz_0, the integral is mostly contributed from the stationary point $\boldsymbol{\alpha} = \boldsymbol{\theta}$ of the phase factor. Thus, using (9.1), we obtain an asymptotic expression,

$$g_c(x,z|0,z_0) \sim \frac{1}{4\pi}\frac{e^{ikr}}{r} e^{ikz_0\cos\theta} A_0(\boldsymbol{\lambda}_s), \qquad kr \to \infty \tag{9.4}$$

where $\boldsymbol{\lambda}_s \equiv (k\sin\theta, \varphi)_{cyl}$ denotes the projection of the scattering wave vector $k\mathbf{r}/r$ onto R_2;

$$k\mathbf{r}/r \equiv (\boldsymbol{\lambda}_s, k\cos\theta)_{cyl} \equiv (k\sin\theta, \varphi, k\cos\theta)_{cyl} \tag{9.5}$$

For another derivation we substitute (8.7) into (8.23), and putting $|\mathbf{r}-\mathbf{r}'| \sim r - (\mathbf{r}\cdot\mathbf{r}')/r, r' \ll r$, if the image source is distributed near the origin, then

$$g_c(\mathbf{x}, z|0, z_0) = \frac{1}{4\pi}\int_{R_3} \frac{e^{ik|\mathbf{r}-\mathbf{r}'|}}{|\mathbf{r}-\mathbf{r}'|} Q_c(\mathbf{r}')d\mathbf{r}' \tag{9.6}$$

$$\sim \frac{e^{ikr}}{4\pi r}\int_{R_3} e^{-ik(\mathbf{r}\cdot\mathbf{r}')/r} Q_c(\mathbf{r}')d\mathbf{r}' \tag{9.7}$$

$$= \frac{e^{ikr}}{4\pi r} e^{ikz_0\cos\theta}\int_{R_2} e^{-ik(\mathbf{r}\cdot\mathbf{x}')/r} q_c(\mathbf{x}')d\mathbf{x}' \tag{9.8}$$

which is reduced to (9.4) because of (9.5) and (8.25).

9.2 Coherent Radiation Power

Asymptotic representation for the total coherent part G_c given by (8.21) can be similarly obtained,

$$G_c(\mathbf{x}, z|0, z_0) \sim \frac{1}{4\pi}\frac{e^{ikr}}{r}\left[e^{-ikz_0\cos\theta} \mp e^{ikz_0\cos\theta}(1 + A_0(k\sin\theta, \varphi))\right], \quad kr \to \infty \tag{9.9}$$

where the term $e^{\pm ikz_0\cos\theta}$ shows the phase difference between the origin and the source P_0 or the image P_0'. Using this we can calculate the coherent power scattered into a unit solid angle in the (θ, φ) direction:

$$\begin{aligned} P_c(\theta, \varphi; z_0) &= \lim_{r\to\infty} rIm\left[\overline{G_c}\frac{\partial G_c}{\partial r}\right] \\ &= P_{00}|e^{-ikz_0\cos\theta} \mp e^{ikz_0\cos\theta}[1 + A_0(k\sin\theta, \varphi)]|^2 \end{aligned} \tag{9.10}$$

where $P_{00} \equiv 1/(4\pi)^2$ denotes the power flow per unit solid angle radiated from a point source.

9.3 Asymptotic Form of the Incoherent Green Function

Let us evaluate an asymptotic representation for the incoherent part of the Green function g_{ic}. For simplicity we deal with only the first Wiener kernel and neglect the higher order corrections to calculate g_{ic}. First we rewrite (8.20) as

$$K(\mathbf{x}, z, z_0|\boldsymbol{\lambda}_1) = \frac{1}{16\pi^2}\int_0^{2\pi} d\beta \times \int_C e^{ikrcos(\boldsymbol{\alpha}-\boldsymbol{\theta})} e^{iS(\boldsymbol{\lambda}-\boldsymbol{\lambda}_1)z} a_1(\boldsymbol{\lambda}_1|\boldsymbol{\lambda}-\boldsymbol{\lambda}_1)\cos\alpha\sin\alpha d\alpha \tag{9.11}$$

where C denotes the contour in the complex α-plane as in (9.1). In the same manner as the coherent case, we obtain the asymptotic expression for K;

$$K(x, z, z_0|\lambda_1) \sim \frac{1}{4\pi^2}\frac{e^{ikr}}{r} k\cos\theta e^{iS(\boldsymbol{\lambda}_s-\boldsymbol{\lambda}_1)z_0} a_1(\boldsymbol{\lambda}_1|\boldsymbol{\lambda}_s-\boldsymbol{\lambda}_1), \qquad kr\to\infty \tag{9.12}$$

where $\boldsymbol{\lambda}_s \equiv (k\sin\theta, \varphi)_{cyl}$ as defined by (9.5). Substituting (9.12) into (8.18), we obtain the asymptotic representation of the incoherent part of Green function:

$$g_{ic}(\mathbf{x}, z|0, z_0; \omega) \sim \frac{1}{4\pi^2}\frac{e^{ikr}}{r} k\cos\theta \int_{R_2} e^{iS(\boldsymbol{\lambda}_s-\boldsymbol{\lambda})z_0} a_1(\boldsymbol{\lambda}|\boldsymbol{\lambda}_s-\boldsymbol{\lambda}) dB(\boldsymbol{\lambda}) \tag{9.13}$$

9.4 Incoherent Radiation Power

The incoherent power scattered into a unit solid angle in the (θ, φ) direction can be calculated as follows:

$$P_{ic}(\theta, \varphi; z_0) = \lim_{r\to\infty}\left\langle rIm\left[\overline{g_{ic}}\frac{\partial g_{ic}}{\partial r}\right]\right\rangle = P_{00}k^2\cos^2\theta\int_{R_2} e^{-2ImS(\boldsymbol{\lambda})z_0}|a_1(\boldsymbol{\lambda}_s-\boldsymbol{\lambda}|\boldsymbol{\lambda})|^2 d\boldsymbol{\lambda} \tag{9.14}$$

$$\simeq P_{00}k^2\cos^2\theta\int_{\lambda^2<k^2}|a_1(\boldsymbol{\lambda}_s-\boldsymbol{\lambda}|\boldsymbol{\lambda})|^2d\boldsymbol{\lambda} \tag{9.15}$$

$$=P_{00}\int_0^{2\pi}\int_0^{\pi/2}\frac{P(\theta,\varphi|\theta_0,\varphi_0)}{\cos\theta_0}\sin\theta_0 d\theta_0 d\varphi_0 \tag{9.16}$$

where $P_{00}=1/(4\pi)^2$ and (9.15) is an approximate evaluation by neglecting the surface wave part for $kz_0\gg 1$.

9.5 Power Conservation for Radiation

As shown in Fig. 9.1 let S_0 denote a small sphere with center at P_0 and radius $a(\to 0)$, and S the hemisphere with large radius $R(\to\infty)$ above the random surface. By the divergence theorem again we have the almost sure equality for the total power flow through S_0 and S:

$$\frac{1}{k}\int_{S_0}\mathrm{Im}\left[\overline{G}\frac{\partial G}{\partial r}\right]_{r=a}dS=\frac{1}{k}\int_{S_0}\mathrm{Im}\left[\overline{G}\frac{\partial G}{\partial r}\right]_{r=R}dS\qquad(a.s) \tag{9.17}$$

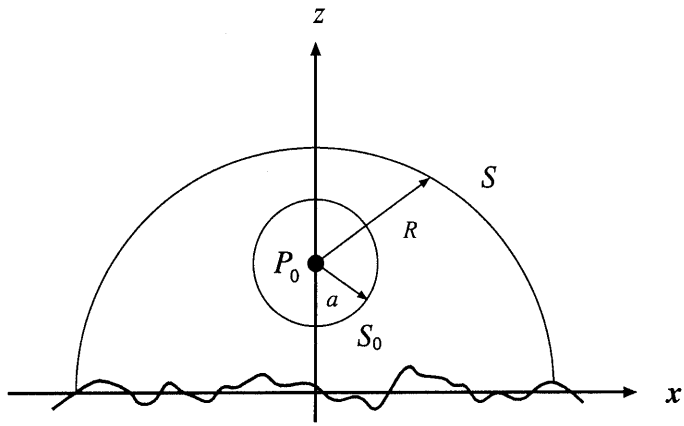

Figure 9.1. Spheres S and S_0 for integrating the power flow from the source P_0 above the random surface.

In the limit $a \to 0$, $R \to \infty$, we get the equality

$$\frac{1}{4\pi} \equiv 4\pi P_{00} = \frac{1}{k} \int_0^{2\pi} d\varphi \int_0^{\pi/2} \left[\overline{G} \frac{\partial G}{\partial r} r^2 \right]_{r=\infty} \sin\theta d\theta \qquad (a.s.) \quad (9.18)$$

where the lefthand side equals the total radiation power from the point source. In what follows a power is always normalized by the monopole radiation power. Since (9.18) is an almost sure equality with a constant on the lefthand side, we can take the average to obtain equality. Therefore, substituting $G = G_c + g_{ic}$ into (9.18) to take an average, we get the equality,

$$1 = \frac{1}{4\pi P_{00}} \int_0^{2\pi} d\varphi \int_0^{\pi/2} \frac{1}{k} \mathrm{Im} \left[\overline{G_c} \frac{\partial G_c}{\partial r} r^2 + \left\langle \overline{g_{ic}} \frac{\partial g_{ic}}{\partial r} \right\rangle r^2 \right]_{r=\infty} \sin\theta d\theta \quad (9.19)$$

which can be rewritten as a power conservation formula in terms of P_c and P_{ic};

$$1 = \frac{1}{4\pi P_{00}} \int_0^{2\pi} d\varphi \int_0^{\pi/2} [P_c(\theta, \varphi; z_0) + P_{ic}(\theta, \varphi; z_0)] \sin\theta d\theta \qquad (9.20)$$

In the special case of a flat surface with $\sigma^2 = 0$, we have $P_{ic} = 0$ and P_c is obtained from (9.10) by putting $A_0 = 0$. Then the righthand side gives

$$P_{asym} = \frac{1}{4\pi} \int_0^{2\pi} d\varphi \int_0^{\pi/2} |2 \left\{ \begin{matrix} \sin \\ \cos \end{matrix} \right\} (kz_0 \cos\theta)|^2 \sin\theta d\theta \quad (9.21)$$

$$= 1 \mp \frac{1}{2} \frac{\sin 2kz_0}{kz_0} \quad (9.22)$$

where $\mp$ sign refers to the Dirichlet and Neumann conditions. It is noticed that P_{asym} may not be equal to 1 because of asymptotic evaluation: however, P_{asym} is nearly equal to 1 if $kz_0 \gg l$.

10. Radiation Characteristics

We show some examples for the angular distribution of the coherent and the incoherent power flow from a point source above the random surface.

10.1 Dirichlet Condition

Figure 10.1 shows the angular coherent distribution of the total coherent power (9.10) for the source altitude $kz_0 = 10$. Oscillatory patterns reaching the top ($P_c/P_{00} = 4$) corresponds to $\sigma^2 = 0$ (flat surface), which is due to the interference of the direct wave from the source P_0 and the reflected wave from the image source P_0', the number of peaks being roughly kz_0/π. For small roughness as treated here, the interference pattern is only slightly modified by the coherent-scattering amplitude A_0 shown in Fig. 6.1. The angular distribution of the incoherent power flow $P_{ic}(\theta; z_0)$ can be calculated from (9.14). The distribution is not dependent on the source altitude z_0 if $kz_0 > 10$ since the surface waves are less excited. Figure 10.2 shows $P_{ic}(\theta; z_0)$ for $k\sigma = \pi/10$ and $kz_0 = 10$.

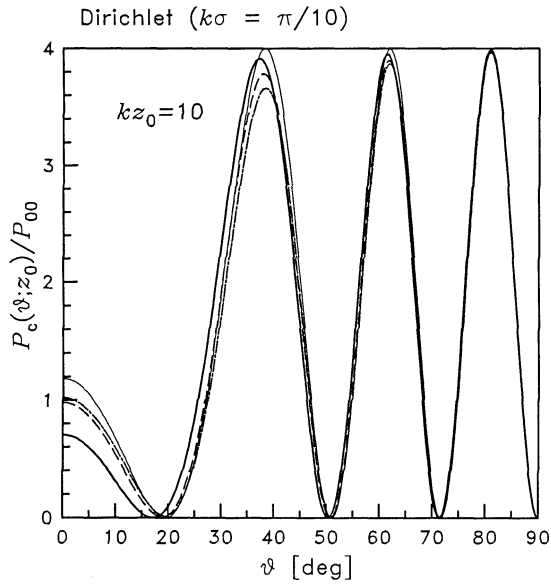

Figure 10.1. Angular distribution of total coherent power flow (Dirichlet). $k\sigma = \pi/10$, $kz_0 = 10$; $kl = 0.5$ **(solid line), 1.0 (broken line), 2.0 (chain line). The thin solid line corresponds to the flat surface** ($\sigma^2 = 0$). $P_c(\theta; z_0)$ **is normalized by** P_{00}, **the total power flow from the source.**

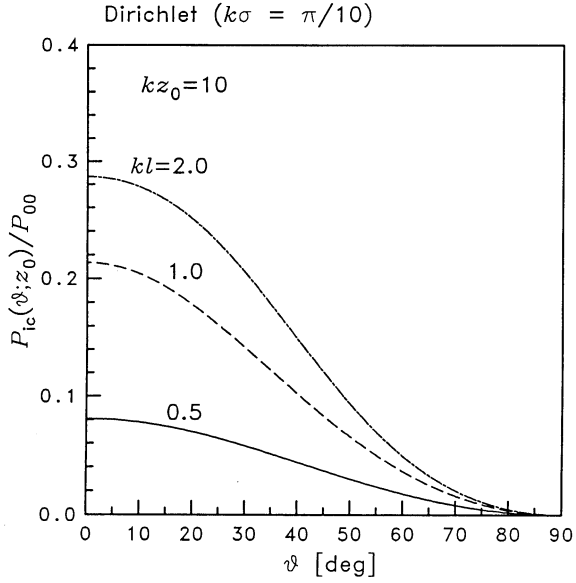

Figure 10.2. Angular distribution of incoherent power flow (Dirichlet). $k\sigma = \pi/10$, $kz_0 = 10$; $kl = 0.5$ **(solid line), 1.0 (broken line), 2.0 (chain line).** $P_{ic}(\theta; z_0)$ **is normalized by** P_{00}.

10.2 Neumann Condition

Figure 10.3 shows the angular coherent distribution of the total coherent power $P_c(\theta; z_0)$ calculated from (5.33) and (9.10). As compared with Dirichlet's case in Fig. 10.1, there is a remarkable difference in the distribution near $\theta = 90°$. This is because, as shown by (5.33) and (5.37), $A_0(\boldsymbol{\lambda}) = 0$ for the flat surface with $\sigma^2 = 0$, whereas for $\sigma^2 > 0$, however small it is, we have $A_0(\mathbf{k}) = -2(1 + A_0 = -1)$, which means that in the random Neumann case the coherent reflection near $\theta = 90°$ looks almost like Dirichlet's. This is one of the distinguishing characteristics of the Neumann random surface closely related to the anomalous scattering. The angular distribution of the incoherent power flow $P_{ic}(\theta; z_0)$ calculated from (9.14) and (5.38) are shown in Fig. 10.4 for $k\sigma = \pi/10$ and $kz_0 = 10$. The distribution is again independent of the source altitude z_0.

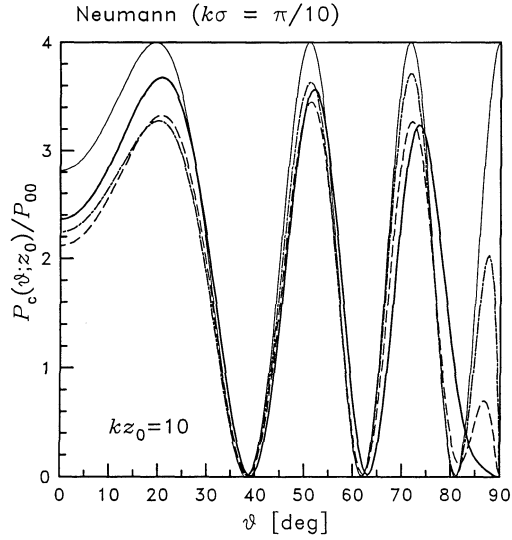

Figure 10.3. Angular distribution of total coherent power flow (Neumann). $k\sigma = \pi/10$, $kz_0 = 10$; $kl = 0.5$ (solid line), 1.0 (broken line), 2.0 (chain line). The thin solid line corresponds to the flat surface ($\sigma^2 = 0$). $P_c(\theta; z_0)$ is normalized by P_{00}, the total power flow from the source.

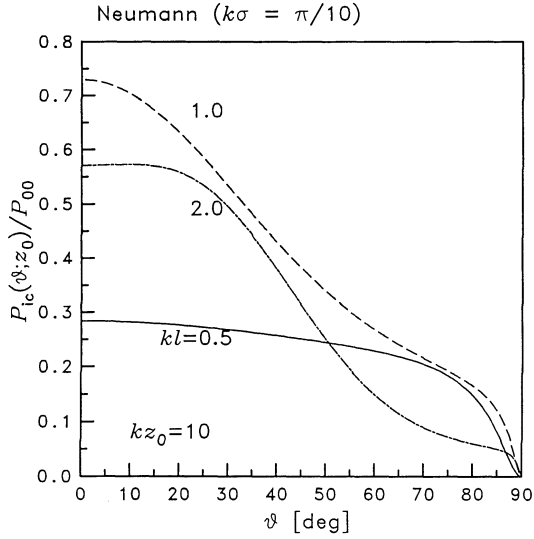

Figure 10.4. Angular distribution of incoherent power flow (Dirichlet). $k\sigma = \pi/10$, $kz_0 = 10$; $kl = 0.5$ (solid line), 1.0 (broken line), 2.0 (chain line). $P_{ic}(\theta; z_0)$ is normalized by P_{00}.

11 Propagation over a Random Surface - Far Field along the Surface

In the radio-wave transmission, the altitude z of the receiving antenna is usually of the same order as the altitude z_0 of the transmitting antenna, even if the propagation distance ρ is increased $(k\rho \to \infty)$. This means that the zenith angle of $\mathbf{x}$ in (9.5) is almost $\theta = \pi/2$, so that the asymptotic expressions (9.9) and (9.13) given in the preceding chapter are no longer valid since the saddle point λ_s coincides with a branch point $\lambda = k$. Therefore, we evaluate a new asymptotic form of the Green function for $k\rho \to \infty$ with kz and kz_0 fixed.

11.1 Asymptotic Form of the Coherent Green Function

11.1.1 Coherent Part of the Green Function.

For simplicity we assume the random surface is isotropic so that by (2.27) and (3.22) we have $F(\boldsymbol{\lambda}) = F(\lambda)$, $A_0(\boldsymbol{\lambda}) = A_0(\lambda)$, $\lambda = |\boldsymbol{\lambda}| = \sqrt{\lambda_x^2 + \lambda_y^2}$, and without loss of generality the azimuth angle of the observation point be put $\varphi = 0$ and $\mathbf{x} = (\rho, 0)_{cyl}$. Then the coherent part of the secondary wave (8.17) can be written

$$g_c(\mathbf{x}, z|0, z_0) = \frac{i}{8\pi^2} \int_{R_2} e^{i\lambda\rho\cos\alpha + iS(\lambda)(z+z_0)} \frac{A_0(\lambda)}{S(\lambda)} \lambda d\lambda d\alpha \quad (11.1)$$

$$\sim \frac{i}{4\pi} \frac{1}{\sqrt{2\pi}} \int_{-\infty}^{\infty} \frac{e^{i\lambda\rho}}{\sqrt{i\lambda\rho}} e^{iS(\lambda)(z+z_0)} \frac{A_0(\lambda)}{S(\lambda)} \lambda d\lambda \quad (11.2)$$

where (11.2) is obtained using either the asymptotic form of Bessel function or the stationary phase method and the the contour of integration is taken as in Fig. 11.1 to detour around the branch cuts. To proceed further with the asymptotic evaluation, we make the transformation of variable;

$$s = (k^2 - \lambda^2)^{1/2}, \quad \lambda(s) = (k^2 - s^2)^{1/2} \quad (11.3)$$

so that the two-valued neighborhood at the branch point $\lambda = k$ is transformed into a single-valued neighborhood at $s = 0$. Then, by deforming the contour as in Fig. 11.2 assuming $\rho > 0$, (11.2) can be rewritten

$$g_c(\mathbf{x}, z|0, z_0) \sim \frac{1}{4\pi} \sqrt{\frac{i}{2\pi\rho}} \int_{-\infty}^{\infty} e^{i\lambda(s)\rho + iS(\lambda)(z+z_0)} \frac{A_0(\lambda(s))}{\sqrt{\lambda(s)}} ds \quad (11.4)$$

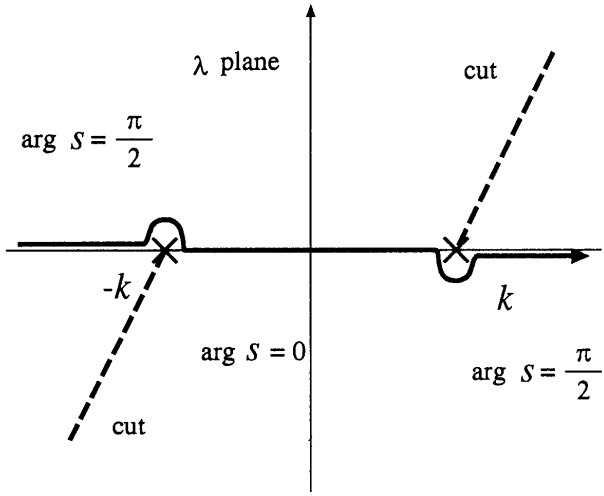

Figure 11.1. Contour of integration on λ plane and the branch cuts of $S(\lambda)$.

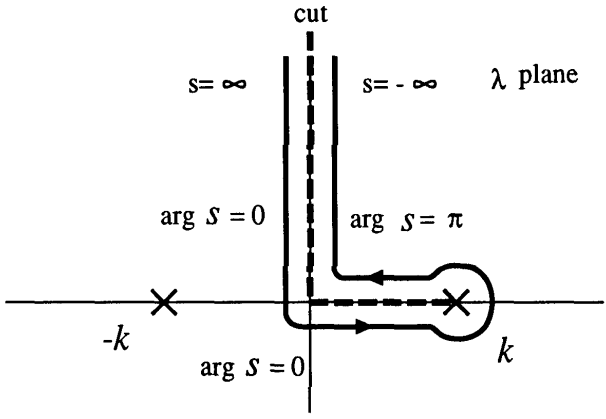

Figure 11.2. Deformed contour in λ plane.

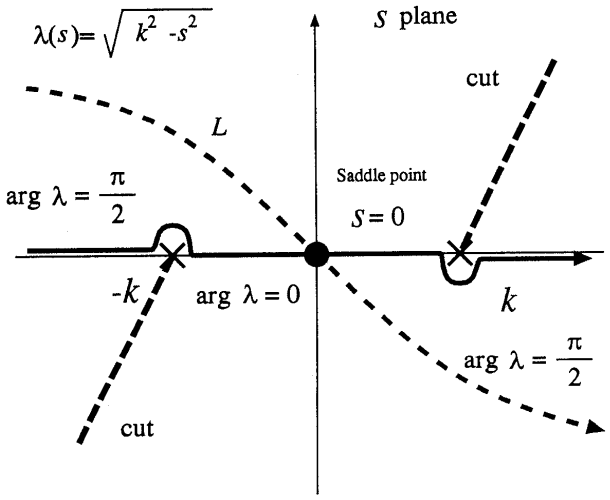

Figure 11.3. Contour in s plane and saddle point $s = 0$.

where the contour is shown in Fig. 11.3. We make similar argument to obtain an asymptotic integral representation for the total coherent part (8.21),

$$G_c(\mathbf{x}, z|0, z_0) \sim \frac{1}{4\pi}\sqrt{\frac{i}{2\pi\rho}}\int_{-\infty}^{\infty} e^{i\lambda(s)\rho} f(s)ds \tag{11.5}$$

$$f(s) \equiv \frac{1}{\sqrt{\lambda(s)}}\left\{e^{-is(z-z_0)} \mp e^{is(z+z_0)}[1 + A_0(\lambda(s))]\right\} \tag{11.6}$$

$$= \frac{1}{\sqrt{\lambda(s)}}\left\{e^{-is(z-z_0)} - e^{is(z+z_0)}[1 \pm sa_0(\lambda(s))]\right\} \tag{11.7}$$

$$a_0(\lambda) = -\frac{2\xi}{1 + s\xi}, \quad \text{(Dirichlet)} \tag{11.8}$$

$$a_0(\lambda) = \frac{2\eta}{s + \eta}, \quad \text{(Neumann)} \tag{11.9}$$

where (5.16) and (5.37) are used for a_0. The above representation is valid for $\rho > 0$ and no longer depends on whether $z > z_0$ or $z < z_0$.

11.1.2 Asymptotic Form due to the Saddle Point Method.

We apply the saddle point method [41] to (11.5). Since $\lambda'(0) = 0$, saddle point is $s = 0(\lambda(0) = k)$, we make the change of variable $s \to t$, by which the path of steepest descent is defined;

$$\begin{aligned} i\lambda(s) \equiv & \sqrt{s^2 - k^2} = ik - t^2, \quad -\infty < t < \infty \\ s \equiv & s(t) \equiv t\sqrt{t^2 - 2ik} \end{aligned} \tag{11.10}$$

Then, $s \cong \sqrt{-2ik}t(t \cong 0)$ by (11.10), and we see that the path of steepest descent L passes the saddle point $s = 0$ at the angle $\pi/4$ (Fig. 11.3). We obtain the asymptotic expansion;

$$\int_{-\infty}^{\infty} e^{i\lambda(s)\rho} f(s) ds = e^{ik\rho} \int_{-\infty}^{\infty} e^{-t^2\rho} F(t) dt \tag{11.11}$$

$$\sim \frac{e^{ik\rho}}{\sqrt{\rho}} \sum_{n=0}^{\infty} \frac{F^{(2n)}(0)}{(2n)!} \frac{\Gamma(n + \frac{1}{2})}{\rho^n} \tag{11.12}$$

where

$$F(t) \equiv f(s)\frac{ds}{dt} = \sum_{n=0}^{\infty} \frac{F^{(n)}(0)}{n!} t^n \tag{11.13}$$

$$\begin{aligned} F(0) = & f(0)\sqrt{-2ik} \\ F''(0) = & f''(0)[-2ik]^{3/2} + f(0)\frac{3}{\sqrt{-2ik}}, \cdots \end{aligned} \tag{11.14}$$

where the primes denote differentiation. In view of (11.7) we have at the saddle point

$$f(0) = 0 \tag{11.15}$$

in either boundary condition, which means the first term vanishes in the asymptotic expansion, and that the second term has to be calculated. Thus, using (11.7) (11.14) we obtain

$$G_c(\mathbf{x}, z|0, z_0) \sim \frac{1}{8\pi}\sqrt{k}k^3 f''(0)\frac{e^{ik\rho}}{(k\rho)^2} \tag{11.16}$$

$$f''(0) = \frac{2}{\sqrt{k}}\left[2zz_0 \mp i(z + z_0)a_0(k) \mp \frac{\partial}{\partial s}a_0(k)|_{s=0}\right] \tag{11.17}$$

where we have regarded $a_0(\lambda)$ as a function of the form $a_0(\lambda(s), s)$ upon differentiation. Substituting (5.16) and (5.37) into $a_0(k)$ we obtain the asymptotic expression for the coherent Green function:

$$G_c(\mathbf{x}, z|0, z_0) \sim \frac{k^3}{\pi} \frac{e^{ik\rho}}{(k\rho)^2} \left[zz_0 + i(z + z_0)\xi(k) - \xi^2(k) \right] \quad \text{(Dirichlet)} \tag{11.18}$$

$$\sim \frac{k^3}{2\pi} \frac{e^{ik\rho}}{(k\rho)^2} \left[zz_0 + i(z + z_0) \frac{1}{\eta(k)} - \frac{1}{\eta^2(k)} \right] \quad \text{(Neumann)} \tag{11.19}$$

$$k\rho \gg |k/\eta|^2 \simeq 1/(k\sigma)^4$$

$$\xi(k) \simeq \int_{R_2} S(\lambda) |F(|\boldsymbol{\lambda} - \boldsymbol{k}|)|^2 d\boldsymbol{\lambda} \tag{11.20}$$

$$\eta(k) \simeq \int_{R_2} \frac{[k^2 - \boldsymbol{\lambda} \cdot \boldsymbol{k}]^2}{S(\lambda)} |F(|\boldsymbol{\lambda} - \boldsymbol{k}|)|^2 d\boldsymbol{\lambda} \tag{11.21}$$

where we have put $\xi(k) = \xi(\boldsymbol{k})$ and $\eta(k) = \eta(\boldsymbol{k})$. The condition attached to (11.19) is explained below.

11.1.3 Asymptotic Form in the "Medium Range" over a Neumann Random Surface (Effect of a Pole on the Saddle).

In the Neumann case, as shown by (11.9), $a_0(\lambda(s))$ has a pole, $s \simeq -\eta(k)$, which gets closer to the saddle point $s = 0$ as the random surface becomes smoother; $\eta \simeq (k\sigma)^2 \to 0$. The asymptotic evaluation (11.16) is valid under the condition that in (11.11) the distance from the saddle point to the pole is sufficiently larger than the saddle width; that is, $|\eta|/\sqrt{2k} \gg 1/\sqrt{\rho}$. Since η is of the order of $(k\sigma)^2$, this can be rewritten

$$k\rho \gg |k/\eta|^2 \sim 1/(k\sigma)^4 \tag{11.22}$$

which is the condition for (11.19).

On the other hand, when $|\eta|$, or the surface roughness $k\sigma$ is sufficiently small or the distance $k\rho$ is not very large such that the pole gets in the saddle region, the saddle-point evaluation is subject to change as follows [45]. Let us call it "medium range", when the observation point along the surface is in the Fraunhofer region relative

to the distance $z + z_0$ between the source and its image, but still it is relatively near in such a way that

$$[k(z + z_0)]^2 \ll k\rho \ll |k/\eta|^2 \cong 1/(k\sigma)^4 \tag{11.23}$$

and we discriminate it from the "far range" satisfying (11.22). To obtain the asymptotic form in the medium range we employ (11.6) for $f(s)$, putting

$$f(s) = f_0(s) + f_1(s) \tag{11.24}$$

$$f_0(s) \equiv \frac{1}{\sqrt{\lambda(s)}} \left\{ e^{-is(z-z_0)} + e^{is(z+z_0)} \right\} \tag{11.25}$$

$$f_1(s) \equiv \frac{1}{\sqrt{\lambda(s)}} e^{is(z+z_0)} A_0(\lambda(s)) = -2\eta \frac{1}{\sqrt{\lambda(s)}} e^{is(z+z_0)} \frac{1}{s+\eta} \tag{11.26}$$

For simplicity we fix $\eta = \eta(k)$, and make the change of variable by (11.10) to obtain

$$\begin{aligned} &\int_{-\infty}^{\infty} e^{i\lambda(s)\rho} f_1(s) ds \\ &\cong -2\eta \frac{e^{ik\rho}}{\sqrt{k}} \int_{-\infty}^{\infty} e^{-t^2\rho} e^{(1+i)\sqrt{k}(z+z_0)t} \frac{1}{t+\eta_0} dt \qquad (11.27) \\ &= -2\eta \frac{e^{ik\rho}}{\sqrt{k}} \left\{ (1+i)\sqrt{k}(z+z_0)\sqrt{\frac{\pi}{\rho}} \right. \\ &\qquad \left. + \left[1 - \eta_0(1+i)\sqrt{k}(z+z_0) \right] I(\rho) \right\} \qquad (11.28) \end{aligned}$$

where we have put

$$\eta_0 \equiv \frac{1}{\sqrt{-2ik}}\eta = \frac{1}{2\sqrt{k}}(1+i)\eta \equiv p + iq \tag{11.29}$$

$$I(\rho) \equiv \int_{-\infty}^{\infty} e^{-t^2\rho} \frac{dt}{t+\eta_0} \equiv I_1(\rho) - iI_2(\rho) \tag{11.30}$$

$$I_1(\rho) \equiv \int_{-\infty}^{\infty} e^{-t^2\rho} \frac{t+p}{(t+p)^2+q^2} dt \tag{11.31}$$

$$I_2(\rho) \equiv \int_{-\infty}^{\infty} e^{-t^2\rho} \frac{q}{(t+p)^2+q^2} dt \tag{11.32}$$

Therefore, we obtain the following asymptotic form in the medium range for the coherent part g_c,

$$g_c(\mathbf{x}, z|0, z_0) \sim \frac{i}{8\pi^2}\sqrt{\frac{2\pi}{i\rho}}\int_{-\infty}^{\infty} e^{i\lambda(s)\rho} f_1(s)ds \tag{11.33}$$

$$\sim -\eta\frac{i}{2\pi}\frac{e^{ik\rho}}{\rho}(z+z_0) - \eta\frac{1+i}{4\pi^2}\sqrt{\frac{\pi}{k\rho}}e^{ik\rho}[1-i\eta(z+z_0)]I(\rho) \tag{11.34}$$

and for the total coherent part G_c including the primary wave G_0, we have

$$G_c(\mathbf{x}, z|0, z_0) \sim \frac{1}{2\pi}\frac{e^{ik\rho}}{\rho}[1-i\eta(z+z_0)] - \eta\frac{1+i}{4\pi^2}\sqrt{\frac{\pi}{k\rho}}e^{ik\rho}[1-i\eta(z+z_0)]I(\rho)$$
$$[k(z+z_0)]^2 \ll k\rho \ll |k/\eta|^2 \tag{11.35}$$

11.1.4 Asymptotic Behavior of the Coherent Green Function

First we note the asymptotic behavior of the Green function G_0 for a perfectly flat surface $(\sigma^2 = 0)$, i.e., (8.9):

$$G_0(\mathbf{x}, z|0, z_0) \sim \frac{k^3}{2\pi}\frac{e^{ik\rho}}{(k\rho)^2}zz_0 \qquad \text{(Dirichlet)} \tag{11.36}$$

$$G_0(\mathbf{x}, z|0, z_0) \sim \frac{k}{2\pi}\frac{e^{ik\rho}}{k\rho} \qquad \text{(Neumann)} \tag{11.37}$$

Expression (11.36) agrees with the first term of (11.18), implying that the radiation along the surface looks like a dipole field decaying in proportion to $1/(k\rho)^2$. This is because of the cancellation of the monopole fields from the source and the image decaying in proportion to $1/k\rho$, whereas (11.37) is just twice of (8.7), implying that the two monoploe fields add up in phase along the surface.

However, when the surface is random $(\sigma^2 > 0)$ the asymptoric form of the coherent Green function for the Dirichlet random surface is given by (11.18) in both medium and far ranges, which decays in

proportion to $1/(k\rho)^2$ as $k\rho \to \infty$. For the Neumann random surface the asymptotic form has different expressions in the two ranges. In the medium range with small η, the first term in (11.35) is dominant and G_c decays like (11.37) in proportion to $1/k\rho$, but the second term becomes more effective as $k\rho$ gets larger. In the far range, however, the asymptoric form (11.19) behaves like the Dirichlet case (11.18), decaying in proportion to $1/(k\rho)^2$ faster than in the medium range. This means that in the far region (11.22) the Neumann random surface looks like a Dirichlet surface. We note further that their dependence on the roughness parameter σ^2 is quite different in (11.18) and (11.19). The former consists of the terms with positive powers $(\sigma^0, \sigma^2, \sigma^4)$, but the latter has the terms with negative powers $(\sigma^0, 1/\sigma^2, 1/\sigma^4)$ although it is subject to the condition (11.22). The latter property, though seemingly contradictory, can be explained in the following way: The asymptotic field (11.37) for $\sigma^2 = 0$ that the factor $(k\rho)^{-1}$ decays with distance much slower than (11.19) with the factor $(k\rho)^{-2}$; that is, at a large distance in the far region, the field for $\sigma^2 = 0$ has much larger amplitude than (11.19). Therefore, it is most likely that in the Neumann case the field in the far region along the surface is increased as σ^2 is made smaller. As shown below, similar behavior appears in the asymptotic form of the incoherent amplitude.

11.2 Asymptotic Form of the Incoherent Green Function

11.2.1 Asymptotic Form of the Wiener Kernel.

To obtain the asymptotic form of the coherent part g_{ic} given by (8.18), we evaluate the asymptotic form of the Wiener kernel $K(\mathbf{x}, z, z_0 | \boldsymbol{\lambda}_1)$ for $k\rho \to \infty$. For this purpose we divide the parameter space $\boldsymbol{\lambda}_1 \in R_2$ into two domains D_1 and D_2 as we define below, and we use two expressions (8.19) and (8.20) for K according to D_1 and D_2:

$$K(\mathbf{x}, z, z_0 | \boldsymbol{\lambda}_1) = \frac{i}{8\pi^2} e^{i\boldsymbol{\lambda}_1 \cdot \mathbf{x}} \int_0^\infty \lambda d\lambda \times \int_0^{2\pi} e^{i\lambda\rho\cos\alpha + iS(\boldsymbol{\lambda}+\boldsymbol{\lambda}_1)z + iS(\boldsymbol{\lambda})z_0} a_1(\boldsymbol{\lambda}_1 | \boldsymbol{\lambda}) d\alpha \qquad \boldsymbol{\lambda}_1 \in D_1 \tag{11.38}$$

$$
\begin{aligned}
&= \frac{i}{8\pi^2} \int_0^\infty \lambda d\lambda \\
&\quad \times \int_0^{2\pi} e^{i\lambda\rho\cos\alpha + iS(\boldsymbol{\lambda})z + iS(\boldsymbol{\lambda}-\boldsymbol{\lambda}_1)z_0} a_1(\boldsymbol{\lambda}_1|\boldsymbol{\lambda}-\boldsymbol{\lambda}_1) d\alpha \\
&\qquad\qquad \boldsymbol{\lambda}_1 \in D_2
\end{aligned}
\tag{11.39}
$$

where, in view of the reciprocity (3.26), we can employ the following relation;

$$
a_1(\boldsymbol{\lambda}_1|\boldsymbol{\lambda}-\boldsymbol{\lambda}_1) = a_1(\boldsymbol{\lambda}_1|-\boldsymbol{\lambda}) \tag{11.40}
$$

Without loss of generality we assume the azimuth angle of $\mathbf{x}$ be $\varphi = 0$: $\mathbf{x} = (\rho, 0)_{cyl}$, $\boldsymbol{\lambda}_1 = (\lambda_1, \alpha_1)$. For $k\rho \to \infty$, we first evaluate the integral over α by the stationary phase method. Summing the contributions from two stationary points $\alpha = 0, \pi$, we get

$$
\begin{aligned}
&K(\mathbf{x}, z, z_0|\boldsymbol{\lambda}_1) \\
&= x\sqrt{\frac{i}{2\pi\rho}} e^{i\boldsymbol{\lambda}_1\cdot\mathbf{x}} \int_{-\infty}^{\infty} e^{i\lambda\rho} \frac{1}{\sqrt{\lambda}} \left[e^{iS(\boldsymbol{\lambda}+\boldsymbol{\lambda}_1)z + iS(\boldsymbol{\lambda})z_0} a_1(\boldsymbol{\lambda}_1|\boldsymbol{\lambda}) \right]_{\alpha=0} \lambda d\lambda \\
&\qquad\qquad \boldsymbol{\lambda}_1 \in D_1
\end{aligned}
\tag{11.41}
$$

$$
\begin{aligned}
&= \frac{1}{4\pi}\sqrt{\frac{i}{2\pi\rho}} \int_{-\infty}^{\infty} e^{-i\lambda\rho} \frac{1}{\sqrt{\lambda}} \left[e^{iS(\boldsymbol{\lambda})z + iS(\boldsymbol{\lambda}+\boldsymbol{\lambda}_1)z_0} a_1(\boldsymbol{\lambda}_1|\boldsymbol{\lambda}) \right]_{\alpha=0} \lambda d\lambda \\
&\qquad\qquad \boldsymbol{\lambda}_1 \in D_2
\end{aligned}
\tag{11.42}
$$

where $\boldsymbol{\lambda}_1 \cdot \mathbf{x} = \lambda_1\rho\cos\alpha_1$, and we have used (11.40) in (11.42). In the integrand of (11.41) or (11.42) we note that $S(\boldsymbol{\lambda})$ has the branch points $\lambda = \pm k$ and that $S(\boldsymbol{\lambda} + \boldsymbol{\lambda}_1)$ has the branch points (cf. Figs. 11.4,11.5),

$$
\begin{aligned}
&\lambda_\pm = -\lambda_{1x} \pm \sqrt{k^2 - \lambda_{1y}^2} \\
&\qquad \lambda_{1x} \equiv \lambda_1\cos\alpha_1, \quad \lambda_{1y} \equiv \lambda_1\sin\alpha_1
\end{aligned}
\tag{11.43}
$$

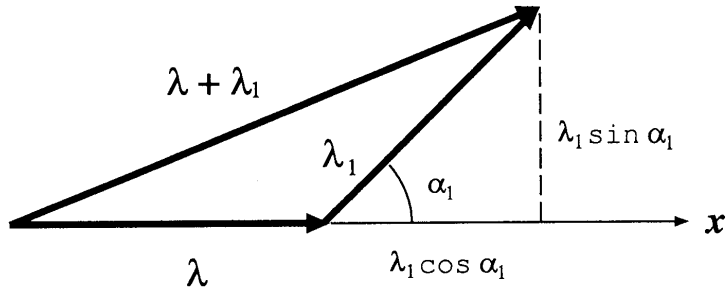

Figure 11.4. Vector triangle.

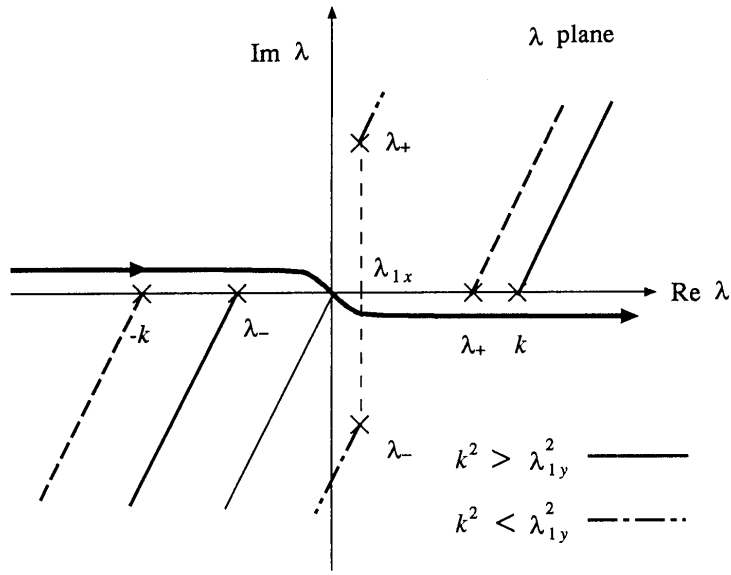

Figure 11.5. Branch cuts and the integration contour in the λ plane. A broken line shows a cut when $k^2 > \lambda_{1y}^2$, and a chain line indicates a cut when $k^2 < \lambda_{1y}^2$.

Thus the contour of integration and the branch cuts on the λ-plane are to be taken as shown in Fig. 11.5. We define the domain D_1 for the integral (11.41) in such a way that the branch point λ_+ always lies on the left side of the branch point k just as in Fig. 11.3, that is,

$$D_1 : Re\lambda_+ < k \tag{11.44}$$

which means that the domain D_1 on the $\boldsymbol{\lambda}_1 = (\lambda_{1x}, \lambda_{1y})$ plane is defined by the inequalities:

$$(\lambda_{1x} + k)^2 + \lambda_{1y}^2 > k^2, \qquad |\lambda_{1y}| < k$$

$$\lambda_{1x} > -k, \qquad |\lambda_{1y}| > k \tag{11.45}$$

as shown by the hatched domain in Fig. 11.6. Let D_2 denote the complementary domain to D_1. In a similar manner, the domain D_1' where the branch point λ_- lies on the right side of the branch point $-k$, i.e,

$$D_1' : Re\lambda_- > -k \tag{11.46}$$

is given by $D_1' = \{\boldsymbol{\lambda}; -\boldsymbol{\lambda} \in D_1\}$, and apparently $D_2 \subset D_1'$.

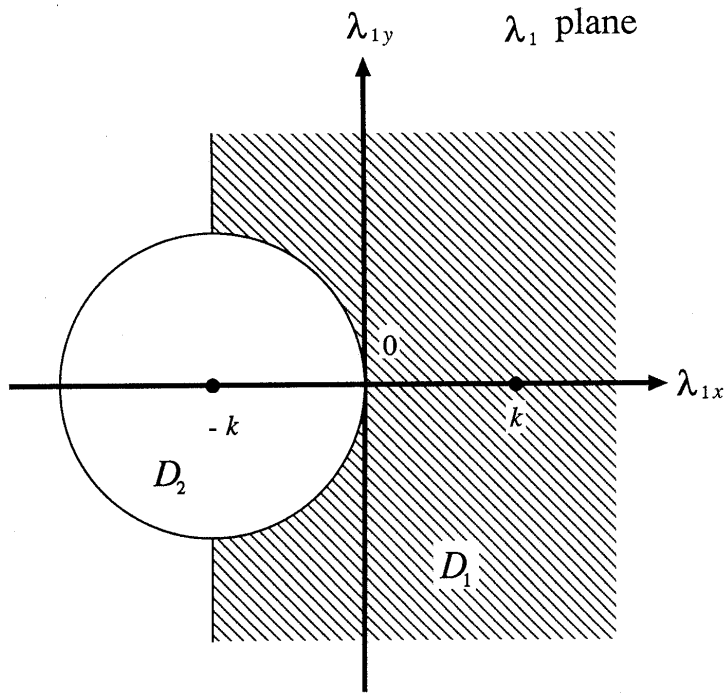

Figure 11.6. Domain D_1 and D_2 on the λ_1 plane.

Therefore, we can deform the contour of the integral in (11.41) around the branch point $\lambda = k$ as in Fig. 11.2 at least in its neighborhood because of the relation (11.44), and similarly, we deform the contour for (11.42) in the other way around the branch point $\lambda = -k$ because of (11.46). Then, we make the change of variable (11.3), $\lambda \to s$, in each of (11.41) and (11.42) as in (11.4). The saddle point $s = 0$ is then free from the branch points and the asymptotic evaluation at the saddle point can be made in the same way as (11.16): that is, using (11.40), we obtain

$$K(\mathbf{x}, z, z_0|\boldsymbol{\lambda}_1) = \frac{1}{4\pi}\sqrt{\frac{i}{2\pi\rho}}e^{i\boldsymbol{\lambda}_1\cdot\mathbf{x}}\int_L e^{i\lambda(s)\rho}f(s|z, z_0|\boldsymbol{\lambda}_1)ds, \qquad \boldsymbol{\lambda}_1 \in D_1 \tag{11.47}$$

$$= \frac{1}{4\pi}\sqrt{\frac{i}{2\pi\rho}}\int_L e^{-i\lambda(s)\rho}f(s|z_0, z|\boldsymbol{\lambda}_1)ds, \qquad \boldsymbol{\lambda}_1 \in D_2 \tag{11.48}$$

where we have put

$$f(s|z, z_0|\boldsymbol{\lambda}_1) \equiv e^{i\mu(s)z+isz_0}\hat{a}_1(s|\boldsymbol{\lambda}_1)\frac{s}{\sqrt{\lambda(s)}} \tag{11.49}$$

$$\mu(s) \equiv S(\boldsymbol{\lambda}+\boldsymbol{\lambda}_1) \equiv \sqrt{k^2-(\boldsymbol{\lambda}+\boldsymbol{\lambda}_1)^2} = \sqrt{s^2-\lambda_1^2-2\lambda_1\lambda\cos\alpha_1} \tag{11.50}$$

$$\hat{a}_1(s|\boldsymbol{\lambda}_1) \equiv -2iF(\boldsymbol{\lambda}_1)\frac{1}{[1+s\xi(\lambda(s))][1+\mu(s)\xi(\sqrt{k^2-\mu^2(s)})]} \quad \text{(Dirichlet)} \tag{11.51}$$

$$\equiv -2iF(\boldsymbol{\lambda}_1)\frac{s^2-\lambda(s)\lambda_1\cos\alpha_1}{[s+\eta(\lambda(s))][\mu(s)+\eta(\sqrt{k^2-\mu^2(s)})]} \quad \text{(Neumann)} \tag{11.52}$$

On inserting a_1 in the above equations, we have neglected for simplicity the higher order correcting terms ξ^* and η^* appearing in (5.17) and (5.38), respectively.

11.2.2 Saddle Point Evaluation of the Wiener Kernel.

At the saddle point $s = 0$ ($\lambda = k, -k$) we have

$$f(0|z, z_0|\,\boldsymbol{\lambda}_1) = 0 \tag{11.53}$$

so that in the same way as (11.16) we have the asymptotic expression,

$$K(\mathbf{x}|z, z_0|\boldsymbol{\lambda}_1) \sim \frac{1}{8\pi}\sqrt{k}k^3 f_+^{''}(0|z, z_0|\boldsymbol{\lambda}_1)\frac{e^{i(\boldsymbol{\lambda}_1+\boldsymbol{k})\cdot\mathbf{x}}}{(k\rho)^2}, \quad \boldsymbol{\lambda}_1 \in D_1 \tag{11.54}$$

$$\sim \frac{1}{8\pi}\sqrt{k}k^3 f_-^{''}(0|z_0, z|\boldsymbol{\lambda}_1)\frac{e^{i\boldsymbol{k}\cdot\mathbf{x}}}{(k\rho)^2}, \quad \boldsymbol{\lambda}_1 \in D_2 \tag{11.55}$$

where $\boldsymbol{k}\cdot\mathbf{x} = k\rho$, $\boldsymbol{\lambda}_1\cdot\mathbf{x} = \lambda_1\rho\cos\alpha_1$, and we have put

$$\begin{aligned} &f_+^{''}(0|z, z_0|\boldsymbol{\lambda}_1) \\ &= \frac{2}{\sqrt{k}}e^{-\sqrt{\lambda_1^2+2k\lambda_1\cos\alpha_1}z}\left\{iz_0\hat{a}_1(0|\boldsymbol{\lambda}_1) + \frac{\partial}{\partial s}\hat{a}_1(s|\boldsymbol{\lambda}_1)|_{s=0}\right\}_{\lambda=k} \\ &\qquad \boldsymbol{\lambda}_1 \in D_1 \end{aligned} \tag{11.56}$$

$$\begin{aligned} &f_-^{''}(0|z_0, z|\boldsymbol{\lambda}_1) \\ &= \frac{2}{\sqrt{k}}e^{-\sqrt{\lambda_1^2-2k\lambda_1\cos\alpha_1}z_0}\left\{iz\hat{a}_1(0|\boldsymbol{\lambda}_1) + \frac{\partial}{\partial s}\hat{a}_1(s|\boldsymbol{\lambda}_1)|_{s=0}\right\}_{\lambda=-k} \\ &\qquad \boldsymbol{\lambda}_1 \in D_2 \end{aligned} \tag{11.57}$$

We note here the relations;

$$\mu(0) \equiv S(\boldsymbol{k} + \boldsymbol{\lambda}_1) = i\sqrt{\boldsymbol{\lambda}_1\cdot(\boldsymbol{\lambda}_1 + 2\boldsymbol{k})}, \qquad \mu'(0) = 0 \tag{11.58}$$

$$\boldsymbol{\lambda}_1\cdot(\boldsymbol{\lambda}_1 + 2\boldsymbol{k}) = \lambda_1^2 + 2k\lambda_1\cos\alpha_1 > 0, \qquad \boldsymbol{\lambda}_1 \in D_1 \tag{11.59}$$

$$\boldsymbol{\lambda}_1\cdot(\boldsymbol{\lambda}_1 - 2\boldsymbol{k}) = \lambda_1^2 - 2k\lambda_1\cos\alpha_1 > 0, \qquad \boldsymbol{\lambda}_1 \in D_2 \tag{11.60}$$

Substituting (11.51) and (11.52) into (11.56) gives

$$f_+''(0|z,z_0|\boldsymbol{\lambda}_1) \simeq \frac{4}{\sqrt{k}}[z_0 + i\xi(k)]e^{-\sqrt{\lambda_1^2+2k\lambda_1\cos\alpha_1}z}F(\boldsymbol{\lambda}_1), \quad \text{(Dirichlet)} \tag{11.61}$$

$$\simeq \frac{4i}{\sqrt{k}}\frac{1}{\eta(k)}\left[z_0 + i\frac{1}{\eta(k)}\right]e^{-\sqrt{\lambda_1^2+2k\lambda_1\cos\alpha_1}z}F(\boldsymbol{\lambda}_1) \quad k\rho \ll |k/\eta|^2 \quad \text{(Neumann)} \tag{11.62}$$

where we have made approximation using $|k\xi|\,,\ |\eta/k| \ll 1$. The condition of (11.62) is explained later. We obtain similar expressions for f_-''.

Now we summarize the asymptoric form of the Wiener kernel as follows:

$$K(\mathbf{x},z,z_0|\boldsymbol{\lambda}_1) \sim \frac{e^{i(\boldsymbol{k}+\boldsymbol{\lambda}_1)\cdot\mathbf{x}}}{(k\rho)^2}h_1(z,z_0|\boldsymbol{\lambda}_1), \qquad \boldsymbol{\lambda}_1 \in D_1 \tag{11.63}$$

$$\sim \frac{e^{i\boldsymbol{k}\cdot\mathbf{x}}}{(k\rho)^2}h_2(z,z_0|\boldsymbol{\lambda}_1), \qquad \boldsymbol{\lambda}_1 \in D_2 \tag{11.64}$$

$$k\rho = \boldsymbol{k}\cdot\mathbf{x} \to \infty, \qquad z,z_0 > 0$$

$$h_1(z,z_0|\,\boldsymbol{\lambda}_1) \equiv \frac{1}{8\pi}\sqrt{k}k^3 f_+''(0|z,z_0|\,\boldsymbol{\lambda}_1) \tag{11.65}$$

$$h_2(z,z_0|\,\boldsymbol{\lambda}_1) \equiv \frac{1}{8\pi}\sqrt{k}k^3 f_-''(0|z_0,z|\,\boldsymbol{\lambda}_1) \tag{11.66}$$

11.2.3 Asymptoric Form of the Incoherent Green Function - Surface-Wave Part and Propagating Part.

The asymptotic form of the incoherent part of the Green function can now be written as a Wiener integral:

$$g_{ic}(\mathbf{x},z|0,z_0;\omega) = \int_{D_1+D_2} K(\mathbf{x},z;z_0|\boldsymbol{\lambda}_1)dB(\boldsymbol{\lambda}_1) + \cdots \tag{11.67}$$

$$\sim g_{ic}^s(\mathbf{x},z|0,z_0) + g_{ic}^p(\mathbf{x},z|0,z_0) \tag{11.68}$$

$$g_{ic}^{s}(\mathbf{x}, z|0, z_0) = \frac{1}{(k\rho)^2} \int_{D_1} e^{i(\boldsymbol{k}+\boldsymbol{\lambda}_1)\cdot\mathbf{x}} h_1(z, z_0|\boldsymbol{\lambda}_1) dB(\boldsymbol{\lambda}_1) \quad (11.69)$$

$$g_{ic}^{p}(\mathbf{x}, z|0, z_0) = \frac{e^{ik\rho}}{(k\rho)^2} \int_{D_2} h_2(z, z_0|\boldsymbol{\lambda}_1) dB(\boldsymbol{\lambda}_1) \quad (11.70)$$

where g_{ic}^{s} gives the surface-wave part and g_{ic}^{p} the propagating part with the factor $e^{ik\rho}$. Like the coherent part (11.16), the incoherent part decays in proportion to $1/(k\rho)^2$ as $k\rho$ increases. We can calculate the variance and the covariance for (11.69) and (11.70) as follows:

$$\left\langle |g_{ic}^{s}|^2 \right\rangle = \frac{1}{(k\rho)^4} \int_{D_1} |h_1(z, z_0|\boldsymbol{\lambda}_1)|^2 d\boldsymbol{\lambda}_1 \quad (11.71)$$

$$\left\langle |g_{ic}^{p}|^2 \right\rangle = \frac{1}{(k\rho)^4} \int_{D_2} |h_2(z, z_0|\boldsymbol{\lambda}_1)|^2 d\boldsymbol{\lambda}_1 \quad (11.72)$$

$$\left\langle \overline{g_{ic}^{s}} g_{ic}^{p} \right\rangle = 0 \quad (11.73)$$

where the surface-wave part and the propagating part are uncorrelated. It is apparent from (11.61) and (11.62) that g_{ic}^{s} decreases with increasing receiver altitude z, whereas g_{ic}^{p} decreases with increasing transmitter altitude z_0.

The average incoherent power flowing along the surface toward the direction $\mathbf{x}$ is given by

$$\begin{aligned} P_{ic} \equiv & \frac{1}{k} \mathrm{Im} \left\langle \overline{g_{ic}} \frac{\partial g_{ic}}{\partial \rho} \right\rangle = P_{ic}^{s} + P_{ic}^{p} \\ = & \frac{1}{(k\rho)^4} \left\{ \int_{D_1} \frac{k + \lambda_1 \cos\alpha_1}{k} |h_1(z, z_0|\boldsymbol{\lambda}_1)|^2 d\boldsymbol{\lambda}_1 + \int_{D_2} |h_2(z, z_0|\boldsymbol{\lambda}_1)|^2 d\boldsymbol{\lambda}_1 \right\} \end{aligned} \quad (11.74)$$

where the first term P_{ic}^{s} and the second term P_{ic}^{p} represent the average power flow for the surface-wave part and the propagating part, respectively.

11.2.4 Asymptotic Form in the "Medium Range" over a Neumann Random Surface.

In the medium range (11.23), the saddle-point evaluation of (11.47) and (11.48) is again subject to modification due to the pole $s \simeq -\eta$

in the saddle. Then using (11.52) we rewrite (11.49) as

$$f(s|z,z_0|\boldsymbol{\lambda}_1) \equiv \frac{1}{s+\eta} g(s|\boldsymbol{\lambda}_1)s = g(s|\boldsymbol{\lambda}_1) - \eta \frac{g(s|\boldsymbol{\lambda}_1)}{s+\eta} \tag{11.75}$$

$$g(s|\boldsymbol{\lambda}_1) \equiv -2iF(\boldsymbol{\lambda}_1) e^{i\mu(s)z+isz_0} \frac{1}{\sqrt{\lambda(s)}} \frac{s^2 - \lambda(s)\lambda_1 \cos\alpha_1}{\mu(s) + \eta(\sqrt{k^2 - \mu^2(s)})} \tag{11.76}$$

Calculating in the same manner as (11.27), we obtain

$$\int_L e^{i\lambda(s)\rho} f(s|z,z_0|\boldsymbol{\lambda}_1) ds$$

$$\sim \sqrt{\frac{2\pi k}{i\rho}} g(0|\boldsymbol{\lambda}_1) e^{ik\rho} - \eta(k) \int_L e^{i\lambda(s)\rho} \frac{g(0|\boldsymbol{\lambda}_1) + g'(0|\boldsymbol{\lambda}_1)s}{s+\eta} ds \tag{11.77}$$

$$= g(0|\boldsymbol{\lambda}_1)[1 - iz_0\eta(k)] \left\{ \sqrt{\frac{2\pi k}{i\rho}} - \eta(k) I(\rho) \right\} e^{ik\rho} \tag{11.78}$$

where $I(\rho)$ is defined by (11.30) and

$$g(0|\boldsymbol{\lambda}_1) = 2iF(\boldsymbol{\lambda}_1) \frac{1}{\sqrt{k}} e^{i\mu(0)z} \frac{k\lambda_1 \cos\alpha_1}{\mu(0) + \eta(|\boldsymbol{k} + \boldsymbol{\lambda}_1|)} \tag{11.79}$$

$$g'(0|\boldsymbol{\lambda}_1) = iz_0 g(0|\boldsymbol{\lambda}_1) \tag{11.80}$$

The final asymptotic expressions for K are written

$$K(\mathbf{x},z,z_0|\boldsymbol{\lambda}_1) \sim \left[\frac{1}{k\rho} - \frac{\eta(k)}{k} \sqrt{\frac{i}{2\pi k\rho}} I(\rho) \right] \times e^{i(k+\lambda_1 \cos\alpha_1)\rho} J_1(z,z_0|\boldsymbol{\lambda}_1), \qquad \boldsymbol{\lambda}_1 \in D_1 \tag{11.82}$$

$$\sim \left[\frac{1}{k\rho} - \frac{\eta(k)}{k} \sqrt{\frac{i}{2\pi k\rho}} I(\rho) \right] \times e^{ik\rho} J_2(z,z_0|\boldsymbol{\lambda}_1), \qquad \boldsymbol{\lambda}_1 \in D_2 \tag{11.83}$$

$$J_1(z,z_0|\boldsymbol{\lambda}_1) \equiv \frac{\sqrt{k}}{4\pi} k g(0|\boldsymbol{\lambda}_1)[1 - iz_0\eta(k)] \tag{11.84}$$

$$= \frac{1}{2\pi} k^2 F(\boldsymbol{\lambda}_1) \frac{\lambda_1 \cos\alpha_1}{\sqrt{\boldsymbol{\lambda}_1 \cdot (\boldsymbol{\lambda}_1 + 2\boldsymbol{k}) - i\eta(k)}}$$

$$\times e^{-\sqrt{\boldsymbol{\lambda}_1\cdot(\boldsymbol{\lambda}_1+2\boldsymbol{k})}z}[1-iz_0\eta(k)] \tag{11.85}$$

$$J_2(z,z_0|\boldsymbol{\lambda}_1) = \frac{1}{2\pi}k^2F(\boldsymbol{\lambda}_1)\frac{-\lambda_1\cos\alpha_1}{\sqrt{\boldsymbol{\lambda}_1\cdot(\boldsymbol{\lambda}_1-2\boldsymbol{k})-i\eta(k)}}$$
$$\times e^{-\sqrt{\boldsymbol{\lambda}_1\cdot(\boldsymbol{\lambda}_1-2\boldsymbol{k})}z_0}[1-iz\eta(k)] \tag{11.86}$$

Consequently, in the medium range of Neumann surface, the surface-wave part and the propagating part of the incoherent Green function are written

$$g_{ic}^s(\mathbf{x},z|0,z_0;\omega) = \left[\frac{1}{k\rho}-\frac{\eta(k)}{k}\sqrt{\frac{i}{2\pi k\rho}}I(\rho)\right]$$
$$\times\int_{D_1} e^{i(k+\lambda_1\cos\alpha_1)\rho}J_1(z,z_0|\boldsymbol{\lambda}_1)dB(\boldsymbol{\lambda}_1) \tag{11.87}$$

$$g_{ic}^p(\mathbf{x},z|0,z_0;\omega) = \left[\frac{1}{k\rho}-\frac{\eta(k)}{k}\sqrt{\frac{i}{2\pi k\rho}}I(\rho)\right]$$
$$\times e^{ik\rho}\int_{D_2} J_2(z,z_0|\boldsymbol{\lambda}_1)dB(\boldsymbol{\lambda}_1) \tag{11.88}$$

Similarly we have

$$\left\langle|g_{ic}^s|^2\right\rangle = \left|\frac{1}{k\rho}-\frac{\eta(k)}{k}\sqrt{\frac{i}{2\pi k\rho}}I(\rho)\right|^2\int_{D_1}|J_1(z,z_0|\boldsymbol{\lambda}_1)|^2d\boldsymbol{\lambda}_1 \tag{11.89}$$

$$\left\langle|g_{ic}^p|^2\right\rangle = \left|\frac{1}{k\rho}-\frac{\eta(k)}{k}\sqrt{\frac{i}{2\pi k\rho}}I(\rho)\right|^2\int_{D_2}|J_2(z,z_0|\boldsymbol{\lambda}_1)|^2d\boldsymbol{\lambda}_1 \tag{11.90}$$

The average power flow in the direction $\mathbf{x}$ is written

$$P_{ic} \equiv \frac{1}{k}\mathrm{Im}\left\langle\overline{g_{ic}}\frac{\partial g_{ic}}{\partial\rho}\right\rangle = P_{ic}^s + P_{ic}^p$$
$$= \left|\frac{1}{k\rho}-\frac{\eta(k)}{k}\sqrt{\frac{i}{2\pi k\rho}}I(\rho)\right|^2$$
$$\times\left\{\int_{D_1}\frac{k+\lambda_1\cos\alpha_1}{k}|J_1(z,z_0|\boldsymbol{\lambda}_1)|^2d\boldsymbol{\lambda}_1+\int_{D_2}|J_2(z,z_0|\boldsymbol{\lambda}_1)|^2d\boldsymbol{\lambda}_1\right\} \tag{11.91}$$

which should be compared with expression (11.74) in the far region.

12. Propagation Characteristics

We show some numerical results for the amplitude and the power flow of the coherent and incoherent fields in the far region, which are plotted on the abscissa against the altitude z on the ordinate so that their profiles can be viewed in a natural manner.

12.1 Dirichlet Condition

As shown by (11.18), the amplitude of the coherent part decays with increasing distance inversely proportional to $(k\rho)^2$, but its profile, i.e., the distribution versus altitude, can be given by the factor,

$$k^2 \left[z z_0 + i(z + z_0)\xi(k) - \xi^2(k) \right] \tag{12.1}$$

which is symmetric in z and z_0. The first term, corresponding to the flat surface $(\sigma^2 = 0)$, is proportional to the receiver altitude z; this is because, as shown by (9.9), the asymptotic field high above the surface ($z/\rho > 0$) decays in proportion to $1/k\rho$, which is slower than the decay rate $1/(k\rho)^2$ along the surface ($z/\rho \to 0$, $\rho \to \infty$). In the amplitude of (12.1), the first term kzz_o is so dominant that the contribution from other small terms could hardly be recognized, since $\xi(k) = o(\sigma^2)$ by (5.19). Therefore, instead of the amplitude profile (12.1), we show in Fig. 12.1 the complex quantity $k\xi(k)$ calculated by (9.9).

The incoherent power P_{ic} can be calculated by (11.74) using (5.17). It is clear from (11.56) and (11.57) that P_{ic}^s is dominant at a lower altitude z, whereas at a higher altitude P_{ic}^p increases with altitude nearly in proportion to z^2. Figure 12.2 shows the incoherent power $P_{ic} \equiv P_{ic}^s + P_{ic}^p$ versus receiver altitude kz without the distance factor $(k\rho)^{-4}$. The surface-wave part P_{ic}^s is also shown by a thin line for comparison.

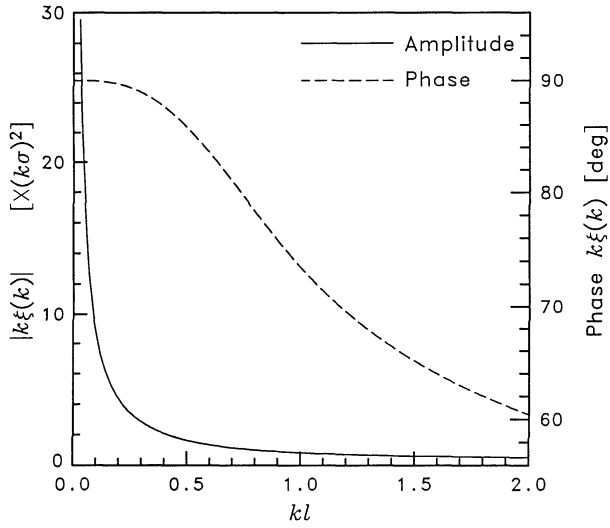

Figure 12.1. Amplitude and phase of $\xi(k)$ versus kl (Dirichlet).

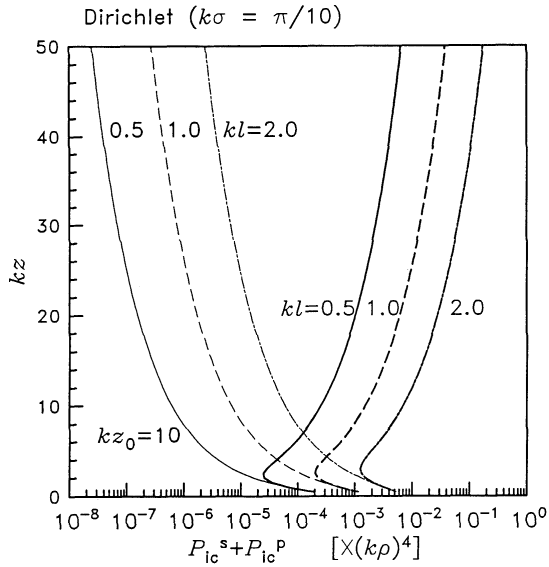

Figure 12.2. Incoherent power P_{ic} versus receiver altitude (Dirichlet). $k\sigma - \pi/10$, $kz_0 = 10$; $kl = 0.5$ (solid line), 1.0 (broken line), 2.0 (chain line).

12.2 Neumann Condition

By (11.19) the profile of the coherent amplitude in the far range $(k\rho \gg |k/\eta|^2)$ can be described by the factor,

$$k^2[zz_0 + i(z + z_0)/\eta(k) - 1/\eta^2(k)] \tag{12.2}$$

Unlike (12.1), as mentioned before, the first term does not give the profile for $\sigma^2 = 0$, and its amplitude changes appreciably with respect to z because $1/\eta(k)$ is of the order of σ^{-2}. Figure 12.3 shows the complex value of $1/\eta(k)$, and Figure 12.4 shows the profile of the complex coherent amplitude plotted against the altitude kz without the factor $1/(k\rho)^4$. We observe that the amplitude for $kl = 0.5$ becomes minimum at $kz \simeq 10$ and that there is some phase delay along the surface. It goes without saying that the amplitude increases proportionally with z at a much higher altitude than that shown in the figure.

Figure 12.5 shows the profile of the incoherent power flow in the far range calculated by (11.74) using (5.38). We again observe that, for $kl = 0.5$, the power becomes minimum around $kz \simeq 10$ and that the surface wave is dominant at low altitude. P_{ic} will increase in proportion to z^2 at a much higher altitude than in the figure. The expressions (11.35) and (11.91), that is, the profiles of the coherent and incoherent power flux in the medium range, are highly dependent on the distance ρ also, and therefore will not be shown here.

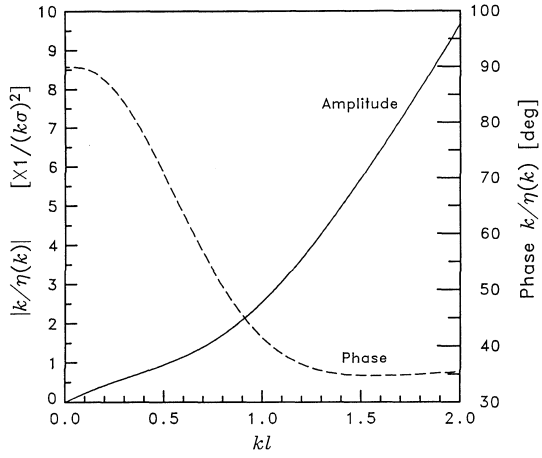

Figure 12.3. Amplitude and phase of $k/\zeta(k)$ versus kl (Neumann).

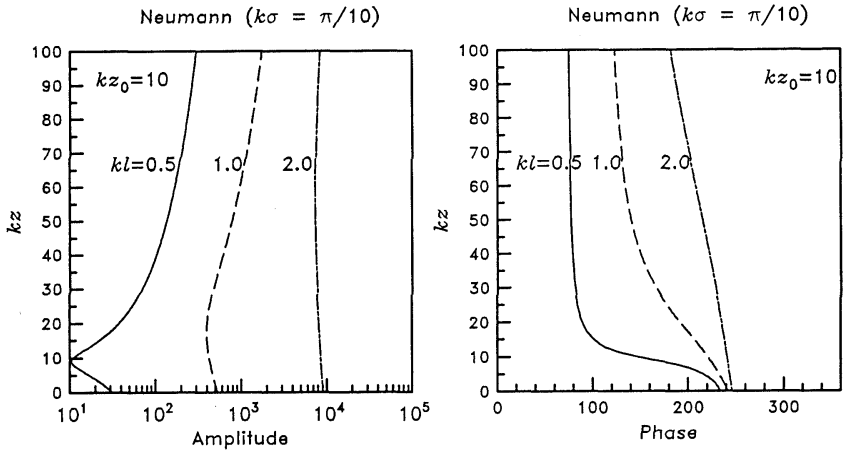

Figure 12.4. Comples coherent amplitude versus receiver altitude (Neumann). Amplitude and pahse of the profile $k^2[zz_0+i(z+z_0)/\eta(k)-1/\eta^2(k)]$ are plotted against z with $k\sigma = \pi/10$, $kz_0 = 10; kl = 0.5$ (solid line), 1.0 (broken line), 2.0 (chain line).

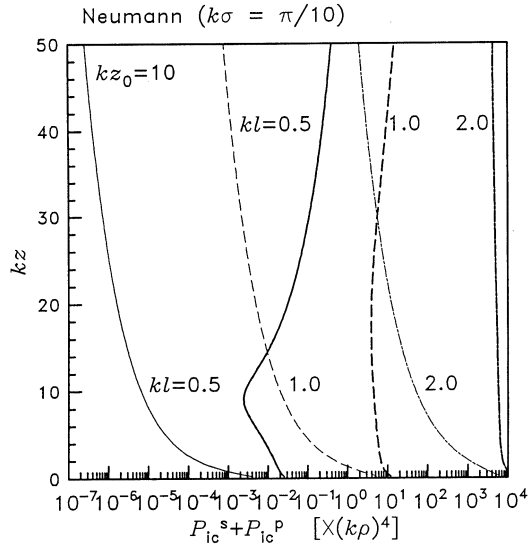

Figure 12.5. Incoherent power P_{ic} versus receiver altitude (Neumann). $k\sigma = \pi/10$, $kz_0 = 10$; $kl = 0.5$ (solid line), 1.0 (broken line), 2.0 (chain line).

Appendix

Stochastic Functional of the Gaussian Random Measure on the Plane

At present the Wiener-Itô theory seems to be the only useful tool to deal with stochastic functionals, which we apply to the stochastic scattering and propagation problems. Although the original theory was given on the basis of the Brownian-motion process on the time axis, we must prepare the formulas based on the Gaussian random measure on a 2D plane for our purpose. For the readers unaccustomed to the Wiener-Itô theory, we give here a brief account of the definitions as well as notations and formulas for ease in reference.

For basic mathematical theories concerning the Wiener-Itô expansion and of orthogonal functionals of the Brownian motion process, the reader should refer to Refs. [28–31], and for practical formulas and description in terms of multivariate Hermite polynomials, see, e.g., [24,32,33] and [34] for the operator formalism.

A. Gaussian Random Measure

Let $\mathrm{d}\,\mathbf{x}$ denote an infinitesimal rectangle at $\mathbf{x} = (x, y)$ with an area $dxdy$ on the 2D plane R_2, and let $dB(\mathbf{x}, \omega) \equiv dB(\mathbf{x})$ (the probability parameter ω is often suppressed for brevity) be a real-valued Gaussian random measure on R_2 with the following properties:

$$\langle dB(\mathbf{x}) \rangle = 0 \tag{A.1}$$

$$\left\langle dB(\mathbf{x}) dB(\mathbf{x}') \right\rangle = \delta(\mathbf{x} - \mathbf{x}') d\mathbf{x} d\mathbf{x}' \tag{A.2}$$

That is, $dB(\mathbf{x})/d\mathbf{x}$ is regarded as Gaussian white noise on R_2.

The homogeneity of the random measure on R_2 is expressed as (c.f.,(2.3))

$$dB(\mathbf{x} + \mathbf{a}, \omega) = dB(\mathbf{x}, T^{\mathbf{a}}\omega), \qquad \mathbf{a} \in R_2 \tag{A.3}$$

where $T^{\mathbf{a}}, \mathbf{a} \in R_2$, denotes the shift transformation on Ω.

Similarly, the isotropy of the random measure is written (c.f.,(2.13))

$$dB(g_\alpha \mathbf{x}, \omega) = dB(\mathbf{x}, T^{\alpha}\omega), \qquad g_\alpha \in G_2 \tag{A.4}$$

where $T^\alpha, g_\alpha \in G_2$, denotes the rotational shift transformation on Ω. $T^{\mathbf{a}}$ and T^α satisfy the commutation relation (2.15).

B. Multiple Wiener Integral

Let a n-tuple Wiener integral of n-variate function f_n with respect to the Gaussian random measure $dB(\mathbf{x})$ be defined by a stochastic integral

$$I_n(f) = \int \cdots \int_{R_2} f_n(\mathbf{x}_1, \cdots, \mathbf{x}_n) h_n[dB(\mathbf{x}_1), \cdots, \cdots, dB(\mathbf{x}_n)] \quad \text{(A.5)}$$

Here, h_n denotes the n-th degree Wiener-Hermite differential[3], and some low degree differentials are

$$h_0 = 1$$

$$h_1[dB(\mathbf{x})] = dB(\mathbf{x})$$

$$h_2[dB(\mathbf{x}_1), dB(\mathbf{x}_2)] = dB(\mathbf{x}_1)dB(\mathbf{x}_2) - \delta(\mathbf{x}_1 - \mathbf{x}_2)d\mathbf{x}_1 d\mathbf{x}_2$$

$$\begin{aligned} h_3[dB(\mathbf{x}_1), dB(\mathbf{x}_2), dB(\mathbf{x}_3)] &= dB(\mathbf{x}_1)dB(\mathbf{x}_2)dB(\mathbf{x}_3) \\ &- [\delta(\mathbf{x}_1 - \mathbf{x}_2)d\mathbf{x}_1 d\mathbf{x}_2 dB(\mathbf{x}_3) + \delta(\mathbf{x}_2 - \mathbf{x}_3)d\mathbf{x}_2 d\mathbf{x}_3 dB(\mathbf{x}_1) \\ &+ \delta(\mathbf{x}_3 - \mathbf{x}_1)d\mathbf{x}_3 d\mathbf{x}_1 dB(\mathbf{x}_2)], \cdots \end{aligned} \quad \text{(A.6)}$$

The Wiener-Hermite differentials satisfy the orthogonality

$$\begin{aligned} &\left\langle h_n[dB(\mathbf{x}_1), \cdots, dB(\mathbf{x}_n)] h_m[dB(\mathbf{x'}_1), \cdots, dB(\mathbf{x'}_m)] \right\rangle \\ &= \delta_{nm}\delta^n_{ij} d\mathbf{x}_1 \cdots d\mathbf{x}_n d\mathbf{x'}_1 \cdots d\mathbf{x'}_m \end{aligned} \quad \text{(A.7)}$$

$$\delta^n_{ij} \equiv \sum_{allpair} \prod_{(i,j)} \delta(\mathbf{x}_i - \mathbf{x'}_j) \quad \text{(A.8)}$$

Where the sum in δ^n_{ij} is to be taken over all distinct products of $\delta(\mathbf{x}_i - \mathbf{x'}_j)$ for possible combintations of the pairs (i, j) made from $i, j = 1, \cdots, n$, the number of such terms being $n!$. Because of (A.7) the n-tuple Wiener integral satisfies the following relations:

$$I_n(f) = I_n(\tilde{f}) \quad \text{(A.9)}$$

$$\left\langle \overline{I_n}(f) I_m(g) \right\rangle = \delta_{nm} n! (\tilde{f}, \tilde{g})_n \tag{A.10}$$

$$\left\langle |I_n(f)|^2 \right\rangle = n! \|\tilde{f}\|_n^2 \tag{A.11}$$

where

$$(f,g)_n = \int \cdots \int_{R_2} \overline{f_n}(\mathbf{x}_1, \cdots, \mathbf{x}_n) g_n(\mathbf{x}_1, \cdots, \mathbf{x}_n) d\mathbf{x}_1, \cdots, d\mathbf{x}_n \tag{A.12}$$

$$\|f\|_n^2 \equiv (f,f)_n \tag{A.13}$$

$$\tilde{f}(\mathbf{x}_1, \cdots, \mathbf{x}_n) \equiv \frac{1}{n!} \sum_{(i)} f(\mathbf{x}_1, \cdots, \mathbf{x}_n) \tag{A.14}$$

$(i) = (i_1, \cdots, i_n)$ running over all permutations of $(1, \cdots, n)$, and the overbar denoting a complex conjugate quantity. The n-tuple Wiener integral $I_n(f)$ is defined for f_n with $\|f\|_n^2 < \infty$. (A.9) is due to the symmetry of h_n with respect to its n variables, so that $f_n(\mathbf{x}_1, \cdots, \mathbf{x}_n)$ can be symmetrized from the beginning. (A.10) gives the othogonality of n-tuple Wiener integral.

C. Complex Gaussian Random Measure

We let R_2 stand for the 2D-space of the spatial frequency $\boldsymbol{\lambda} \equiv (\lambda_x, \lambda_y)$ also, and $d\boldsymbol{\lambda}$ denote an infinitesimal area $d\lambda_x d\lambda_y$ at $\boldsymbol{\lambda}$. For notational simplicity, we write a complex random measure as $dB(\boldsymbol{\lambda}, \omega) \equiv dB(\boldsymbol{\lambda})$, and discriminate it from the real random measure $dB(\mathbf{x})$ by its argument $\boldsymbol{\lambda}$. The complex Gaussian random measure $dB(\boldsymbol{\lambda})$ is a complex valued random variable such that its real and imaginary parts have independent identical Gaussian distributions with

$$\langle dB(\boldsymbol{\lambda}) \rangle = 0 \tag{A.15}$$

$$\left\langle \overline{dB(\boldsymbol{\lambda})} dB(\boldsymbol{\lambda}') \right\rangle = \delta(\boldsymbol{\lambda} - \boldsymbol{\lambda}') d\boldsymbol{\lambda}\, d\boldsymbol{\lambda}' \tag{A.16}$$

and

$$\overline{dB(\boldsymbol{\lambda})} = dB(-\boldsymbol{\lambda}) \tag{A.17}$$

Such a complex random measure is given by the Fourier transform of white noise $dB(\mathbf{x})/d\mathbf{x}$:

$$dB(\boldsymbol{\lambda},\omega) = d\boldsymbol{\lambda}\frac{1}{2\pi}\int_{R_2} e^{-i\boldsymbol{\lambda}\cdot\mathbf{x}} dB(\mathbf{x},\omega) \tag{A.18}$$

As easily verified the shift of homogeneous random measure $dB(\mathbf{x})$ as defined by (A.3) induces the transformation of the complex random measure as follows:

$$dB(\boldsymbol{\lambda}, T^{\mathbf{a}}\omega) = e^{i\boldsymbol{\lambda}\cdot\mathbf{a}} dB(\boldsymbol{\lambda},\omega) \tag{A.19}$$

which means that $dB(\boldsymbol{\lambda},\omega)$ is an eigenfunction of the shift $T^{\mathbf{a}}$ with eigenvalue $e^{i\boldsymbol{\lambda}\cdot\mathbf{a}}$. Similarly, by the rotational shift T^{α} associated with the rotation $g_\alpha \in G_2$ as defined by (A.4), the complex random measure (A.18) is transformed according to

$$dB(\boldsymbol{\lambda}, T^{\alpha}\omega) = dB(g_\alpha\boldsymbol{\lambda},\omega) \tag{A.20}$$

D. Multiple Wiener Integral w.r.t. Complex Gaussian Random Measure

The n-tuple Wiener integral can be similarly defined with respect to $dB(\boldsymbol{\lambda})$:

$$\hat{I}_n(F) \equiv \int\cdots\int_{R_2} F_n(\boldsymbol{\lambda}_1,\cdots,\boldsymbol{\lambda}_n)\hat{h}_n[dB(\boldsymbol{\lambda}_1),\cdots,dB(\boldsymbol{\lambda}_n)] \tag{A.21}$$

where $\hat{h}_n$ denotes a n-th degree complex Wiener-Hermite differential. Some low-degree differentials are given by

$$\hat{h}_0 = 1$$

$$\hat{h}_1[dB(\boldsymbol{\lambda})] = dB(\boldsymbol{\lambda})$$

$$\hat{h}_2[dB(\boldsymbol{\lambda}_1), dB(\boldsymbol{\lambda}_2)] = dB(\boldsymbol{\lambda}_1)dB(\boldsymbol{\lambda}_2) - \delta(\boldsymbol{\lambda}_1+\boldsymbol{\lambda}_2)d\boldsymbol{\lambda}_1 d\boldsymbol{\lambda}_2$$

$$\begin{aligned}\hat{h}_3[dB(\boldsymbol{\lambda}_1), dB(\boldsymbol{\lambda}_2), dB(\boldsymbol{\lambda}_3)] &= dB(\boldsymbol{\lambda}_1)dB(\boldsymbol{\lambda}_2)dB(\boldsymbol{\lambda}_3)\\ &- [\delta(\boldsymbol{\lambda}_1+\boldsymbol{\lambda}_2)d\boldsymbol{\lambda}_1 d\boldsymbol{\lambda}_2 dB(\boldsymbol{\lambda}_3) + \delta(\boldsymbol{\lambda}_2+\boldsymbol{\lambda}_3)d\boldsymbol{\lambda}_2 d\boldsymbol{\lambda}_3 dB(\boldsymbol{\lambda}_1)\\ &+ \delta(\boldsymbol{\lambda}_3+\boldsymbol{\lambda}_1)d\boldsymbol{\lambda}_3 d\boldsymbol{\lambda}_1 dB(\boldsymbol{\lambda}_2)]\end{aligned} \tag{A.22}$$

For use in the text we show a recurrence formula for $\hat{h}_n$ here:

$$\begin{aligned} dB(\boldsymbol{\lambda})\hat{h}_n[dB(\boldsymbol{\lambda}_1),\cdots,dB(\boldsymbol{\lambda}_n)] &= \hat{h}_{n+1}[dB(\boldsymbol{\lambda}),dB(\boldsymbol{\lambda}_1),\cdots,dB(\boldsymbol{\lambda}_n)] \\ &+ \sum_{k=1}^{n} \hat{h}_{n-1}[dB(\boldsymbol{\lambda}_1),\cdots,dB(\boldsymbol{\lambda}_{k-1}),dB(\boldsymbol{\lambda}_{k+1}),\cdots,dB(\boldsymbol{\lambda}_n)] \\ &\times \delta(\boldsymbol{\lambda}+\boldsymbol{\lambda}_k)d\boldsymbol{\lambda}d\boldsymbol{\lambda}_k \end{aligned} \tag{A.23}$$

The complex Wiener-Hermite differentials satisfies the orthogonality relation similar to (A.7):

$$\begin{aligned} &\left\langle \overline{\widehat{h_n}[dB(\boldsymbol{\lambda}_1),\cdots,dB(\boldsymbol{\lambda}_n)]}\widehat{h_m}[dB(\boldsymbol{\mu}_1),\cdots,dB(\boldsymbol{\mu}_m)] \right\rangle \\ =&\delta_{nm}\delta^n_{ij}d\boldsymbol{\lambda}_1\cdots d\boldsymbol{\lambda}_n d\boldsymbol{\mu}_1\cdots d\boldsymbol{\mu}_n \qquad \text{(A.24)} \\ &\delta^n_{ij} \equiv \sum_{allpair} \prod_{(i,j)} \delta(\boldsymbol{\lambda}_i-\boldsymbol{\mu}_j) \qquad \text{(A.25)} \end{aligned}$$

where δ^n_{ij} is defined as in (A.8).

The n-tuple Wiener integral (A.21) has the following property corresponding to (A.9)–(A.ll):

$$\hat{I}_n(F) = \hat{I}_n(\tilde{F}) \tag{A.26}$$

$$\left\langle \overline{\hat{I}_n(F)}\hat{I}_m(G) \right\rangle = \delta_{nm}n!(\tilde{F},\tilde{G})_n \tag{A.27}$$

$$\left\langle |\hat{I}_n(F)|^2 \right\rangle = n!\|\tilde{F}\|^2_n \tag{A.28}$$

$$(F,G)_n \equiv \int\cdots\int_{R_2} \overline{F_n}(\boldsymbol{\lambda}_1,\cdots,\boldsymbol{\lambda}_n)G_n(\boldsymbol{\lambda}_1,\cdots,\boldsymbol{\lambda}_n)d\boldsymbol{\lambda}_1\cdots d\boldsymbol{\lambda}_n \tag{A.29}$$

where $\tilde{F}$ denotes the symmetrization of F as in (A.14).

By (A.23) the product of two Wiener integrals $I_1(F_1)I_n(G_n)$

splits into $(n+1)-$ and $(n-1)-$tuple Wiener integrals as follows:

$$\begin{aligned}
&\hat{I}_1(F_1)\hat{I}_n(G_n)\\
&\equiv \int F_1(\boldsymbol{\lambda})dB(\boldsymbol{\lambda}) \int \cdots \int G_n(\boldsymbol{\lambda}_1,\cdots,\boldsymbol{\lambda}_n)\hat{h}_n[dB(\boldsymbol{\lambda}_1),\cdots,dB(\boldsymbol{\lambda}_n)]\\
&= \int \cdots \int K_{n+1}(\boldsymbol{\lambda}_1,\cdots,\boldsymbol{\lambda}_{n+1})\hat{h}_{n+1}[dB(\boldsymbol{\lambda}_1),\cdots,dB(\boldsymbol{\lambda}_{n+1})]\\
&\quad + \sum_{k=1}^{n} \int \cdots \int L_{n-1}(\boldsymbol{\lambda}_1,\cdots,\boldsymbol{\lambda}_{k-1},\boldsymbol{\lambda}_{k+1},\cdots,\boldsymbol{\lambda}_n)\\
&\quad \times \hat{h}_{n-1}[dB(\boldsymbol{\lambda}_1),\cdots,dB(\boldsymbol{\lambda}_{k-1}),\cdots,dB(\boldsymbol{\lambda}_{k+1}),\cdots,dB(\boldsymbol{\lambda}_n)]
\end{aligned} \tag{A.30}$$

where we have put

$$K_{n+1}(\boldsymbol{\lambda}_1,\cdots,\boldsymbol{\lambda}_{n+1}) \equiv F_1(\boldsymbol{\lambda}_{n+1})G_n(\boldsymbol{\lambda}_1,\cdots,\boldsymbol{\lambda}_n) \tag{A.31}$$

$$L_{n-1}(\boldsymbol{\lambda}_1,\cdots,\boldsymbol{\lambda}_{k-1},\boldsymbol{\lambda}_{k+1},\cdots,\boldsymbol{\lambda}_n) \equiv \int F_1(-\boldsymbol{\lambda}_k)G_n(\boldsymbol{\lambda}_1,\cdots,\boldsymbol{\lambda}_k,\cdots,\boldsymbol{\lambda}_n)d\boldsymbol{\lambda}_k \tag{A.32}$$

Now using (A.26) we can symmetrize the kernels, so that we obtain the following recurrence formula for the multiple Wiener integrals:

$$\begin{aligned}
&\hat{I}_1(F_1)\hat{I}_n(G_n)\\
&=\hat{I}_{n+1}(\tilde{K}_{n+1}) + n\hat{I}_{n-1}(L_{n-1})
\end{aligned} \tag{A.33}$$

$$\begin{aligned}
&\equiv \int \cdots \int \tilde{K}_{n+1}(\boldsymbol{\lambda}_1,\cdots,\boldsymbol{\lambda}_{n+1})\hat{h}_{n+1}[dB(\boldsymbol{\lambda}_1),\cdots,dB(\boldsymbol{\lambda}_{n+1})]\\
&\quad + n\int \cdots \int L_{n-1}(\boldsymbol{\lambda}_1,\cdots,\cdots,\boldsymbol{\lambda}_{n-1})\hat{h}_{n-1}[dB(\boldsymbol{\lambda}_1),\cdots,dB(\boldsymbol{\lambda}_{n-1})]
\end{aligned} \tag{A.34}$$

$$\tilde{K}_{n+1}(\boldsymbol{\lambda}_1,\cdots,\boldsymbol{\lambda}_{n+1}) \equiv \frac{1}{n+1}\sum_{k=1}^{n+1} F_1(\boldsymbol{\lambda}_k)G_n(\boldsymbol{\lambda}_1,\cdots,\boldsymbol{\lambda}_{k-1},\boldsymbol{\lambda}_{k+1},\cdots,\boldsymbol{\lambda}_{n+1}) \tag{A.35}$$

$$L_{n-1}(\boldsymbol{\lambda}_1,\cdots,\boldsymbol{\lambda}_{n-1}) \equiv \int F_1(-\boldsymbol{\lambda}_n)G_n(\boldsymbol{\lambda}_1,\cdots,\boldsymbol{\lambda}_n)d\boldsymbol{\lambda}_n \tag{A.36}$$

where we have assumed G_n is already symmetric, i.e., $G_n = \tilde{G}_n$, and so is L_{n-1}.

By virtue of the tensorial property of the multivariate Hermite polynomial under a linear transformation, the n-tuple Wiener integral (A.5) is transformed into the n-tuple complex Wiener integral (A.21) by the Fourier transformation (A.18):

$$I_n(f) = \hat{I}_n(F) \tag{A.37}$$

where

$$F_n(\boldsymbol{\lambda}_1, \cdots, \boldsymbol{\lambda}_n) = \frac{1}{(2\pi)^n} \int \cdots \int_{R_2} e^{i(\boldsymbol{\lambda}\cdot\mathbf{x})} f_n(\mathbf{x}_1, \cdots, \mathbf{x}_n) d\mathbf{x}_1 \cdots d\mathbf{x}_n \tag{A.38}$$

$$\begin{aligned} &\hat{h}_n[dB(\boldsymbol{\lambda}_1), \cdots, dB(\boldsymbol{\lambda}_n)] \\ &\quad = d\boldsymbol{\lambda}_1 \cdots d\boldsymbol{\lambda}_n \frac{1}{(2\pi)^n} \int \cdots \int_{R_2} e^{-i(\boldsymbol{\lambda}\cdot\mathbf{x})} h_n[dB(\mathbf{x}_1), \cdots, dB(\mathbf{x}_n))] \end{aligned} \tag{A.39}$$

$$(\boldsymbol{\lambda} \cdot \mathbf{x}) \equiv \boldsymbol{\lambda}_1 \cdot \mathbf{x}_1 + \cdots + \boldsymbol{\lambda}_n \cdot \mathbf{x}_n \tag{A.40}$$

The righthand sides of these equations are $2n$-D Fourier transforms on $R_2 \times \cdots \times R_2$. By the shift transformation, the complex Wiener-Hermite differential $\hat{h}_n$ is transformed according to

$$\begin{aligned} &\hat{h}_n[dB(\boldsymbol{\lambda}_1, T^{\mathbf{a}}\omega), \cdots, dB(\boldsymbol{\lambda}_n, T^{\mathbf{a}}\omega)] \\ &\quad = e^{i(\boldsymbol{\lambda}_1 + \cdots + \boldsymbol{\lambda}_n)\cdot\mathbf{a}} \hat{h}_n[dB(\boldsymbol{\lambda}_1, \omega), \cdots, dB(\boldsymbol{\lambda}_n, \omega)] \end{aligned} \tag{A.41}$$

Similarly, for the rotational shift T^α, we have

$$\begin{aligned} &\hat{h}_n[dB(\boldsymbol{\lambda}_1, T^\alpha\omega), \cdots, dB(\boldsymbol{\lambda}_n, T^\alpha\omega)] \\ &\quad = \hat{h}_n[dB(g_\alpha\boldsymbol{\lambda}_1, \omega), \cdots, dB(g_\alpha\boldsymbol{\lambda}_n, \omega)] \end{aligned} \tag{A.42}$$

E. Wiener-Itô Expansion

An L^2 functional $\Psi[\omega]$ is defined by a random variable or a stochastic functional generated by the Gaussian random measure $dB(\mathbf{x})$ or $dB(\boldsymbol{\lambda})$ such that $\langle|\Psi|^2\rangle < \infty$. $L^2[\Omega]$ denotes the Hilbert space of such functionals with the inner product defined by the covariance. An

L^2 functional can be expanded in terms of the orthogonal functionals of the form (A.5) or (A.21) in the sense of quadratic mean convergence:

$$\Psi[\omega] = \sum_{n=0}^{\infty} I_n(f) = \sum_{n=0}^{\infty} \hat{I}_n(F) \tag{A.43}$$

Two types of expansion in the middle and the right members are different representations for the same functional. Functions f_n or $F_n, n = 0, 1, 2, ...$ which are the "expansion coefficients", sometimes called Wiener kernels, can be obtained from Ψ by means of orthogonality (A.7) or (A.24). Wiener-Itô expansion (A.43) implies the decomposition of $L^2[\Omega]$ into the orthogonal subspaces $L_n^2[\Omega]$ spanned by the n-th Wiener-Hermite differential. Using (A.11) and (A.28) we obtain a Parseval formula for the orthogonal expansion (A.43).

$$\left\langle |\Psi|^2 \right\rangle = \sum_{n=0}^{\infty} n! \|\tilde{f}_n\|_n^2 = \sum_{n=0}^{\infty} n! \|\tilde{F}_n\|_n^2 \tag{A.44}$$

A Wiener-Itô expansion of a homogeneous random field $\Psi[T^{\mathbf{x}}\omega]$ can be readily obtained from (A.43) using (A.3) and (A.41):

$$\begin{aligned} &\Psi[T^{\mathbf{x}}\omega] \\ &= \sum_{n=0}^{\infty} \int \cdots \int_{R_2} f_n(\mathbf{x}_1 - \mathbf{x}, \cdots, \mathbf{x}_n - \mathbf{x}) h_n[dB(\mathbf{x}_1), \cdots, \cdots, dB(\mathbf{x}_n)] \end{aligned} \tag{A.45}$$

$$= \sum_{n=0}^{\infty} \int \cdots \int_{R_2} e^{i(\boldsymbol{\lambda}_1 + \cdots + \boldsymbol{\lambda}_n)\cdot \mathbf{x}} F_n(\boldsymbol{\lambda}_1, \cdots, \boldsymbol{\lambda}_n) \hat{h}_n[dB(\boldsymbol{\lambda}_1), \cdots, dB(\boldsymbol{\lambda}_n)] \tag{A.46}$$

where f_n and F_n are symmetric functions with respect to their n variables.

References

1. Beckman, P., and A. Spizzichino, *The Scattering of Electromagnetic Waves from Rough Surfaces*, New York, Pergamon, 1963.
2. Ishimaru, A., *Wave Propagation and Scattering in Random Media,* Vol.II, New York, Academic, 1978
3. Kong, J. A., *Electromagnetic Wave Theory,* Second edition, New York, John-Wiley & Sons, 1990.
4. Ogilvy, J. A., *Theory of Wave Scattering from Random Rough Surfaces*, Bristol, Adam Hilger, 1991.
5. Rice, S. O., "Reflection of electromagnetic waves from slightly rough surface", *Commn. Pure Appl. Math.*, Vol. 4, 351–378, 1951.
6. Bass, F. G., and I. M. Fuks, *Wave Scattering from Statistical Rough Surfaces*, New York, Pergamon 1979.
7. Freilikher, V. D., and I. M. Fuks, "Green's function method for the Helmholtz equation with perturbed boundary conditions," *Radio Phys. Quantum Electron.*, Vol. 13, No. 1, 73–79, 1970.
8. Zipfel, G. G., and J. A. DeSanto, "Scattering of a scalar wave from a random rough surface: A diagrammatic approach," *J. Math. Phys.* Vol. 13, 1903–1911, 1972.
9. DeSanto, J. A., "Green's function for electromagnetic scattering from a random rough surface," *J. Math. Phys.*, Vol. 15, 283–288, 1974.
10. Brown, G. S., "A stochastic Fourier transform approach to scattering from perfectly conducting randomly rough surfaces," *IEEE Trans. Antenna Propag.*, Vol. 30, 1135–1144, 1982.
11. Brown, G. S., "New results on coherent scattering from randomly rough conducting surfaces," *IEEE Trans. Antenna Propag.*, Vol. 31, 5–11, 1983.
12. Ito, S., "Analysis of scalar wave scattering from slightly random suraces: a multiple scattering theory," *Radio Sci.*, Vol. 20, 1–12, 1985.
13. Nakayama, J., H. Ogura, and B. Matsumoto, "A probabilistic theory of scattering from a random rough surface," *Radio Sci.*, Vol. 15, 1049–1057, 1980.
14. Nakayama, J., H. Ogura, and M. Sakata, "Scattering of a scalar wave from a slightly random surface," *J. Math. Phys.*, Vol. 22, 471–477, 1981.
15. Nakayama, J., "Anomalous scattering from a slightly random surface," *Radio Sci.* Vol. 17, 558–564, 1982.

16. Nakayama, J., H. Ogura, and M. Sakata, "A probabilistic theory of electromagnetic scattering from a slightly random surface 1. Horizontal polarization," *Radio Sci.*, Vol. 16, 831–847, 1981.
17. Nakayama, J., M. Sakata, and H. Ogura, "A probabilistic theory of electromagnetic scattering from a slightly random surface 2. Vertical polarization," *Radio Sci.* Vol. 16, 847–853, 1981.
18. Nakayama, J., K. Mizutani, H. Ogura, and S. Hayashi, "Theory of light scattering from a random metal surface: Excitation of surface plasmon in a Ag film," *J. Appl. Phys.*, Vol. 56, 1465–1472, 1984.
19. Ogura, H., and N. Takahashi, "Green function and radiation over a random rough surface," *J. Opt. Soc. Am.*, Vol. A2, 2208–2224, 1985.
20. Ogura, H., and H. Nakayama, "Scattering of waves from a random cylindrical surface," *J. Math. Phys.*, Vol. 29, 851–860, 1988.
21. Ogura, H., N. Takahashi, and M. Kuwahara, "Scattering of waves from a random cylindrical surface," *Wave Motion*, Vol. 14, 273–295, 1991.
22. Ogura, H., N. Takahashi, and M. Kuwahara, "Scattering of an electromagnetic wave from a slightly random cylindrical surface: horizontal polarlization," *Waves in Random Media*, Vol. l, 363–389, 1991.
23. Ogura, H., and N. Takahashi, "Scattering of waves from a random spherical surface - Mie scattering -," *J. Math. Phys.*, Vol. 31, 61–75, 1990.
24. Ogura, H., "Theory of waves in a homogeneous random medium," *Phys. Rev.*, Vol. A11, 942–956, 1975.
25. Ogura, H., and J. Nakayama, "Initial-value problem of the one-dimensional wave propagation in a homogeneous random medium," *Phys. Rev.*, Vol. A11, 957–962, 1975.
26. Ogura, H., T. Aoki, and Y. Yoshida, "Computer simulation of the wave propagation in a homogeneous random medium," *Phys. Rev.*, Vol. A13, 349–356, 1976.
27. Ogura, H., and Y. Yoshida, "Wave propagation in a slightly lossy random medium," *Phys. Rev.*, Vol. A14, 796–801, 1976.
28. Wiener, N., *Nonlinear Problems in Random Theory*, Cambridge, MA, MIT, 1958.
29. Cameron, R. H., and W. T. Martin, "The orthogonal development of nonlinear functionals in series of Fourier-Hermite functionals," *Ann. Math.*, Vol. 48, 385–392, 1947.

30. Ito, K., "Multiple Wiener integrals," *J. Math. Soc. Japan*, Vol. 13, 157–169, 1951.
31. Ito, K., "Complex multiple Wiener integrals," *Jpn. J. Math.*, Vol. 22, 63–86, 1952.
32. Ogura, H., *Theory of Stochastic Processes*, Tokyo, Corona, 1978.
33. Ogura, H., "Orthogonal functionals of the Poisson process" *IEEE Trans. IT*, Vol. 18, 473–481, 1972.
34. Imamura, T., W. C. Meecham, and A. Siegel, "Symbolic calculus of of the Wiener process and Wiener-Hermite functionals," *J. Math. Phys.*, Vol. 6, 696–706, 1965.
35. Siegel, A., T. Imamura, and W. C. Meecham, "Wiener-Hermite expansion in model turbulence in the late decay stage," *J. Math. Phys.*, Vol. 6, 707–721, 1965.
36. Barrett, J. F., "The use of functionals in the analysis of nonlinear physical systems," *J. Electron. Contr.*, Vol. 15, 567–615, 1963.
37. Schetzen, M., *The Volterra and Wiener Theory of Nonlinear Systems*, New York, Wiley, 1980.
38. Meecham, W. C., and W. W. Lin, "Reflection of radiation from random rough surfaces," *Wave Matter Interaction*, Vol. l, 4–12, 1986.
39. Eftimiu, C., "Electromagnetic scattering by rough conducting circular cylinders - I: Angular corrugation, II: Axial corrugation," *IEEE Trans.,* AP-36, 651–658, 659–663, 1988.
40. Doob, J. L., *Stochastic Processes*, New York, John Wiley & Sons, 1953.
41. Yaglom, A. M., *Introduction to the Theory of Stationary Random Functions*, (English translation,) New York, Dover, 1973.
42. Ishimaru, A., J. S. Chen, P. Phu, and K. Yoshitomi, "Numerical, analytical, and experimental studies of scattering from very rough surfaces and backscattering enhancement," *Waves in Random Media*, Vol. 1, 91–107, 1991.
43. Celli, V., A. A. Maradudin, A. M. Marvin, and A. R. McGurn, "Some aspects of light scattering from a randomly rough metal surface," *J. Opt. Soc. Am. A*, Vol. 2, 2225–2239, 1985.
44. Thorsos, E. I., and D. R. Jackson, "The validity of the perturbation approximation for rough surface scattering using roughness spectrum," *J. Acoust. Soc. Am.*, Vol. 86, 261–277, 1989.
45. Felsen, L. B., and N. Marcuvitz, *Radiation and Scattering of Waves*, Englewood Cliffs, N.J., Prentice-Hall, 1973.